Experimental and Numerical Investigations on the Development and Optimization of Latent Heat Storage System

A thesis submitted in partial fulfillment of the requirements for the degree of

Doctor of Philosophy

by

Hakeem Niyas. U.S

(Roll No. 126103017)

Department of Mechanical Engineering

Indian Institute of Technology Guwahati

Guwahati – 781039, India

September 2017

Department of Mechanical Engineering
Indian Institute of Technology Guwahati
Guwahati – 781039, India

THESIS CERTIFICATE

This is to certify that the work contained in the thesis entitled **Experimental and Numerical Investigations on the Development and Optimization of Latent Heat Storage System** by **Hakeem Niyas. U.S**, a student of the Department of Mechanical Engineering, Indian Institute of Technology Guwahati, for the award of the degree of **Doctor of Philosophy** has been carried out under my supervision and that this work has not been submitted elsewhere for any degree.

Prof. P. Muthukumar

Department of Mechanical Engineering

Indian Institute of Technology Guwahati

Guwahati – 781039, India

Dedicated

To

My Mother

Acknowledgement

I express my deepest gratitude and sincere thanks to my supervisor Prof. P. Muthukumar for his invaluable guidance and constant encouragement. I am much inspired by not only his rich experience and knowledge but also the way of approaching a problem, immense patience and extreme care. I am highly obligated to him for his persistent devotion and willingness. During my research, he provided me with the most precious ideas and resources that played a vital role in completing the thesis successfully. I enjoyed every moment working under his supervision and learnt many things from him, which will be an asset for my future research.

I would like to thank Department of Science and Technology (DST), Government of India, for their financial support in the fabrication of the experimental setup (Project No: DST/TM/SERI/2K10/53(G)) and the international travel grant for presenting the research output in the international conference, Solar World Congress 2015 held at Daegu, South Korea (Grant No: ITS/4332/2015-16).

I am thankful to my doctoral committee members, Prof. Subhash Chandra Mishra (Late), Dr. Amaresh Dalal, Dr. Dipankar Narayan Basu and Dr. Nanda Kishore for giving their valuable suggestions and encouragement, which helped to shape myself to meet the requirements of a successful researcher. I would like to express my sincere thanks to Prof. Pinakeswar Mahanta (ex. HOD) and Prof. Anoop Kumar Dass (HOD) for providing all the facilities needed for my research work. I take this opportunity to thank all the faculty members of the department for their valuable suggestions and cooperation during my course work.

I specially thank the departmental personnel, Mr. Dilip Chetri, Mr. Monoj Kumar Baishya, Mr. Mrinal Sarma, Mr. Porag Saikia, Mr. Nip Borah and Mr. Rituraj Saikia for their help during the course of fabrication of the experimental setup.

I am thankful to my lab colleagues, Dr. Satya Sekhar, Dr. Anbarasu, Dr. Niraj Kumar Mishra, Mr. Chilaka Ravi Chandra Rao, Mr. Vivek Selvan, Mr. Gyan Sagar Sinha, Mr. Sujit Roy, Mr. Deva Kanta Rabha, Mr. Kiran Naik Bukke, Mr. Nithin Narmada, Mr. Vigneshwaran, Mr. Lav Kumar Kaushik, Mr. Gurpreet Singh Sodhi, Mr. Sunku Prasad, Mr. Likhendra Prasad, Mr. Atul Keshao Khobragade, Mr. Ankit Kumar Shukla, and Mr. Bhuvnesh Garg for their constant support and valuable friendship.

I would like to express my sincere gratitude to my parents, Mr. Saleem and Mrs. Sarammal, my brothers, Mr. Rasik Fareedh and Mr. Salman Farish, my parents-in-law, Mr. Mohamed Ibrahim and Mrs. Razia Begum, whose blessings and never-ending support is the real stimulus that constantly inspires me to do my best. I also thank my wonderful children, Fathima Shifa and Muhammad Muaadh, for always making me smile. Last but not the least, my deepest gratitude goes to my wife, Mrs. Ayesha Haslin Fathima for her constant encouragement, unlimited sacrifices and patience, sincere prayers, continuous support and motivation for the completion of this thesis work.

HAKEEM NIYAS. U.S

Abstract

Energy plays a major role for the existence of humanity. For quite a long period, much of the energy needs of the humankind have been fulfilled from the non-renewable energy sources such as coal, oil and natural gas. The gruesome point of usage of non-renewable energy sources in the power generation, heating and cooling, and transportation sector is the greenhouse gas emissions, which has several adverse effects like climate change, global warming, ozone depletion, sea level rise, etc. Hence, several countries ramped their investments on renewable energy based technologies to combat these harmful environmental outcomes.

Concentrated solar power (CSP) is one of the promising large-scale power generation technologies among the renewables, which is being widely commercialized now. The major problem that all solar power plants face is the intermittent solar radiation that can be solved by adding storage. Of all the storage options, thermal energy storage (TES) is the most economical, which gives an advantage to CSP plants over solar PV plants since TES can be integrated with CSP to ensure power 24/7. The TES systems are broadly classified into sensible heat storage, latent heat storage (LHS) and thermochemical heat storage. LHS systems using phase change materials (PCMs) are highly attractive due to their high volumetric heat storage capacity, compactness, moderate cost, near constant temperature heat storage/retrieval and adaptability over wider temperature ranges.

In general, LHS system consists of a regenerator type heat exchanger wherein the heat transfer fluid (HTF) is passed through the storage media for charging and discharging processes. During charging, the high-temperature HTF transfers the heat to the storage medium. The stored energy is released during discharging as the low-temperature HTF passes through it. Design and optimization of LHS prototypes require exhaustive analysis on heat transfer characteristics between the PCM and HTF. The number of HTF tubes and fins on the HTF tube's outer surface play a major role in transferring the heat between them. Un-optimized prototype with more number of HTF tubes and fins would lead to higher material inventory. Additionally, the

overall weight of the system will increase too. Hence, a detailed optimization study is needed to have a cost-effective LHS system.

The main objectives of the present work are (i) to study the charging and discharging characteristics of a LHS prototype by considering the natural convection effect, (ii) to develop a 2D mathematical model for optimizing the number of tubes and fins in the shell-and-tube type lab-scale LHS prototype, (iii) to develop a 3D thermal model for predicting the charging and discharging characteristics of the LHS prototype with the optimized number of tubes and fins at different operating conditions and (iv) to test the storage performances of the LHS prototype at various operating conditions.

A numerical study of conjugate heat transfer and phase change process in a shell-and-tube type prototype of 10 MJ LHS capacity filled with a PCM is presented. The PCM used in the present study is a ternary mixture of potassium nitrate, sodium nitrate and sodium nitrite in the weight proportion of 53:7:40. Effective heat capacity method is used in the model to integrate the latent heat of the PCM with the specific heat and Boussinesq approximation is applied to incorporate the buoyancy effect of the molten layer of the PCM. For proper modeling of velocities in the PCM, Darcy law's source term is added. The governing equations involved in the model are solved using a finite element based software product, COMSOL Multiphysics 4.3a. To optimize the number of HTF tubes and number fins on the tubes, a 2D thermal model is developed and the performance is compared by varying the number of HTF tubes (19, 22, 25, 28) and number fins on the tubes (0, 2, 4, 6). Thermal model with 25 tubes and 4 fins is found to be the optimized configuration.

Based on the results of optimization study, a lab-scale shell-and-tube based LHS prototype of 10 MJ LHS capacity is fabricated and the computational study is extended to a 3D thermal model for evaluating the performance of the prototype. Charging and discharging characteristics are investigated at different HTF inlet temperatures (157 / 162 / 167 °C during charging and 117 / 122 / 127 °C during discharging) and flow rates (0.3, 0.45, 0.6 m^3/hr). It is observed that the charging/discharging rate is faster for higher/lower HTF inlet temperature. Similarly, the charging/discharging rate is faster for higher HTF flow rates. The numerical and experimental results are found to have a good agreement.

It is observed that the charging process is faster than the discharging process due to the additional natural convection, which takes place after the phase change temperature. For an HTF inlet temperature of 162 / 122 °C during charging/discharging and HTF flow rate of 0.3 m^3/hr, it took about 124 / 131 min for charging/discharging of the LHS prototype in the experiments. Similarly, it took about 111 / 117 min for charging/discharging of the LHS prototype in the numerical simulations. It is also seen that partial charging/discharging process is efficient than complete charging/discharging process. It took only 73 / 70 % of the complete charging/discharging time for 90 % of heat storage/discharge. In addition, it is found that varying HTF inlet temperature has a greater effect on charging/discharging time when compared with HTF flow rate. Still, the effect of HTF flow rate is more prominent at lower/higher HTF inlet temperature during charging/discharging process.

Based on the above discussions, one can conclude that the shell-and-tube based LHS prototype with multiple tubes and fins can be effectively used for storing the heat. Further, the results presented in this thesis will be useful for developing the commercial LHS devices for industrial applications. Using the developed thermal model, one can predict the performances of shell-and-tube based LHS prototype with fins filled with different PCMs without performing the expensive experimental studies.

In addition to the major objectives of the thesis, two novel concepts namely novel encapsulation and novel fin are proposed in this thesis. The numerical model used for the performance evaluation of the LHS prototype is slightly modified to study the storage characteristics of the novel concepts.

The concept of novel encapsulation technique is intended to achieve better heat transfer in LHS capsules, which has a wide application in steam accumulators. A comparison of the heat transfer characteristics of the basic and novel capsules is done using the numerical model. It is found from the numerical study that it took about 64 / 33 min and 158 / 57 min for the basic/novel capsules for complete charging/discharging. The reduction in the charging/discharging time achieved by the novel capsule when compared with the basic capsule is about 48.4 / 63.9 %. Effect of operating temperature range is also studied and it is observed that the novel capsule with the least temperature difference (20 °C) itself charges/discharges faster than the basic capsule with a higher temperature difference (30 / 40

°C). The scope for commercial viability of the novel concept is also explored and the results showed a positive step towards the commercialization of the novel concept. While upscaling, the reduction in the charging and discharging time achieved by the novel capsule (1 MJ capacity) when compared with the basic capsule (0.5 MJ capacity) are 4.7 % and 19 %. Different arrangements of novel and basic capsules in circular and rectangular forms are studied for less volume occupancy and it is found that the novel capsules arranged in the rectangular fashion occupies the least volume. In addition, a mass reduction of approximately 21.4 % can be achieved with the novel capsule when compared with the basic capsule in the current study.

The concept of novel fin is envisioned to accomplish an efficient heat transfer in tube-in-tube LHS modules. A comparison of the storage characteristics of the novel fin configuration with no fin and standard fin configurations is made using the numerical model. It is found from the numerical study that it takes about 548 / 788 min, 514 / 742 min and 487 / 665 min for complete charging/discharging of the LHS module with no fin, standard fin and novel fin. It can be noted that the charging/discharging time has decreased by about 11.1 / 15.6 % and 5.25 /10.4 % when using novel fin configuration with respect to no fin and standard fin configurations. The novel fin proposed has also an additional advantage of weight and cost reduction of fins by a factor of 0.5.

Nomenclature

A_{MUSH}	:	Mushy zone constant
C_P	:	Specific heat (J kg^{-1} K^{-1})
E_L	:	Latent energy stored/discharged (J)
E_S	:	Sensible energy stored/discharged (J)
E_T	:	Total energy stored/discharged (J)
F	:	Body force (N m^{-3})
g	:	Gravitational acceleration (m s^{-2})
k	:	Thermal conductivity (W m^{-1} K^{-1})
L_F	:	Latent heat of fusion (J kg^{-1})
P	:	Pressure (Pa)
S	:	Source term (N m^{-3})
T	:	Temperature (°C)
T_M	:	Phase change temperature (°C)
t	:	Time (s)
v	:	Velocity (m s^{-1})

Greek symbols

β	:	Thermal expansion coefficient (K^{-1})
ρ	:	Density (kg m^{-3})
μ	:	Dynamic viscosity (Pa s)
γ	:	Kinematic viscosity (m^2 s^{-1})
θ	:	Melt fraction

Subscripts

b	:	Boundary
C	:	Charging
D	:	Discharging
EFF	:	Effective

ini	:	Initial
L	:	Liquid, liquidus
S	:	Solid, solidus

Symbols

∇	:	Differential operator

Abbreviations used

BDF	:	Backward differentiation formula
EHC	:	Effective heat capacity
FEM	:	Finite element method
FVM	:	Finite volume method
HTF	:	Heat transfer fluid
LHS	:	Latent heat storage
MWCNT	:	Multi-walled carbon nano tube
PCM	:	Phase change material

Contents

List of Figures

List of Tables

Chapter 1
Introduction

1.1 Preface

Energy plays a pivotal role in the development of all nations. The global primary energy consumption in 2015 was 5.83×10^{20} J, equal to an average power consumption of 18.5 TW (Perez and Perez, 2015). Majority of the world's current energy consumption is met by the non-renewable energy sources, which occupies a huge proportion of 80.8 % (Sawin et al., 2016). If we continue to rely on the non-renewable energy sources at the same pace for another century, we will be mostly ruin out of the resources. Nowadays, the humankind faces massive challenges: population growth, exhausting fossil fuels, growing energy demand, increasing energy prices and global warming. All these factors contribute to the immediate urge in the transformation of the energy sector, which predominantly depends on the non-renewable energy sources, to the one that uses renewable energy sources and energy efficient technologies. Opting for renewable energy is one of the strategic solutions to the existing challenges faced by the world. Most of the countries have already implemented the production and usage of renewable energy through various approaches.

Fig. 1.1 depicts the global potential of various non-renewable and renewable energy resources. It can be observed from Fig. 1.1 that the solar energy is the best available renewable energy source in terms of energy potential. Traditionally, solar energy is used in heating and drying applications. Nowadays, it finds a remarkable place in the field of electricity generation. Solar energy can be converted to electricity, directly using photovoltaics (PV), or indirectly using concentrated solar power (CSP). Photovoltaics converts the sunlight into electric current using

the photoelectric effect. CSP plants use reflective lenses or mirrors and tracking systems to focus a large amount of sunlight into a small point or beam by which the working fluid gets heated to a higher temperature. In direct steam generation (DSG) plants, the working fluid is generally water and the steam produced is directly fed to the turbine for electricity production. In non-DSG plants, the primary working fluid is generally a synthetic oil that gets heated from the concentrated sunlight. Synthetic oil transfers the heat to the secondary working fluid (water/steam), which is then supplied to the turbine for power generation. The major disadvantage with the PV and CSP plants is the inability to generate electricity during night and overcast day, which reduces the operating time. Perhaps this issue can be solved in CSP plants by incorporating thermal energy storage (TES). Hasnain (1998), Dincer and Rosen (2002) and Kuravi et al. (2013) discussed in detail about the various aspects of TES technologies and their applications for CSP plants. Though several prototypes of TES were developed across the world, only a few large-scale TES systems have been commissioned in the CSP plants (Gil et al., 2010).

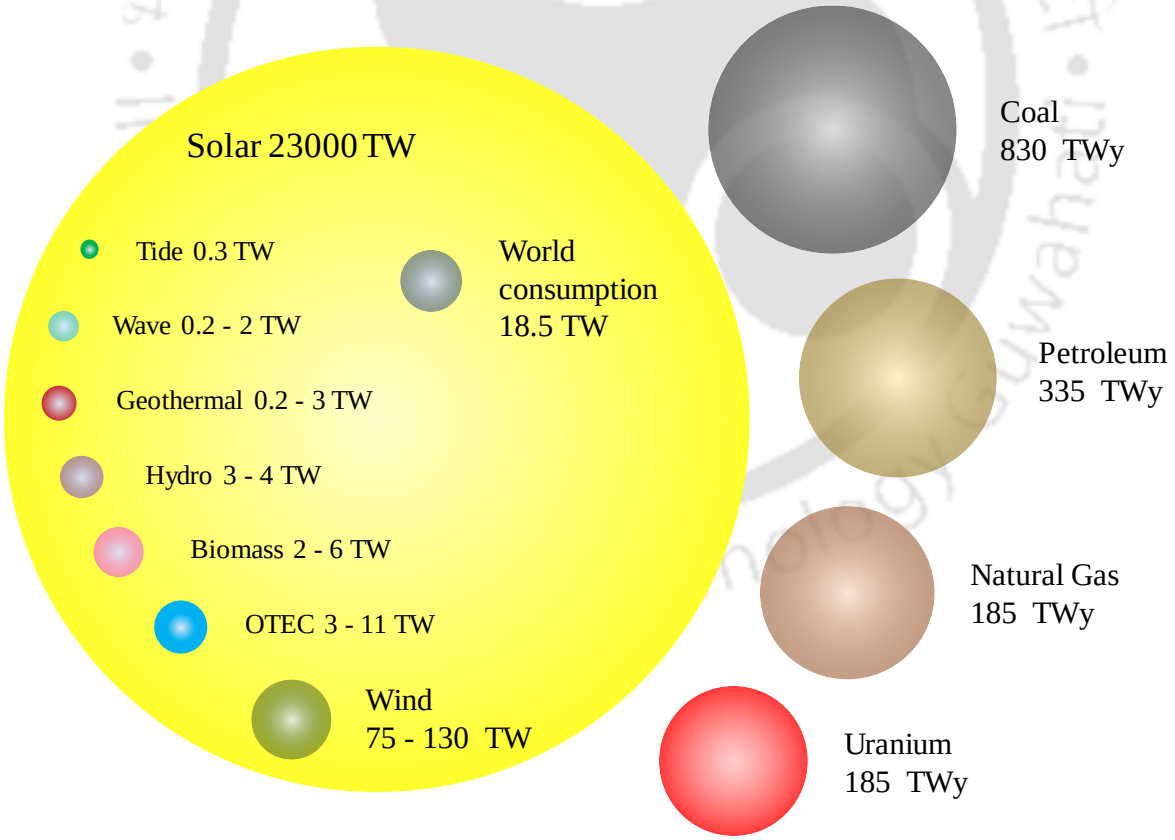

Fig. 1.1 Global potential of various energy sources (Perez and Perez, 2015).

1.2 Thermal energy storage

The main problem with using solar energy for power is the intermittent nature of sunlight. This necessitates the development of energy storage that can bridge the gap between demand and production of electricity. Of all the energy storage options, thermal energy storage (TES) is the most economical. It is also most appropriate for CSP plants. In addition, TES systems can increase the plant reliability and reduce the Levelized Cost of Energy (LCOE) for CSP plants. In general, the TES system consists of a regenerator type heat exchanger wherein the heat transfer fluid (HTF) passes through the storage media for charging and discharging only. During charging, the high-temperature HTF transfers the heat to the storage medium. The stored energy is released from the TES system during discharging as the low-temperature HTF passes through it. Fig.1.2. depicts the schematic representation of a CSP plant incorporated with the TES system.

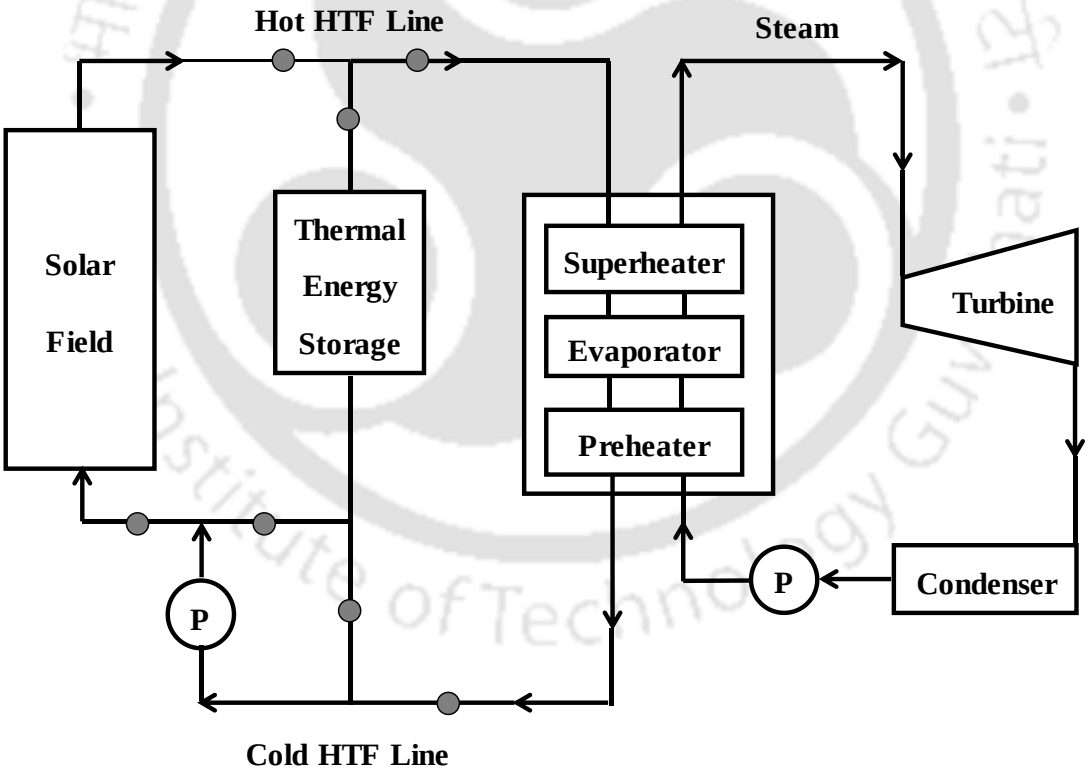

Fig. 1.2 Schematic view of a CSP plant with TES system

The TES system can be put into operation with the CSP plant in the following modes:

1) Storage charging only.
2) Steam generation and storage charging.
3) Steam generation from storage discharge only.
4) Steam generation from solar field and storage discharge.

The first mode is generally applicable when there is a solar field output, but the solar field output can be more effectively used at a different time of the day. The high-temperature HTF from the solar field is passed through the TES system and then recirculated to the solar field itself. In the second mode, the excess thermal energy that is not used to generate steam is stored in the TES system. The HTF flows from the solar field to both the heat exchangers i.e. steam generator and TES in parallel and recirculated back to the solar field. The third mode applies when there is no solar field output and steam is required. The HTF flows in the loop between the storage heat exchanger and steam generator. The fourth mode is applicable when there is some amount of solar field output, but it is desirable to supplement that output with certain energy from the storage. The HTF flows from solar field and storage heat exchanger (both solar field and storage heat exchanger act in parallel) to the steam generation unit and recirculated back to the pump.

1.3 Thermal energy storage methods

There are currently three major methodologies available for storing the thermal energy. They are:

1) Sensible heat storage.
2) Thermochemical heat storage.
3) Latent heat storage.

1.3.1 Sensible heat storage

In sensible heat storage (SHS), thermal energy is stored in the storage material by raising the temperature. SHS utilizes the heat capacity of the storage material to store the thermal energy. For a given quantity of energy to store at a prescribed temperature gradient, material with a higher specific heat requires less mass of storage material. The thermal energy stored in the SHS material is given by Eq. 1.1.

$$E = mC_P \Delta T \tag{1.1}$$

SHS materials are a group of materials that undergo no phase change in the temperature range of the energy storage/retrieval process (Fernandez et al., 2010). SHS materials are broadly classified into two types; viz. (i) liquid based materials and (ii) solid based materials. The major problems with liquid media storage system are that it requires two bulky storage tanks and expensive heat exchangers. Although, one storage tank can be eliminated by adapting the thermocline based storage system, but high temperature of freezing of liquid media (salts) is still a problem. In addition, the commonly used two tanks molten salt storage system is the one with the highest environmental impact and hence it should be substituted by other systems. This higher impact is mainly due to the complexity of the system and the usage of more amount of storage material.

1.3.2 Thermochemical heat storage

Thermochemical heat storage (THS) systems rely on the energy absorbed and released in breaking and reforming molecular bonds of certain materials in a completely reversible chemical reaction. As the binding energy in a chemical reaction is typically large, the temperature required to break the bond is generally high. In this case, the amount of energy stored depends on the mass of storage material (m), the endothermic heat of reaction (Δh_e) and the extent of conversion – fraction reacted (α). For long-term storage, THS is a feasible option, but technological complexity and high costs limit their usage.

$$E = m \Delta h_e \alpha \tag{1.2}$$

1.3.3 Latent heat storage

In latent heat storage (LHS), thermal energy is stored in the materials during the phase change of the material at a constant or near constant temperature. Three types of phase change are physically possible such as solid-to-solid, solid-to-liquid and liquid-to-vapor. In solid-to-solid transition, heat is stored when the material is transformed from one lattice structure to another. This transition has a comparatively lesser latent heat and volume change than solid-to-liquid transition. However, a higher latent heat is associated with liquid-to-vapor transition, but the change of phase causes a drastic volume change that ruled out their usage in storage systems. Hence, solid-to-liquid phase change is a favorable option in the LHS systems. The total energy stored in the LHS material is given by Eq. 1.2.

$$E = m\left[C_{ps} \left(T - T_m \right) + L_F \, \theta + C_{pl} \left(T_m - T_{ini} \right) \right] \tag{1.3}$$

Among the discussed TES techniques, LHS is particularly attractive due to its ability to provide higher storage density and achieve energy storage/retrieval at a near constant temperature.

1.4 Thermal energy storage concepts

Fig. 1.3 depicts the various storage concepts available in the TES systems. Depending upon the role played by the storage medium, storage concept can be classified into two types, viz. active and passive storage systems. In active storage systems, storage material itself circulates through a heat exchanger and this heat exchanger can be a solar receiver or a steam generator. Generally, the active storage system uses one or two massive storage tanks containing the corresponding storage material. Active storage system is further classified into direct and indirect systems. In active direct system, the storage material acts as the HTF also, while in active indirect system, a secondary fluid such as oil is used to extract the energy from the storage material. Hence, the cost of the indirect storage system is comparatively more due to the additional heat exchanger. Passive storage system consists of a regenerator type heat exchanger in which the HTF is passed through the storage media in the charging and discharging processes only. During the charging process, the high temperature HTF transfers the heat to the storage medium. This stored heat is released back to the HTF during the discharging process when the low temperature HTF is passed through it.

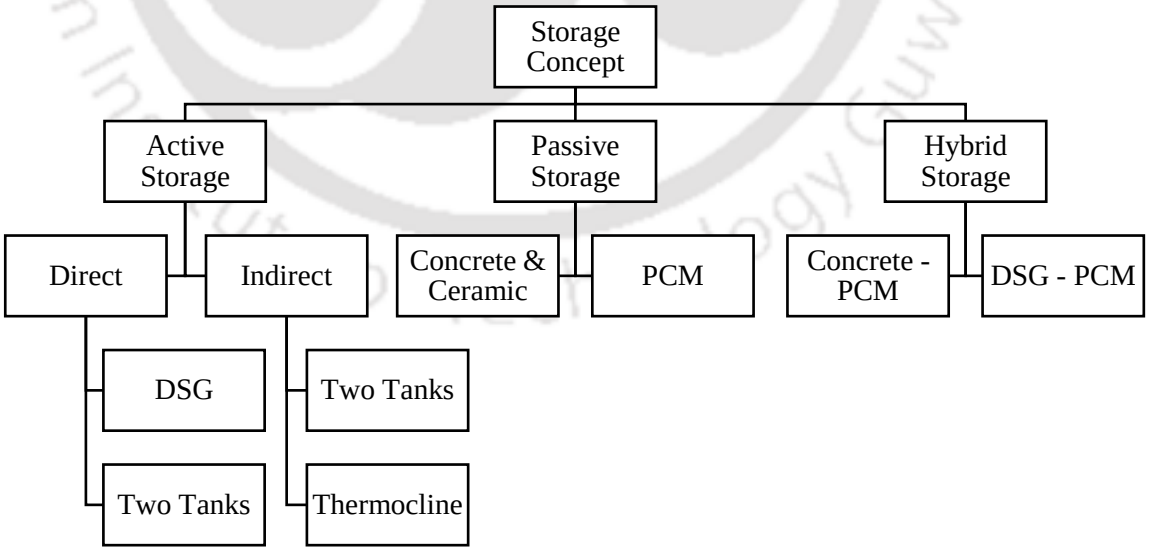

Fig. 1.3 Storage concepts of TES system.

1.5 Phase change materials

Phase change materials (PCMs) are a group of families of materials, which will undergo a phase change while heating/cooling it above/below the phase transition temperature. Initially, the PCMs act like SHS materials; their temperature increases as they absorb heat. However, when PCMs reach the phase transition temperature, they absorb a large amount of heat (called as latent heat) at a near constant temperature. The PCM continues to absorb heat without a significant increase in temperature until all the material has transformed to the liquid phase. Once the entire PCM is melted, the temperature of the PCM again increases when heat is supplied to it.

The main criteria that govern the selection of PCMs are (Abhat, 1983):

- Possess a phase transition temperature in the desired operating temperature range.
- Have a high latent heat of fusion, so that a smaller amount of PCM can store the desired amount of energy.
- Possess high specific heat to provide additional SHS effects.
- Have a high thermal conductivity for faster charging and discharging rates.
- Small volume changes during phase transition, so that a simple type of heat exchanger can be used.
- Exhibit little or no sub-cooling during freezing.
- Possess chemical stability, no chemical decomposition.
- Should not contain poisonous, flammable and explosive elements/compounds.
- No corrosion issue
- Available in large quantities at a cheaper cost.

A classification of PCMs is given in Fig. 1.4. PCMs are broadly classified into inorganic, organic and eutectics. Inorganic PCMs generally include hydrated salts and metals, which are suitable for medium to high temperature storage applications such as process industries and thermal power plants. Organic PCMs on the other hand include paraffins and fatty acids, which are normally used in thermal comfort in buildings, preservation of food/medicines, cooling of electronics, etc. Eutectics are compounds formed by mixing two or more PCMs (organic or inorganic) which melts/solidifies in the same temperature interval. A large number of PCMs

are available in any required temperature range. The comprehensive list of PCMs are well documented in several literatures (Sharma and Sagara, 2005; Kenisarin and Mahkamov, 2007).

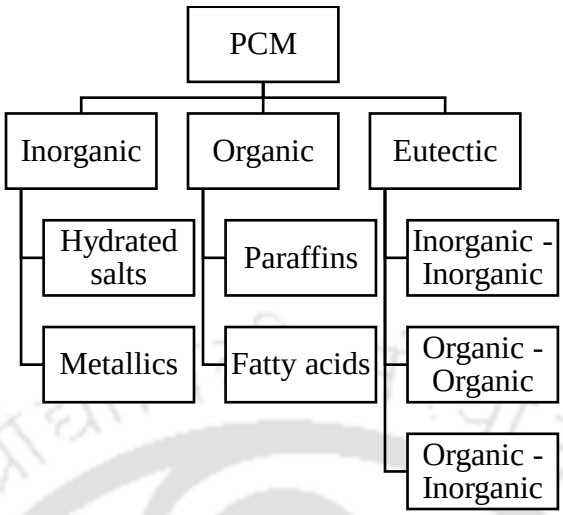

Fig. 1.4 Classification of PCMs.

1.6 Storage heat exchanger design

Once the PCM is selected primarily based on the temperature range of the application, the subsequent vital factors to consider are the geometry of the LHS heat exchanger and the optimum sizing of the heat exchanger required for a given amount of the PCM. All these factors have a direct influence on the storage characteristics of the PCM and eventually affects the charging and discharging rates of the LHS unit. To ensure long-term thermal performance of any LHS unit, the size and shape of the unit must be carefully selected. Depending on the heat exchange mechanism between the HTF and PCM, three different types of storage containments are currently available.

1) Shell-and-tube type LHS prototypes – In this type, PCM is filled in the shell region and the HTF flows through the tubes. Higher/lower heat capacity HTF such as thermic oil/air is generally passed through the tubes in the laminar/turbulent regime.
2) Packed bed LHS prototypes – Here, several spherical capsules containing the PCM is packed in a container and HTF is allowed to pass through the container generally in the turbulent regime to exchange the heat between the HTF and PCM.
3) Staggered LHS capsules – In this configuration, several macro encapsulated LHS capsules are kept in a container, which are arranged in a staggered fashion with a finite minimum distance between the capsules. The HTF is passed through the container for heat storage/extraction in/from the PCM.

The most intensely analyzed LHS configuration is the shell-and-tube system. This is because most of the engineering systems use cylindrical pipes and heat loss from the shell-and-tube system is minimal (Kuravi et al., 2013).

1.7 Applications of PCMs

PCMs play an important role in various research activities of thermal storage over the past four decades and it is being used in a number of applications. Some of the important applications of PCMs are given in Table. 1.1. Most of the commercial solar thermal power plants use liquid based SHS storage systems and a lot of research is now going on in incorporating the PCMs in the CSP plants.

Table. 1.1 Applications of PCMs

Applications	**PCM**	**Reported works**
Greenhouse heating	$CaCl_2 \cdot 6H_2O$	Kurklu (1998)
	PCM 21, PCM 17	Najjar and Hasan (2008)
Solar cooking	Acetamide	Sharma et al. (2000)
	$Mg(NO_3)_2 \cdot 6H_2O$	Hussein et al. (2008)
	NaNO3 – KNO3 (60-40 %)	Veremachi et al. (2016)
Solar water heater	Paraffin	Prakash et al. (1985)
	$Na_2SO_4 \cdot 10H_2O$	Tayeb (1993)
	Stearic acid	Buddhi and Sahoo (1997)
Solar thermal power plants	$NaNO_3$	Laing et al. (2013)
Space cooling	$Na_2HPO_4 \cdot 12H_2O$	Saitoh and Hirose (1986)
	Dimethyl sulfoxide	Farid et al. (1998a)
	Rubitherm RT22	Tan and Zhao (2015)
Space heating	$CaCl_2 \cdot 6H_2O$ – $KF \cdot 4H_2O$	Vakilaltojjar and Saman (2001)
	Lauric acid – Stearic acid	Sari and Kaygusuz (2002b)
	M91	Panayiotou et al. (2016)
Waste heat recovery systems	Erythritol	Ona et al. (2001)
	Lauric acid	Gu et al. (2004)
	Paraffin RT82	Merlin et al. (2016)

1.8 Motivation of the Thesis

LHS systems store/release a large amount of energy at a near constant temperature interval in a compact space, which is being considered as a replacement of liquid based SHS systems. The charging and discharging times of the LHS systems should be low. Hence, proper design and optimization of LHS systems is of vital importance. The development of a 3D numerical model is necessary to evaluate the performance characteristic of the storage system without conducting expensive experimental studies. A detailed experimental study is also required to crosscheck the developed numerical model for further applicability of the model to the development of real time storage systems. In the present thesis, the performances of lab-scale shell-and-tube type LHS prototype with multiple tubes and fins is studied. A major importance is given to the heat transfer that takes place between the PCM and HTF.

1.9 Thesis structure

The performance of LHS device mainly depends on the heat transfer aspects of the storage prototypes at different operating conditions. The objective of the present thesis is to investigate the performance of the PCM based LHS devices at different operating conditions. This thesis is organized in seven chapters.

Chapter 1 starts with the brief introduction of various methods and concepts of TES systems. The advantages of LHS system using PCMs is elucidated. The classification of PCMs, various applications and motivation of the present work are presented.

In Chapter 2, a state-of-art on various aspects of LHS technology is presented. The literature published on the conjugate heat transfer and phase change studies, influence of natural convection, storage module configuration and heat-transfer augmentation techniques are presented. Various numerical models and experimental investigations at different operating conditions during charging and discharging processes of PCM based LHS systems are also reviewed. Based on the conclusions of the literature survey, objectives of the present thesis work are framed.

Chapter 3 is devoted for the design and numerical formulation of the 3D shell-and-tube based thermal model for predicting the conjugate heat transfer characteristics of the lab-scale LHS

prototype. The results obtained from the numerical model during both charging and discharging processes are presented and the implications of the results are discussed.

Chapter 4 describes the prototype configuration, experimental setup and the procedure followed for testing the lab-scale LHS prototype. The results acquired from the experimental studies during the charging and discharging processes are presented.

Chapter 5 covers the novel encapsulation concept proposed in this thesis. The results of the comparative study on the performances of the basic and novel encapsulation are presented. Possible commercial viability options explored are also mentioned in this chapter.

Chapter 6 defines the novel fin concept used for efficient heat transfer in tube-in-tube LHS devices. The advantages of the proposed concept with the performance comparison of other configurations are explained in this chapter.

Chapter 7 encompasses the major conclusions arrived from the numerical and experimental studies of lab-scale LHS prototype. The outcomes of the novel concepts are also presented. Scope for future work and recommendations are also given in this chapter.

1.10 Summary

This chapter starts with the brief introduction of various methods and concepts of TES systems. Various advantages of the LHS systems when compared with the other TES systems are also explained. The classification of PCMs and its usage in several applications are presented. The motivation of the thesis is discussed and finally the thesis structure is clearly explained in sequence.

Chapter 2

State of the Art

2.1 Preface

Over the last four decades, the renewable energy based power stations, especially CSP plants are being considered as a favorable alternative to the traditional coal based power plants. This is due to the overwhelming awareness of the global nations on the ill effects of the coal-based power plants such as greenhouse gas emissions, air and water pollution, global warming, etc. However, the intermittent availability of the solar radiation necessitates the inclusion of a TES system. This stimulated the research on the various TES technologies and a phenomenal amount of work were reported in the literature. Quest is always there for a compact and efficient storage system and hence LHS got the attention of several researchers due to its high energy density storage capability at near constant temperature. Development of a stable and real-time applicable numerical model is highly important, which can save money over expensive experiments. On the other hand, experimental studies are also important to get the realistic idea of the systems and to check the correctness of the developed numerical models. Hence, several researchers developed various mathematical models covering aspects such as heat-transfer enhancement techniques, influence of natural convection and new solving methodologies. Many performance tests on LHS systems conducted at different operating conditions are also reported in the literature.

In this chapter, a detailed literature survey on the mathematical models and experimental investigations of the LHS systems, influence of natural convection during phase change and heat-transfer enhancement techniques are presented.

2.2 Mathematical modeling of melting and solidification processes

Due to the several complications involved in the modeling of melting and solidification processes such as inclusion of latent heat, considering the natural convection and the conjugate heat transfer between the HTF and PCM, initially, researchers developed certain relatively simplified analytical models. Later on with the improvement in the computational facilities, several researchers developed 2D and 3D transient numerical models to solve the melting/solidification problem that exists in the LHS systems. In this section, a detail literature survey on the various mathematical models developed for the simulation of melting and solidification processes are presented. Hu and Argyropoulos (1996), Verma et al. (2008), Dutil et al. (2011) and Al-abidi et al. (2013) presented a detailed review on the various mathematical models considering the phase change, their applications and limitations.

2.2.1 Analytical models

Problems involving phase change phenomenon such as melting and solidification are generally called as moving boundary problems, due to the movement of the solid-liquid interface during the phase change. The simplest phase change problem is the single-phase problem that was first solved analytically by Stefan (1891). It was considered that only one of the phases (preferably liquid) was active and the other phase (solid) was assumed to be at the phase-change transition temperature. Neumann (1912) extended the Stefan problem by considering both the phases and given an analytical solution in terms of a similarity variable. The Neumann's model was able to predict the solid-liquid interface position and temperature of the solid and liquid phases. Nevertheless, the Neumann's solution is limited to the rectangular coordinate system only. Later, Paterson (1952) solved the Neumann's model for the cylindrical coordinate system. However, these analytical solutions were also limited to the semi-infinite problems only. This issue was solved by Goodman and Shea (1960) using an approximate method called as heat-balance integral method, which was primarily developed based on the Karman–Pohlhausen's method of the momentum integral in the boundary layer theory. They found the melting rate of a finite solid slab that is initially at a uniform temperature below the melting point. The slab was given a constant heat flux at one end and the other end was either insulated or kept at its initial temperature. Although these analytical results aid in getting the theoretical concepts of the phase change process, they were not able to solve the real-time practical problems.

2.2.2 Numerical models

The problem of predicting the phase change behavior of any system is complex owing to its intrinsic non-linear nature at the moving solid-liquid interface. The velocity of the moving interface is controlled by the latent heat absorbed or lost at the boundary. Two types of solution techniques were developed to handle the moving interfaces numerically, viz. time-dependent grid method and fixed grid method. In the time-dependent grid method, the melt/solidification front is tracked continuously, and the latent heat release/absorption during the phase change is treated as a moving boundary condition. This type of boundary condition demands the incorporation of a deforming/moving mesh so that the melt interface coincides with the grid elements (Lynch, 1982; Albert and Oneill, 1986; Shyy et al., 1993). In addition, the time-dependent grid method could not be applied for multidimensional problems. Fixed grid method found wide application due to its simplicity and ease of implementation. The primary advantage of the fixed grid approach is that the latent heat evolution is accounted in the governing equation by defining either an enthalpy or an effective specific heat or a heat source (Gong and Mujumdar, 1997).

Bonacina et al. (1973) developed the effect heat capacity method for predicting the heat transfer characteristics during the phase change. The latent heat is accounted in the modified specific heat of the material. As the temperature dependent coefficients in the resulting governing equations were estimated at the intermediate time level, the difficulty of solving a set of nonlinear algebraic equations at each time step was avoided.

Shamsundar and Sparrow (1975) employed the enthalpy method with a fully implicit finite difference scheme for solving the solidification process in a square geometry with convective cooling boundary conditions. They checked the correctness of the model through the demonstration of the equivalence between the enthalpy form and the conventional form of the energy conservation equations. For achieving this, an integral relation was used in the model.

Poirier and Salcudean (1988) reported that the enthalpy method is more complex and expensive than other fixed grid methods. They observed that the computational cost increases with the improvement in the mesh. Oscillation of solution appeared during the phase change process when the ratio of latent heat to sensible heat is large.

Farid et al. (1998b) developed a 2D numerical model to predict the interface motion of paraffin wax during melting and solidification using the EHC method. They assumed a phase-change temperature range of 2–4 °C, which is the actual phase-change range for most of the commercially available PCMs. They simplified the problem to the case of solving the unsteady heat conduction equation in one phase and solved using an explicit finite difference scheme. They concluded that the EHC method is successful in analyzing the heat transfer with phase change and predicting the heat transfer rate during the phase change of materials, which have narrow as well as wide melting ranges. Further, the model was used for simulating a case of successive solidification and melting.

Kuravi et al. (2009) formulated a 2D numerical model based on the effective heat capacity method to investigate the heat transfer performance of nano-encapsulated PCM slurry in microchannels. They incorporated the latent heat of the PCM slurry in the form of a sine profile. The modified effective heat capacity model was validated with the experimental results reported in the literature and a close agreement was found between them.

Some researchers compared the various fixed grid methods for accurate solutions. Lamberg et al. (2004) and Zhang Y et al. (2014) developed two numerical models based on the effective heat capacity (EHC) method and enthalpy method. They compared the numerical results of both the numerical models with their experimental data. They found that the results of EHC method were found to be more accurate than the enthalpy method.

2.3 Effect of natural convection

Extensive research works have been reported on the heat transfer characteristics of the LHS systems. Several researchers developed numerous thermal models and conducted many experiments to deduce the major heat transfer process during the entire charging and discharging processes. However, majority of the initial works (Goodman and Shea, 1960; Meyer, 1973; Comini et al., 1974) considered only the conduction heat transfer during melting and solidification; it was made clear only by the later works (Huang, 1985; Zhang YW et al., 1993; Ng et al., 1998; Fomin and Saitoh, 1999; Tan FL and Leong, 1999; Khodadadi and Zhang, 2001; Sari and Kaygusuz, 2002a; Lamberg, 2004; Trp et al., 2006; Avci and Yazici, 2013; Hosseini et al., 2014; Seddegh et al., 2015) that the effect of natural convection is of high importance during melting and it could be observed in both horizontal and vertical LHS units.

Huang (1985) presented an analytical solution to the 1D momentum equation considering the buoyancy flow during the melting of a vertical semi-infinite region. The motive of the work was to analyze the nature of the velocity profiles during the early stages of melting. The author found that the flow is upward in the warmer region and downward in the colder region. It is also observed that the upward flow has slightly greater velocity than the downward flow.

Zhang et al. (1993) conducted several experiments to study the melting characteristics of n-octadecane kept in a rectangular enclosure. The experiments were mainly meant for testing the possibility of using PCMs in the cooling of electronic components. One side of the rectangular enclosure was discretely heated at a constant flux, and the remaining sides were maintained at adiabatic conditions. They found that the temperature in the upper region of the enclosure was higher than that of the lower region during the melting process. It was due to the natural convection heat transfer, which was developed after the formation of molten PCM.

Ng et al. (1998) formulated a 2D numerical model to study the melting behavior of n-octadecane in a horizontal cylindrical annulus isothermally heated from the inner wall. The outer wall was given adiabatic boundary condition. They observed that melting rate is enhanced by the increase in natural convection. Meanwhile, the melting of the PCM in the bottom part of the annulus is very inefficient due to the convective flow in the melt.

Fomin and Saitoh (1999) analytically and numerically studied the close-contact melting phenomenon of n-octadecane in a spherical capsule. As the flow in the capsule is axisymmetric about the vertical axis of the capsule, 2D spherical polar coordinate system was employed in the model. The lubrication theory approach was implemented for the thermal modeling of heat and mass transfer processes at the bottom of the capsule, as the thickness of the liquid layer was very small when compared to the size of the capsule. They reported that ignoring the natural convection in the molten layer of the PCM leads to overestimation of the melting rate.

Tan and Leong (1999) experimentally investigated the heat transfer behaviour of n-hexadecane kept in a rectangular cavity enclosure during solidification. The experiments were conducted under constant heat rate condition in one of the vertical walls and the remaining walls are maintained adiabatic conditions. Several experiments were conducted with different heat rates. They observed that the solidification front is parallel to the cold wall showing that the presence of natural convection is negligible.

Khodadadi and Zhang (2001) developed a 2D computational model to study the effects of free convection on the constrained melting of silicon. FVM based enthalpy formulation was used for simulating the phase change process. The effect of phase change on convection was implemented using a Darcy's law-type porous media treatment. They found that the conduction heat transfer was the predominant mode during the initial period of melting, leading to concentric temperature contours. After a while once the growth of melt zone became prominent, the heat transfer was mainly due to natural convection. The study was extended to lower thermal conductivity materials and it was observed that the effect of natural convection was more in the low thermal conductivity materials. They have also visually confirmed the presence of natural convection during melting in a series of experiments using a glass bulb containing a wax as the PCM, immersed in an aquarium containing water at a constant temperature.

Sari and Kaygusuz (2002a) experimentally studied the heat transfer characteristics of lauric acid in a vertical tube-in-tube LHS system during melting and solidification. They reported that the melting was dominated by natural convection and the solidification process was controlled by heat conduction. They also observed that the solidification was slowed due to the conduction thermal resistance of the solidified layer, which was formed around the HTF tube.

Lamberg (2004) developed a simplified 1D analytical model to predict the temperature distribution of the fin and the solid-liquid interface location during the solidification process in a finned LHS system. The model was solved using the quasi-stationary approximation method. It was found that the solidification process was dominated by heat conduction, while the natural convection flow occurs only during the commencement of the solidification process. The results of the developed model were compared with a 2D numerical model and a fair agreement was found between them. The error made in the estimation of PCM solid fraction using the analytical model was ± 10 % when compared with the 2D numerical model.

Trp et al. (2006) formulated a fully implicit transient 2D model to study the storage phenomenon of paraffin during melting and solidification in a vertical shell-and-tube LHS storage unit. They validated the developed numerical model with the experimental results acquired from their in-built experimental setup. They reported that the temperature distribution of the PCM was non-isothermal during melting and isothermal during solidification. They also conducted a detailed study on the effect of HTF operating conditions and geometric parameters.

It was concluded that the design and optimization of the LHS system is of high importance for better storage performance of the system.

Avci and Yazici (2013) performed an experimental study for evaluating the storage characteristics of paraffin in a horizontal shell-and-tube storage unit during charging and discharging processes. Paraffin was kept in the shell region and water was allowed to flow through the inner tube of the system. They found that the temperature field is radially uneven during the melting process in the horizontal annulus, which is mainly due to natural convection. They also reported that the increase/decrease of HTF inlet temperature during the charging/discharging process is found to enhance the melting/solidification of the PCM.

Hosseini et al. (2014) performed an experimental and numerical study to understand the role of buoyancy driven convection during melting and solidification of paraffin RT50 in a horizontal shell-and-tube storage unit. Boussinesq approximation was included in the numerical model to consider the buoyancy effects. They found that the buoyancy-driven convection is dominant during the charging process and negligible during the discharging process.

Seddegh et al. (2015) developed two numerical models for evaluating the performance of the shell-and-tube LHS systems, viz. conduction model and combined conduction-convection model. They found that the results of combined conduction-convection model agreed well with the experimental data than that of conduction model. They also concluded that charging is a natural convection dominant process and discharging is a conduction dominant process.

2.4 Shell-and-tube LHS systems

Several researchers reported the numerical and experimental investigations of the LHS systems with various configurations at different operating conditions. The most intensely studied LHS system among various configurations is the shell-and-tube system. More than 70% of the published research on LHS system reported shell-and-tube configuration having a single HTF tube (Agyenim et al., 2010a). In the shell-and-tube configuration, PCM is usually filled in the shell, and the HTF flows through the tubes. This section covers the various works conducted using the shell-and-tube LHS systems.

Lacroix (1993) developed a 2D theoretical model to analyze the transient behavior of n-octadecane kept in a shell-and-tube LHS system during charging and discharging processes. A series of about 27 numerical experiments were undertaken to evaluate the effects of shell diameter, HTF velocity and inlet temperature. The results showed that for a selected PCM, the geometric parameters must be carefully chosen in order to improve the performance of the storage systems.

Esen et al. (1998) theoretically compared two different models of a cylindrical shell based LHS system, viz. model A (PCM kept in the tube) and model B (PCM kept in the shell). They studied the effects of various geometric and thermal parameters; *viz*., cylinder radius, PCM volume, mass flow rates and inlet temperatures of HTF on the charging time. They found that the model B recorded a shorter charging time than model A. They concluded that as the thickness of PCM increases, charging time of the PCM also increases due to the higher thermal conduction resistance exerted by the layer of PCM.

Vyshak and Jilani (2007) numerically studied the melting of PCM for three geometrical configurations namely rectangular, cylindrical and cylindrical shell. The 1D thermal model developed was discretized using the Crank-Nicholson finite difference scheme and solved using the Thomas algorithm. The PCM used in the study was calcium chloride hexahydrate. They found that for same volume and surface area, the cylindrical shell took the least time to melt and this effect was prominent at increased mass of PCM.

Agyenim et al. (2010b) experimentally studied the effect of using multiple HTF tubes in the shell-and-tube LHS units containing erythritol as the PCM. They compared the storage performances of a single-tube LHS unit with a four-tube LHS unit. The multi-tube system showed superior performance than the single tube system aided with the distribution of heat in multiple layers around each tube of the system.

Allouche et al. (2015) experimentally studied the performance of a microencapsulated PCM slurry consisting of paraffin RT15 kept in a 100-liter storage tank. A tube-bundle heat exchanger was used for exchanging the heat between the HTF and PCM. When compared the results with the previously published results for other configurations, the tube-bundle storage tank configuration was found to perform better than a coil-in-tank configuration. They also mentioned that shell-and-tube type of heat exchanger has the additional advantage of

incorporating fins to the HTF tubes, which can significantly enhance the heat transfer. The same author group, Allouche et al. (2016) developed a 3D numerical model to study the heat transfer characteristics of the microencapsulated PCM slurry in a tube-bundle type heat exchanger. They validated the results of the numerical model with their experimental data and a close agreement was found between them.

Esapour et al. (2016) formulated a 2D numerical model to analyze the effect of the number of HTF tubes in an LHS system during the charging process. The PCM used in the model was RT35. They compared different cases with one, two, three and four HTF tubes in each configuration. However, the total surface area was made constant by having lesser diameter tubes in cases with more number of tubes. They reported that by increasing the number of HTF tubes, the bottom region of the shell is influenced by the additional heat transfer thereby reducing the total melting time by about 29% for the four tubes system.

Arrangement and orientation of HTF tubes and fins also have an impact on the performance of the LHS system. Symmetric configuration is generally recommended for better performance. Yazici et al. (2014a, 2014b) experimentally studied the effect of eccentric placing of HTF tube in a horizontal shell-and-tube LHS system during charging and discharging processes. The inner tube of the storage unit was lowered to create an eccentricity in the system. They found a decrease in charging time due to the enhancement of natural convection. However, the discharging time was considerably increased due to the increase in conduction resistance. Seddegh et al. (2016) compared the performances of horizontal and vertical shell-and-tube LHS systems. They concluded that the horizontal LHS system showed a better storage performance during the charging process and no notable difference was found between the two systems during the discharging process.

The direction of HTF flow during the charging and discharging processes also influences the performance of the LHS systems. Gong and Majumdar (1997) developed a 2D FEM based model to investigate the effects of two alternative operation modes, introducing the cold and hot fluid from the same and opposite ends of HTF tube. Numerical experiments showed that injecting the cold and hot fluid from the same end of the storage exchanger was more appropriate than introducing the cold and hot fluid from opposite ends of the storage unit.

2.5 Heat transfer augmentation techniques

Low thermal conductivity of PCMs leads to the poor heat transfer between the HTF and PCM. Hence, the design of a cost-effective LHS system requires the development of proper heat-transfer enhancement technique (Liu et al., 2012). Several works were reported on the effect of incorporating certain heat transfer enhancement techniques such as adding fins, graphite flakes, sprinkling high thermal conductivity micro/nano particles, etc (Jegadheeswaran and Pohekar, 2009; Fan and Khodadadi, 2011; Ibrahim et al., 2017). Some of the major contributions on the heat-transfer enhancement techniques are reviewed here.

2.5.1 Incorporation of fins

Sparrow et al. (1981) conducted several experiments on freezing of n-eicosane in a finned and unfinned vertical tube-in-tube cylindrical heat exchanger. Water was used as the HTF in the experiments and the finned module consists of four longitudinal fins. The top layer of the heat exchanger was covered with a plexiglass to capture the solidification profiles of the PCM. It was observed that the retardation rate of solidification was much higher in the case of unfinned system due to the high thermal conductive resistance. They observed that the solidification rate in the region, midway between the fins also was improved. They concluded that the usage of fins could triple the amount of PCM that freezes around the tube in their study.

Choi and Kim (1992) experimentally investigated the storage characteristics of magnesium chloride hexahydrate during the discharging process. Air was used as the HTF, which is allowed to pass through the inner tube of the setup. They conducted experiments in two different configurations, one without fins and the other with five circular fins. They compared the heat transfer coefficients of the finned and unfinned systems and found its ratio to be 3.5 for the geometry investigated.

Costa et al. (1998) developed a 1D theoretical model based on the enthalpy formulation and fully implicit finite difference method to predict the behaviour of a latent heat energy storage system containing n-octadecane as the PCM. They used the thermal model to compare the performances of a finned and an unfinned system. It was found that for the conduction mode of heat transfer, the presence of fins significantly increases the rate of heat transfer and hence

the melting of the PCM. They concluded that the usage of fins could alleviate the problem of low thermal conductivity of the PCM.

Castell et al. (2006) experimentally studied the influence of fins on the heat transfer phenomenon of PCM kept in a vertical tube-in-tube heat exchanger during the discharging process. The no fin configuration (case 1) was compared with finned modules with two different fin sizes, viz. 20 mm width (case 2) and 40 mm width (case 3). They observed a reduction of 23.5 % and 58.8 % in the solidification time for the case 2 and case 3 when compared with the case 1.

Mat et al. (2013) formulated a 2D thermal model with the FVM based enthalpy method using the Fluent software to evaluate the storage characteristics of RT82. The effect of natural convection during melting was included in the model. They compared the performances of a triplex tube LHS system with different configurations of fins, viz. external fin, internal fin and external – internal fin using the developed model. They concluded that there was no significant difference among the different fin configurations in terms of heat transfer enhancement, but when compared with LHS system without fins, the charging time with fin was decreased by 43.3 %.

Khalifa et al. (2014) developed a 2D numerical tool and an experimental setup to study the energy discharge characteristics of paraffin RT82 during solidification. The numerical tool was formulated based on the effective heat capacity method. The experimental setup comprised of axially finned and unfinned heat pipe based storage prototypes to compare the heat transfer performance of the bare and finned heat pipe. The results showed that the energy extracted by the finned heat pipe LHS system is 86 % more than the bare heat pipe LHS system. In addition, the effectiveness of the heat pipe was increased by about 24 % due to the incorporation of fins.

Tiari et al. (2015) formulated a 2D transient numerical model to analyze the charging performances of potassium nitrate kept in a finned heat pipe–assisted LHS system. They conducted several numerical experiments by varying the number of heat pipes (1, 3, 5) and fins (10, 20). They reported that increasing the number of heat pipes and fins increases the melting rate of the PCM. Still optimization of the LHS system was recommended as the performance improvement between the LHS systems with 3 and 5 heat pipes was minimal. They also

reported that the effect of natural convection was present in the finned cases also and it reduced the melting time by about 30 %.

Zhai et al. (2015) experimentally and numerically investigated the influence of fin in a shell-and-tube type cold LHS system containing a mixture of capric acid and lauric acid as the PCM. The LHS unit is a horizontal tube-in-tube type heat exchanger in which water flows through the inner tube during the cooling process. They used 4 annular and 4 longitudinal fins surrounding the HTF tube, which divide the shell region of the storage system into 20 smaller pockets of PCM. The results showed that the phase change time for the finned unit decreased by about 71.2 % when compared with the unit without fins.

2.5.2 Dispersion of porous materials

Fukai et al. (2003) experimentally studied the influence of the addition of carbon fibers to the PCM during charging and discharging processes. The volume fraction of carbon fibers used in the study was about 1 %. It was found that in the discharging process, the discharge rate using the carbon fibers is 30 % higher than that using no fibers. In the charging process, it was found that even though the carbon fibers prevent the natural convection, the charge rate was 10–20 % higher than that with no fiber.

Elgafy and Lafdi (2005) reported that the porosity of the graphite impregnated to the PCM plays a critical role in the storage effectiveness of the PCM. When using graphite having small pores, there might be a decrease in the latent heat of the PCM as the small pores hinder the molecular movement and it could be difficult to impregnate the porous medium with the PCM. Besides, increasing the pore size diminishes the capillary force, which results in the leakage of liquid PCM.

Wu and Zhao (2011) conducted an experimental investigation on the heat transfer enhancement of PCMs using metal foams and expanded graphite during the charging process. Sodium nitrate was used as the PCM and the heating is achieved through an electrically controlled infrared heater. Four different cases were analyzed during the experiments, viz. pure $NaNO_3$ (case 1), $NaNO_3$ with metal foam (case 2), $NaNO_3$ with expanded graphite (case 3) and $NaNO_3$ with metal foam and expanded graphite (case 4). It was observed that during the sensible heating of solid $NaNO_3$, the heat transfer rate was enhanced by a factor of 2.10, 1.90, 2.50 for the cases,

2, 3, 4, respectively, when compared with the case 1. However, after melting of the PCM, during the sensible heating of the liquid PCM, the heat transfer performance of the composite NaNO3 was inferior to that of the pure NaNO3. Moreover, the authors reported that the corrosion and mixing process of the PCM with the porous materials had some opposing impact for the use of metal foam and expanded graphite as a heat-transfer enhancement material.

Zhang P et al. (2015) carried out several experiments and developed a thermal model to study the heat transfer enhancement achieved due to the addition of metal foam to a PCM. A eutectic salt comprising sodium and potassium nitrate in the weight proportion of 50:50 was employed as the PCM. Two metal foams, copper and nickel foams were considered for heat transfer enhancement. The experiments were conducted at various heating and cooling temperatures to study the storage characteristics during charging and discharging processes. Due to the hindrance in the natural convection because of the porous structure of carbon/nickel foam, the reduction in the charging rate achieved was about 21.6 / 12.2 %, when compared with the pure eutectic salt. However, the reduction in the discharging rate accomplished with the carbon/nickel foam was 28.8 / 19.3 % as compared to the pure eutectic salt. This was due to the increase in the effective thermal conductivity of the system.

2.5.3 Sprinkling of high thermal conductivity nanoparticles

Khodadadi and Hosseinizadeh (2007) simulated the solidification of a nanofluid (formed by the dispersion of nano copper particles in water) kept in a square storage module. The movement of the solid/liquid interface during the phase change was observed for pure PCM and for PCM with different particle mass fractions. Although, the speed of the interface was initially not prominent due to the addition of particles, the effect was more pronounced after a certain period. This lead to a significant reduction in the solidification time. The authors also reported that the latent heat of PCM was decreased as the mass fraction of embedded particles was increased.

Dhaidan et al. (2013) conducted experiments to investigate the effect of the addition of CuO nanoparticles to n-octadecane on the melting rate. The have compared the temperature variation in four different cases, pure PCM and PCM with 1 / 3 / 5 % wt fraction of CuO. A major improvement in the heat transfer was only observed with the addition of 1 % of nanoparticles and not in the cases of 3 / 5 % addition of CuO. They reported that this retardation in the

improvement of heat transfer was due to the agglomeration/precipitation of nanoparticles and increase in dynamic viscosity of the liquid composite PCM, both decreases the natural convection heat transfer of the system.

Ho and Gao (2013) experimentally studied the melting process of n-octadecane mixed with Al_2O_3 nano particles kept in a differentially heated vertical enclosure. They discussed the effect of adding nanoparticles on the overall heat transfer phenomena. The results shown that increasing the fraction of the nanoparticles have a tendency to degrade the natural convection heat transfer in the molten region of the enclosure when compared with that of the base PCM.

Li et al. (2013) carried out several experiments to study the heat transfer and thermal performances of stearic acid with different volume fractions of multi-walled carbon nano tube (MWCNT) during charging and discharging processes. They witnessed that the presence of MWCNT improved the thermal conductivity effectively, but weakens the natural convection of the PCM in the liquid phase. In addition, it was observed that the discharge rate of the storage system only improved when the volume fraction of the MWCNT added was lower than 5 %.

Though the addition of high thermal conductivity nano particles increases the effective thermal conductivity of the storage material, majority of the metal particles have comparatively high densities, which lead to their settlement at the bottom surface of the storage vessel. This would reduce the heat transfer rate of the system. In addition, some metal particles are not compatible with certain group of PCMs (Fukai et al., 2000).

2.5.4 Comparison of various heat transfer enhancement techniques

Velraj et al. (1999) carried out a detailed study on improving the heat transfer during the solidification of PCM. Paraffin RT 58 was used as the PCM and three different heat-transfer enhancement techniques were compared, viz. longitudinal fins, steel lessing rings and bubble agitation. They suggested longitudinal fin for the tube configuration case for better solidification rate.

Agyenim et al. (2009) designed an LHS unit with a horizontal concentric tube heat exchanger, containing erythritol as the PCM. They compared the storage performances with two different fin configurations, circular and longitudinal during the charging and discharging processes. It

was observed that the temperature gradients in all the directions were found uniform in the longitudinal fin case than the circular fin case. They concluded that the LHS unit with the longitudinal fins showed the best heat transfer performance.

Darzi et al. (2016) formulated a 2D thermal model to compare the performances of LHS systems with certain heat-transfer enhancement techniques such as adding nanoparticles, attaching longitudinal fins on the inner tube and using elliptic shaped inner tube. They observed that there was a suppression in the natural convection heat transfer in the cases of nanoparticles and elliptic tube. They established that the best method to increase both the melting and solidification rate among the analyzed techniques is by adding longitudinal fins on the HTF tube.

2.6 Macro encapsulation of PCM

Dimaano and Watanabe (2003) developed a simplified 1D numerical model and conducted experiments to analyze the transient behavior of capric acid and lauric acid mixture during melting and solidification in a vertical cylindrical tube. They have validated the numerical results with the experimental results and a close agreement was found between them. Still, the developed model was able to predict only the radial temperature variations.

Regin et al. (2006) studied the critical parameters influencing the melting rate of paraffin wax employing numerical model and performing experiments. They found that the phase-change temperature range and the capsule diameter mainly govern the melting rate of the capsule. They also reported that the rate of increase in the melting time of capsules while increasing the capsule diameter is steadily increasing which limits the capsule diameter to a certain value in practical applications.

Steinmann and Eck (2006) studied various buffer storage options for direct steam generation solar power plant. Steam accumulators were found to be a viable option for buffer storage. However, the main demerit of the steam accumulators is that the steam generally experiences a drop in pressure while discharging the steam. They found that the integration of LHS system in the form of macro-encapsulated capsules allows an increase in the volumetric storage capacity of the steam accumulators and reduces the decline in pressure of the steam during the discharge.

Few studies reported on the usage of fins/metallic particles within the storage capsules/enclosures to improve the melting/solidification rate.

Koizumi (2004) carried out an experimental study to analyze the heat transfer phenomena during the unconstrained melting of n-octadecane contained within spherical capsules. The PCM was filled in glass spherical capsules, which have an outer diameter of 50 mm and a wall thickness of 1 mm. Three copper plates were kept within the spherical capsule to enhance the heat transfer rate. The study performed dealt with the opposing flow mixed convection, where the direction of the forced flow is opposite to that of the free flow. They found that the addition of copper plates and the opposing flow mixed convection together increases the heat transfer rate of the system.

Ettouney et al. (2006) conducted several experiments to study the heat transfer enhancement achieved by the inclusion of metal beads within the spherical capsules containing paraffin RT52 during charging and discharging processes. The diameter of the copper spherical capsule was about 3 cm. Stainless steel beads of three different diameters (4, 5 and 6 mm) are used for improving the melting and solidification rate. The volume ratio of the beads inside the capsule were between 0.5 – 20 %. It was found that the melting and solidification rates were increased by only 15 %. This is due to the reduction in the natural convection heat transfer.

Siva et al. (2010) developed a numerical model to evaluate the storage characteristics of formic encapsulated in internally finned spherical and cylindrical capsules. It was observed the reduction in the melting/solidification time achieved by the empty cylinder capsule when compared with the empty spherical capsule was 47 / 67 %. They also reported a 60-70 % improvement in the melting/solidification rate using the finned capsules when compared with unfinned capsules.

Soares et al. (2015) experimentally studied the heat transfer phenomenon of paraffin wax placed in a vertical stack of rectangular cavities during the charging and discharging processes. The separation surface between the cavities acts as a form of longitudinal fins to improve the heat transfer in the PCMs. They observed that the heat transfer rate was improved due to the fins and the thermal regulation was proper and evenly distributed as the PCM was separated by the cavity layers.

Fan et al. (2016) tested the heat transfer performance of n-octadecane kept in a circumferentially finned spherical enclosure. The periphery of the spherical capsule is given a constant temperature heat flux through the water bath. They observed a decrease of 30 % in the melting time when compared with the unfinned spherical enclosure. They also reported that the excess volume occupied by the external fin arrangement could hardly allow the approach to apply in a larger scale with many capsules.

2.7 Literature closure

From the literature survey, the following conclusions are made.

- Several researchers developed numerous thermal models for studying the charging / discharging characteristics of LHS systems. Nevertheless, majority of the developed models are based on simple heat exchanger configurations such as rectangular, spherical and shell-and-tube with a single HTF tube. Very few models are developed on the multi-tube based shell-and-tube based configuration.

- Allouche et al. (2016) developed a 3D thermal model to study the heat transfer characteristics of tube-in-tube bundle type heat exchanger. However, they have not optimized the number of tubes and incorporated any heat-transfer enhancement techniques. Other than this work, majority of the numerical analyses reported are confined to only 1-D and 2-D modeling.

- Many researchers recommended the inclusion of natural convection in the mathematical modeling of phase change process. Nevertheless, the consideration of natural convection during melting and solidification in a 3D shell-and-tube model demands higher computational facilities, because of which there is a lack of numerical studies on LHS systems with natural convection.

- Most of the heat-transfer enhancement techniques such as inclusion of fins, nanoparticles, metallic beads, etc. are numerically modeled in basic LHS systems such as shell-and-tube configuration with a single HTF tube and a spherical capsule.

- The reported works are mainly focused on the improvement of the heat transfer characteristics of the LHS systems during melting and solidification. However, a detailed optimization study of the entire storage module including the optimization of the number of tubes and fins is not reported so far.

- Majority of the experimental studies are conducted to study the storage / discharge characteristics of low temperature PCMs. There is a lack of studies undertaken with medium and high temperature PCMs, which have more potential usage in solar thermal power plants.

- Many researchers experimentally investigated the charging and discharging performances of LHS systems employing basic heat exchanger configuration only. However, the storage capacity of the industrial-scale LHS systems in solar thermal power plants is usually in the order of GJ, which needs bulky shell-and-tube heat exchangers with multiple HTF tubes.

In the view of the above closure of literature review, the following aspects are considered in the Ph.D. thesis work.

- To study the charging and discharging characteristics of the lab-scale LHS prototype by considering the natural convection.

- To develop a 2D mathematical model to optimize the number of tubes and fins of the lab-scale shell-and-tube LHS prototype.

- To develop a 3D mathematical model for predicting the charging and discharging characteristics of the LHS prototype with optimized configuration at different operating conditions.

- To design and develop LHS prototype of 10 MJ capacity

- To test the performances of charging and discharging processes of the lab-scale LHS prototype at various operating conditions.

- Validation of the numerical results with the experimental data.

Additionally, two more minor aspects are also included in this thesis, which the author conceptualized during the course of research work.

- Development of a novel encapsulation technique to upscale the LHS capacity in steam accumulators.

- Development of a novel type of fin and comparison of the storage performance with basic fin configuration.

2.8 Summary

In this chapter, a detailed literature survey on the various mathematical models and experimental investigations of the LHS systems and influence of natural convection during phase change are presented. Several heat-transfer enhancement techniques implemented in the LHS systems are reviewed. The closure of literature survey is reported clearly. Finally, the core and minor objectives of the Ph.D. thesis work are framed and presented in sequence.

Chapter 3

Lab scale Prototype – Numerical Studies

3.1 Preface

Design and optimization of LHS prototypes require an exhaustive analysis of the heat transfer characteristics, between the PCM and HTF. The number of the HTF tubes and fins on the HTF tube's outer surface play a significant role in transferring the heat between them. Un-optimized prototype with more number of the HTF tubes and fins would lead to higher material inventory. Additionally, the overall weight of the system will increase too. Hence, a detailed optimization study is needed to have a cost-effective LHS system. To achieve this, many experiments with different geometric configurations, by varying the number of the HTF tubes and fins, need to be conducted. This approach has two major disadvantages; (i) the development cost of the different prototypes to be tested is high and (ii) for up scaling, new prototypes need to be developed for getting the optimized module.

Development of a numerical tool for the optimization of geometric configuration and performance evaluation of LHS prototype is an ideal solution to overcome the above limitations. But the mathematical modeling of the LHS prototypes, especially in the multidimensional case is complex (Bonacina et al., 1973). The major problems involved in the modeling are (i) inclusion of latent heat of PCM, (ii) natural convection of the melt and (iii) conjugate heat transfer between the PCM and HTF.

This chapter presents a 3D transient numerical model, which is developed using the EHC method to study the performance characteristics of a shell-and-tube type lab-scale LHS

prototype of 10 MJ LHS capacity. Longitudinal fins adopted for heat transfer enhancement in the experimental studies are also included in the numerical model. Optimization of the number of tubes and fins for the LHS system is performed using a 2D transient model, the output (the number of tubes and fins) of which is used in the 3D model.

A eutectic ternary mixture comprising of potassium nitrate, sodium nitrate and sodium nitrite in the weight proportion of 53:7:40, which has the melting point of approximately 142 °C is selected as the PCM for the numerical simulation. Hi–Tech Therm 60, a synthetic thermic oil is selected as the HTF. The thermo-physical properties of the selected PCM and HTF are given in Tables 3.1 and 3.2. Various performance parameters such as melt fraction, charging/discharging time, and energy storage/discharge rate are evaluated at different operating conditions. The axial and angular temperature variations of PCM during charging and discharging are also studied. These numerical results will be useful in designing the efficient industrial scale LHS systems. Although, the developed numerical model is applied to the shell-and-tube type configuration in this chapter, it can be easily extended to other configurations such as U-tube heat exchanger or encapsulated LHS capsules (discussed in Chapter 5), if the domains of different materials and boundary conditions are properly defined.

Table. 3.1 Thermo-physical properties of the PCM (Bohlmann, 1972).

Properties	**Values**
Latent heat of fusion (kJ kg^{-1})	81.5
Melting point (°C)	142
Thermal conductivity (W m^{-1} K^{-1})	0.571
Density (kg m^{-3})	
Solid (122 °C)	1996
Liquid (162 °C)	1956
Specific heat (J kg^{-1} K^{-1})	
Solid	1340
Liquid	1562
Dynamic viscosity (Pa s)	0.02
Thermal expansion coefficient (K^{-1})	3.629×10^{-4}

Table. 3.2 Thermo-physical properties of Hi–Tech Therm 60 at different temperatures.

T	ρ	C_p	k	γ	μ
°C	kg m^{-3}	J kg^{-1} K^{-1}	W m^{-1} K^{-1}	mm^2 s^{-1}	Pa s
40	860	2081.8	0.1314	20.00	0.017200
100	823	2306.2	0.1238	3.82	0.003144
150	790	2493.2	0.1175	1.75	0.001383
200	755	2680.2	0.1119	0.90	0.000680

3.2 Design of the LHS prototype

The prototype is designed for an LHS capacity of about 10 MJ. The volume (V) of PCM required depends on the heat storage capacity (Q), density (ρ) and latent heat of fusion (L_F). For storing a heat of 10 MJ, the PCM volume required is calculated using Eq. (3.1). Based on the volume found, the inner diameter of the shell (D) is calculated using Eq. (3.2). The outer diameter (d) and thickness of HTF tubes are 12.7 mm and 2 mm. The height (h) and thickness (b) of the longitudinal fins attached to the tubes are 10 mm and 1 mm. The number of HTF tubes and fins were optimized based on the discharging time. The optimization details are given in the sub-section 3.10.1. The number of HTF tubes (N_T) and fins (N_F) on each tube in the optimized LHS prototype are 25 and 4. The HTF tubes and fins are made of copper. The outer shell of the prototype is made of stainless steel (SS304) of diameter 335 mm OD and 5 mm thickness.

$$Q = \rho V L_F \tag{3.1}$$

$$V = \left[\frac{\pi}{4}(D^2 - N_T d^2) - N_T N_F b h\right] L \tag{3.2}$$

3.3 Model description

Fig. 3.1 shows the sectional view of the 3D shell-and-tube type LHS model containing a PCM in the shell region and HTF in the tube region, both separated by an HTF tube. The LHS unit is a regenerative type heat exchanger, which absorbs/releases heat by passing the hot/cold HTF, respectively through the HTF tubes.

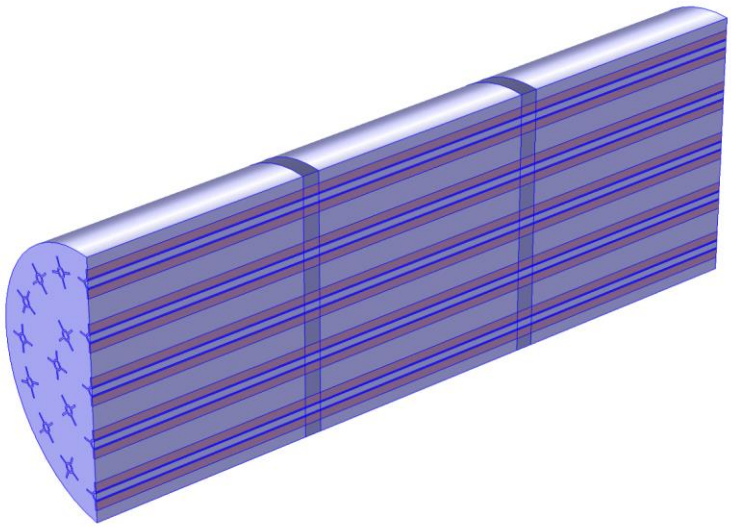

Fig. 3.1 Computational model of the LHS prototype

During the charging cycle, high-temperature HTF is supplied from one side of the model to exchange the heat through convection to the HTF tube, and this heat is further conducted to the PCM. During the discharging cycle, cold HTF is passed from the same side, which extracts the stored heat from the PCM. The LHS unit is divided into three cartridges, separated by a thin layer of concrete. The outer surface of the LHS model is given adiabatic condition to mimic the insulation provided in the experimental setup.

3.4 Assumptions

To study the thermal storage behavior of a shell-and-tube type LHS prototype, four physical processes have to be simulated i.e. HTF flow, conduction, convection, and phase change. The thermal model is developed based on following assumptions:

- HTF is incompressible and Newtonian.
- HTF flow is laminar and exhibits negligible viscous dissipation.
- The initial temperature of PCM is uniform.
- Phase change during melting/solidification occurs in a temperature interval.
- Thermal losses through the outer wall of the PCM are negligible.
- PCM is homogeneous and isotropic.

3.5 Governing equations

The model developed is based on a conjugate heat transfer problem, which simultaneously solves the flow behavior of HTF and phase change behavior of PCM. The biggest problem associated with adapting an existing sensible heat based model for an LHS model is the incorporation of latent heat required to melt/solidify the PCM. This issue is solved by using the EHC method, which includes both specific heat and latent heat of the PCM in a single term called EHC. The EHC method was first developed by Bonacina et al. (1973) and later used by several authors (Morgan et al., 1978; Kuravi et al., 2009; Yang and He, 2010; Ogoh and Groulx, 2012) with slight improvements. The heat capacity of the PCM is modified as shown in Eq. (3.3) and the EHC is calculated using Eq. (3.4).

$$C_P = \begin{cases} C_{P,S} \; for \; T < T_S \\ C_{P,EFF} \quad for \; T_S \le T \le T_L \\ C_{P,L} \; for \; T > T_L \end{cases} \tag{3.3}$$

$$C_{P,EFF} = \frac{C_{P,S} + C_{P,L}}{2} + \frac{L_F}{T_L - T_S} \tag{3.4}$$

Phase change is considered to occur during a temperature interval. Problems of this type are often referred to as mushy region problems. The discontinuous modified heat capacity is implemented in the COMSOL Multiphysics software using a smoothed Heaviside function with a continuous second derivative. Accordingly, continuity, momentum, and energy equations are given in Eq. (3.5–3.7). The effect of convection heat transfer is taken care by the material derivative term DT/Dt in Eq. (3.7).

$$\nabla . \vec{v} = 0 \tag{3.5}$$

$$\frac{\partial \vec{v}}{\partial t} + (\vec{v} . \nabla)\vec{v} = \frac{1}{\rho}\left(-\nabla P + \mu \nabla^2 \vec{v} + \vec{F} + \vec{S} \right) \tag{3.6}$$

$$\rho C_P \frac{DT}{Dt} = k \nabla^2 T \tag{3.7}$$

To include the effect of buoyancy and reduce the complexity in solving the Navier-Stokes equations, Boussinesq approximation (Shenoy and Mashelkar, 1978; Yao and Cherney, 1981; Rieger et al., 1982) is added to the momentum equation, which is given by Eq. (3.8). To nullify the velocities in the solid region of the PCM, Darcy law's source term (Voller and Prakash, 1987; Brent et al., 1988) is added to the momentum equation, which is given by Eq. (3.9).

$$\vec{F} = \rho \vec{g} \beta (T - T_M) \tag{3.8}$$

$$\vec{S} = \frac{(1-\theta)^2}{(\theta^3 + \varepsilon)} A_{MUSH} \vec{v} \tag{3.9}$$

$$\theta = \frac{T - T_S}{T_L - T_S} = \frac{T - T_M + \Delta T_M}{2\ \Delta T_M} = \begin{cases} 0 \ \ for\ T < T_S \\ 0-1 \ \ for\ T_S \le T \le T_L \\ 1 \ \ for\ T > T_L \end{cases} \tag{3.10}$$

The mushy zone constant defines the transition of velocity in the mushy region. Mushy zone constant values between 10^3 and 10^7 are recommended for most computations. For higher values of mushy zone constant, the damping curve becomes steeper, and the velocity drops to zero faster as the material solidifies. Very large values of mushy zone constant may cause the solution to fluctuate as elements interchangeably melt and solidify with minor perturbations in liquid volume fraction. Here, a value of 10^4 is taken based on the works presented by Kheirabadi and Groulx (2015) on the effect of mushy zone constant.

During charging cycle, the Darcy law's source term dominates all other terms in the momentum equations and forces the predicted velocities to near zero before melting of the PCM. Once a molten layer of the PCM is formed, the melt fraction of the PCM increases and hence the source term decreases. After complete melting of the PCM, the melt fraction becomes unity, and therefore the source term becomes zero. The momentum equations then behave normally in terms of actual fluid velocities. Similarly, during the discharging cycle, where the local melt fraction assumes a value of 1 initially, the source term is zero and the momentum equations are in terms of actual fluid velocities. Once the solidification of PCM is started, the source term increases and approximates the Darcy law in the mushy region. Finally, the Darcy law's source term dominates all other terms in momentum equations and forces the predicted velocities to near zero at the end of the discharging cycle.

3.6 Performance parameters

The major performance parameters to evaluate the storage characteristics of the LHS systems are melt fraction, charging/discharging time and energy storage/discharge rate. These parameters are explained in this section.

3.6.1 Melt fraction

Most of the PCMs, especially a mixture of salts, often melt over a finite temperature range. The temperature range wherein, the melt exists in both solid and liquid phases is generally called mushy zone. The highest temperature at which, the material is completely in the solid state is called solidus temperature and the lowest temperature at which, the material is completely in the liquid state is called liquidus temperature. Melt fraction is a non-dimensional parameter, which quantifies the percentage of liquid phase in the mushy region. Melt fraction of the PCM can be calculated based on the lever rule applied between the solidus and liquidus temperatures and it is given by Eq. (3.10).

3.6.2 Charging time

Charging time of LHS prototype is defined with respect to the temperature rise of PCM. The LHS prototype is said to be fully charged when the entire PCM is melted i.e. when the melt fraction reaches a value of unity. The LHS prototype should be designed and optimized in such a way that, it possess a lesser charging time.

3.6.3 Discharging time

Discharging time of LHS prototype is defined with respect to the temperature decrease of PCM. The LHS prototype is said to be fully discharged when the entire PCM is solidified i.e. when the melt fraction reaches a value of zero. The design and configuration of the LHS prototype has a great impact on the discharging time and hence the system should be carefully designed to alleviate performance issues.

3.6.4 Energy stored

Energy gets stored in the PCM in two forms during charging, *viz*. sensible and latent heat. Initially, when the PCM is in the solid state, the rate of SHS would be greater than the rate of LHS due to the higher temperature difference between the initial temperature and solidus temperature of the PCM. Once the PCM starts melting, the rate of LHS would become greater. Sensible, latent and total heat stored in the PCM during the charging process can be calculated using the Eq. (3.11) – (3.13), respectively.

$$E_{S,C} = m\left[C_{ps}\left(T - T_m\right) + C_{pl}\left(T_m - T_{ini}\right)\right] \quad (3.11)$$

$$E_{L,C} = m L_F \theta \quad (3.12)$$

$$E_{T,C} = m\left[C_{ps}\left(T - T_m\right) + L_F \theta + C_{pl}\left(T_m - T_{ini}\right)\right] \quad (3.13)$$

3.6.5 Energy discharged

Similar to the charging phenomenon, energy in the forms of sensible and latent heat is discharged from the PCM during the discharging process. Sensible, latent and total heat discharged from the PCM during the discharging process can be calculated using the Eq. (3.14) – (3.16) respectively.

$$E_{S,D} = m\left[C_{ps}\left(T_{ini} - T_m\right) + C_{pl}\left(T_m - T\right)\right] \quad (3.14)$$

$$E_{L,D} = m L_F (1 - \theta) \quad (3.15)$$

$$E_{T,D} = m\left[C_{ps}\left(T_{ini} - T_m\right) + L_F (1 - \theta) + C_{pl}\left(T_m - T\right)\right] \quad (3.16)$$

3.7 Initial and boundary conditions

Initially (t = 0), HTF domain is given zero velocity (no flow condition), and all the domains (PCM, HTF, and HTF tube) are given a constant lower/higher temperature of $T_{initial}$ during charging/discharging process. At any time (t > 0), the inlet of HTF tubes is specified a constant higher/lower temperature of T_{inlet} and a constant fluid velocity during charging/discharging processes. All the outer surfaces are given adiabatic condition to avoid heat loss to the ambient. To account for zero velocity on the HTF tube walls, no-slip boundary condition was used. To incorporate negligible temperature gradients in the normal direction near the HTF outlet, outflow boundary condition was used.

3.8 Mesh generation

Free tetrahedral and triangular meshes are used for meshing the domains and boundaries. Care has been taken to assure that relatively smaller sections (HTF tubes and fins) are discretized with a sufficient number of elements. Special meshing features of COMSOL Multiphysics such as boundary layers, corner refinement and distribution are used to have a finer mesh near the critical zones of the LHS model, viz. HTF inlet/outlet conditions, HTF boundary layer, and

thermal boundary conditions. Fig. 3.2 shows the meshed view of the LHS model. A grid independence test is also conducted for the developed model and the details are presented in the sub-section 3.10.3.

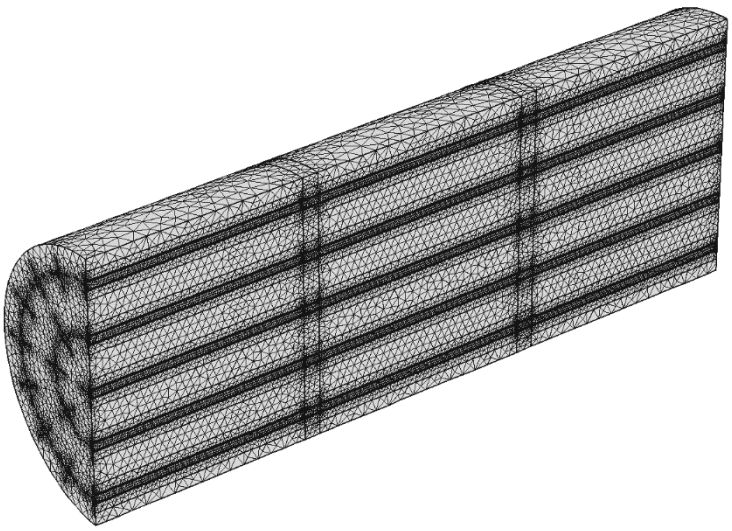

Fig. 3.2 Meshed model of the LHS prototype.

3.9 Numerical treatment

The governing equations described above were solved using the finite element based software product, COMSOL Multiphysics 4.3a. The primary finite element discretization method in COMSOL Multiphysics is the Galerkin method. The EHC method made the system of equations to be solved nonlinear. A time-dependent solver, PARDISO (Schenk and Gartner, 2004) was used to solve the equations. The time stepping was done based on the backward differentiation formula (BDF) for both charging and discharging simulations. In BDF, there is an initial minimum time step and a maximum time step. The time stepping is dynamic and it varies based on the error value of the previous iteration. In the current simulation, the initial minimum time step is set to 0.01 s and the maximum time step is not set. The motive of not setting the maximum time step is to automatically maximize the time step, to solve the problem in the least possible run time. Due to the highly nonlinear nature of the problem, the solution of the numerical model diverges for the convergence criterion of any value smaller than 10^{-3}. Hence, the convergence criterion for temperature and velocities is set to 10^{-3}. As the problem is symmetric on the y-axis, half of the physical LHS prototype was considered as the computational domain. Simulations were carried out using a Dell Precision T7610 workstation, equipped with two Intel Xeon E5-2650 v2 processors and 64 GB 1866 MHz RAM.

3.10 Results and discussions

In the following sub-sections, optimization of the LHS prototype, validation, grid independent test and various results obtained from the numerical simulations of the lab-scale LHS prototype during charging and discharging processes are presented.

3.10.1 Optimization

The major constraint of PCMs is its lower thermal conductivity, which necessitates the implementation of heat-transfer enhancement techniques such as finned tubes. Increasing the number of tubes and fins on the tubes outer surface increases the overall heat-transfer surface area of the system. To optimize the number of tubes and fins in the LHS prototype, a 2D thermal model is developed based on the governing equations, Eq. (3.5 – 3.7) to compare the performances of the selected systems, *viz*. models with 19, 22, 25 and 28 tubes and 25 tubes model with 0, 2, 4 and 6 fins. To maintain the same PCM volume in the various models, the shell diameter is kept different in the models. The shell diameter values of various models are given in Tables 3.3 and 3.4. Figs. 3.3 and 3.4 show the various models considered for optimization. The optimization is done based on the discharging time, as discharging is a comparatively slower process than charging. The discharging time of different configurations is given in Tables 3.3 and 3.4. It can be seen from Tab. 3.3 that the there is a vast reduction in the discharging time of LHS prototype (19.8 %) with 22 tubes when compared to 19 tubes and 25 tubes when compared to 22 tubes (14.3 %). However, there was only a marginal reduction in the discharging time of LHS prototype with 28 tubes when compared to 25 tubes (8.3 %). Similarly, it can be seen from Tab. 3.4 that there is a vast reduction in the discharging time of LHS prototype (29.4 %) with 2 fins when compared to 0 fins and 4 fins when compared to 2 fins (21.3 %). However, there was only a marginal reduction in the discharging time of LHS prototype with 6 fins when compared to 4 fins (9.0 %). Hence, shell-and-tube type heat exchanger with 25 tubes and 4 fins attached to each tube is found to be the optimized configuration for the current heat storage/discharge requirement.

Table. 3.3 Optimization of tubes.

No of tubes	Shell diameter (mm)	Charging time (min)	% reduction in time	Discharging time (min)	% reduction in time
19	318.9	184		262	
22	319.6	166	9.8	210	19.8
25	320.4	151	9.0	180	14.3
28	321.1	138	8.6	165	8.3

Table. 3.4 Optimization of fins.

No of fins	Shell diameter (mm)	Charging time (min)	% reduction in time	Discharging time (min)	% reduction in time
0	320.4	151		180	
2	322.3	117	22.5	127	29.4
4	324.3	93	20.5	100	21.3
6	326.3	78	16.1	91	9.0

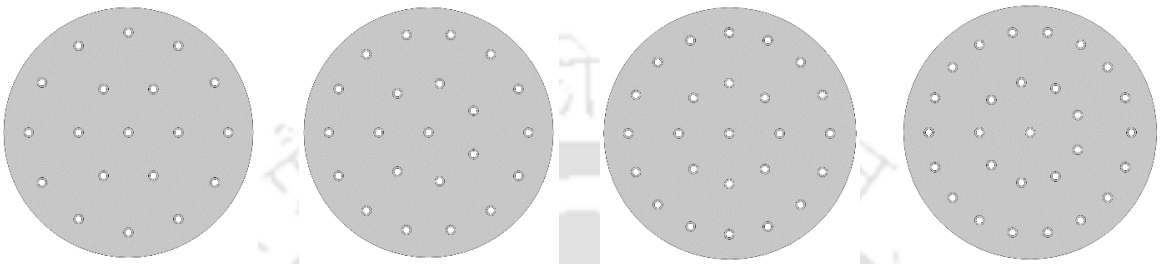

Fig. 3.3 Optimization of tubes (a) 19 tubes, (b) 22 tubes, (c) 25 tubes and (d) 28 tubes.

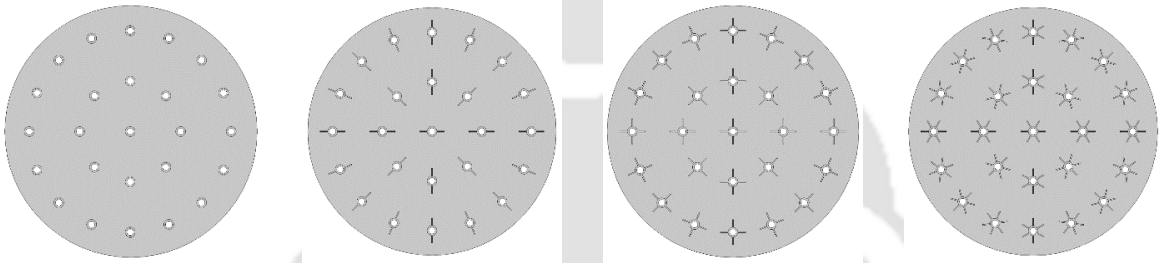

Fig. 3.4 Optimization of fins (a) no fins, (b) 2 fins, (c) 4 fins and (d) 6 fins.

3.10.2 Model validation

For any numerical model developed, validation with the real – time experimental data is vital for the practical applicability and further improvement of the model. To validate the developed numerical model for the charging and discharging process, the results obtained for the temperature variation of the PCM at 2 locations in the LHS prototype, viz. middle of 1st and 3rd cartridges [B (-141 mm, 30 mm)] were compared with the corresponding temperature values of the experiments. The thermocouple position selected for validation is point B, which is shown in Fig. 3.5(a). The PCM is initially at 122 / 162 °C during the charging/discharging process. At any time t > 0, the inlet of the tubes is given an HTF flow of 0.3 m^3/hr and inlet temperature of 162 / 122 °C during the charging/discharging process. Fig. 3.5(b) and (c) illustrates the comparison between the experimental and numerical values for the charging and discharging processes. It can be noted from Fig. 3.5(b) and (c) that there is a close agreement between the experimental and numerical data. The maximum deviation is about 3.36 °C and 2.74 °C during the charging and discharging processes, respectively.

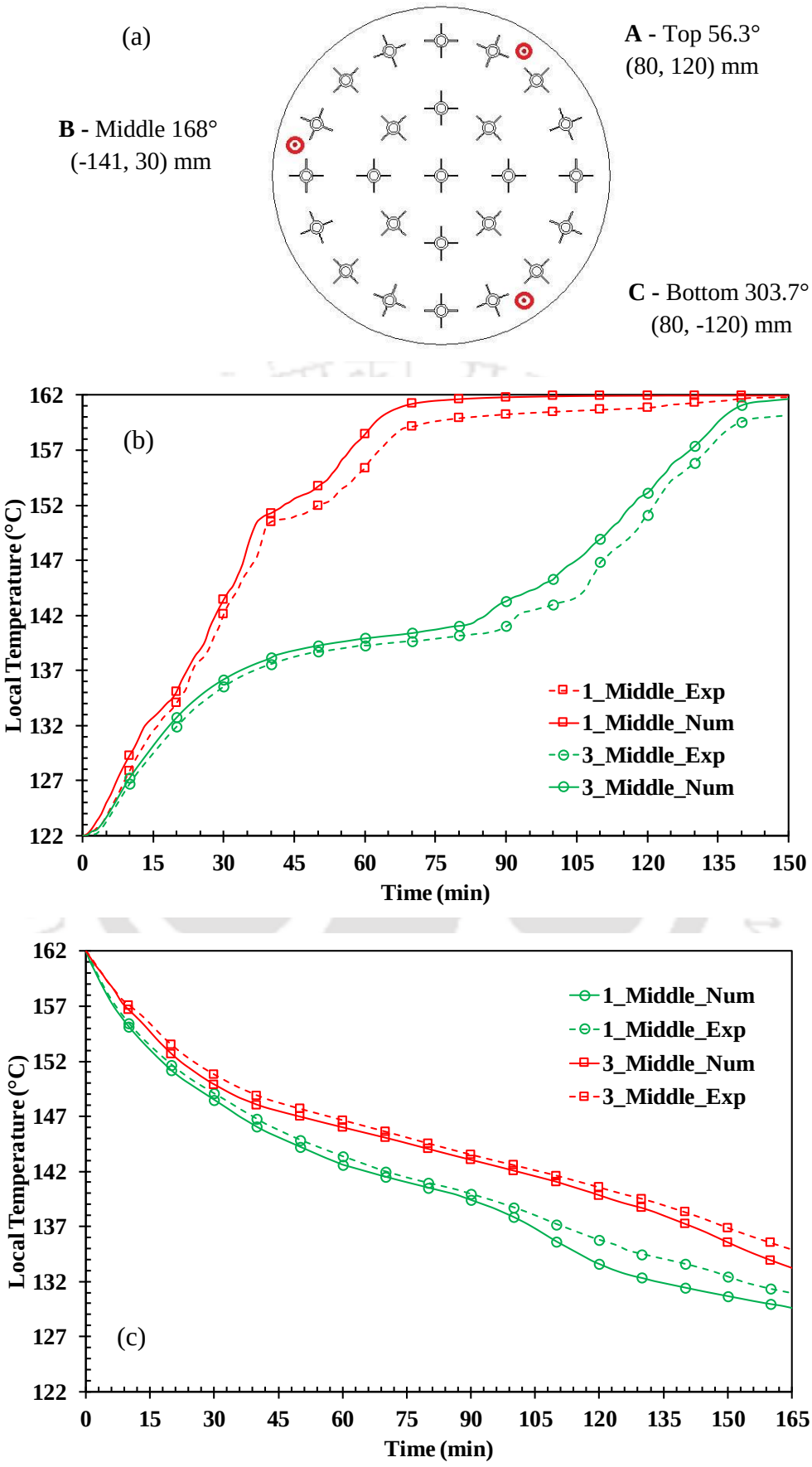

Fig. 3.5 Model validation (a) thermocouple position, (b) charging and (c) discharging.

3.10.3 Grid independent test

The variation of mesh element sizes has a major control in the numerical results of all models. To test the dependency of numerical results on the mesh element size, simulations with different mesh element sizes were run for charging and discharging processes. Fig. 3.6(a) and (b) shows the average temperature variation of the LHS prototype with a different number of mesh elements *viz*. 786342, 890548 and 995643 elements for charging process and 743148, 842412 and 944674 for discharging processes. Convergence issues were found for the developed model with mesh elements lesser than 786342 and 743148 for charging and discharging processes. It can be observed from Fig. 3.6(a) and (b) that the charging/melting simulation demands more number of mesh elements, due to the free convective movement of the PCM. For all the cases of grid independent test, the PCM is initially at 122 / 162 °C during charging/discharging process. At any time t > 0, the inlet of the tubes is given an HTF flow of 0.3 m^3/hr and inlet temperature of 162 / 122 °C during charging/discharging process. It is observed from Fig. 3.6(a) and (b) that the models with 890548 and 842412 elements are found to be grid independent for charging and discharging processes.

3.10.4 Temperature variation

Fig. 3.7(a) and (b) depicts the average temperature variation of the LHS prototype during the charging and discharging processes. The average temperature is the volumetric average temperature of all the mesh elements of the numerical model. Initially, the LHS prototype is at 122 / 162 °C during the charging/discharging process. When the HTF at 162 / 122 °C is passed through the HTF tubes, heat transfer takes place between the HTF and PCM. It can be noted from Fig. 8(a) and 8(b) that the initial part of the average temperature variation curve shows a steady increase/decrease of temperature during charging/discharging process. This steady increase/decrease is due to the higher heat transfer potential available during the initial period of the processes. After 30 min, the slope of the temperature variation curve started reducing. During this time, LHS prototype stores/discharges a large amount of latent heat. The PCM average temperature reaches approximately about 161 / 132.3 °C in 150 / 165 min during the charging/discharging process. The PCM temperature increase during charging is faster than the PCM temperature decrease during discharging. This is mainly due to the additional convective heat transfer that increases the overall heat transfer rate of the prototype during the charging process.

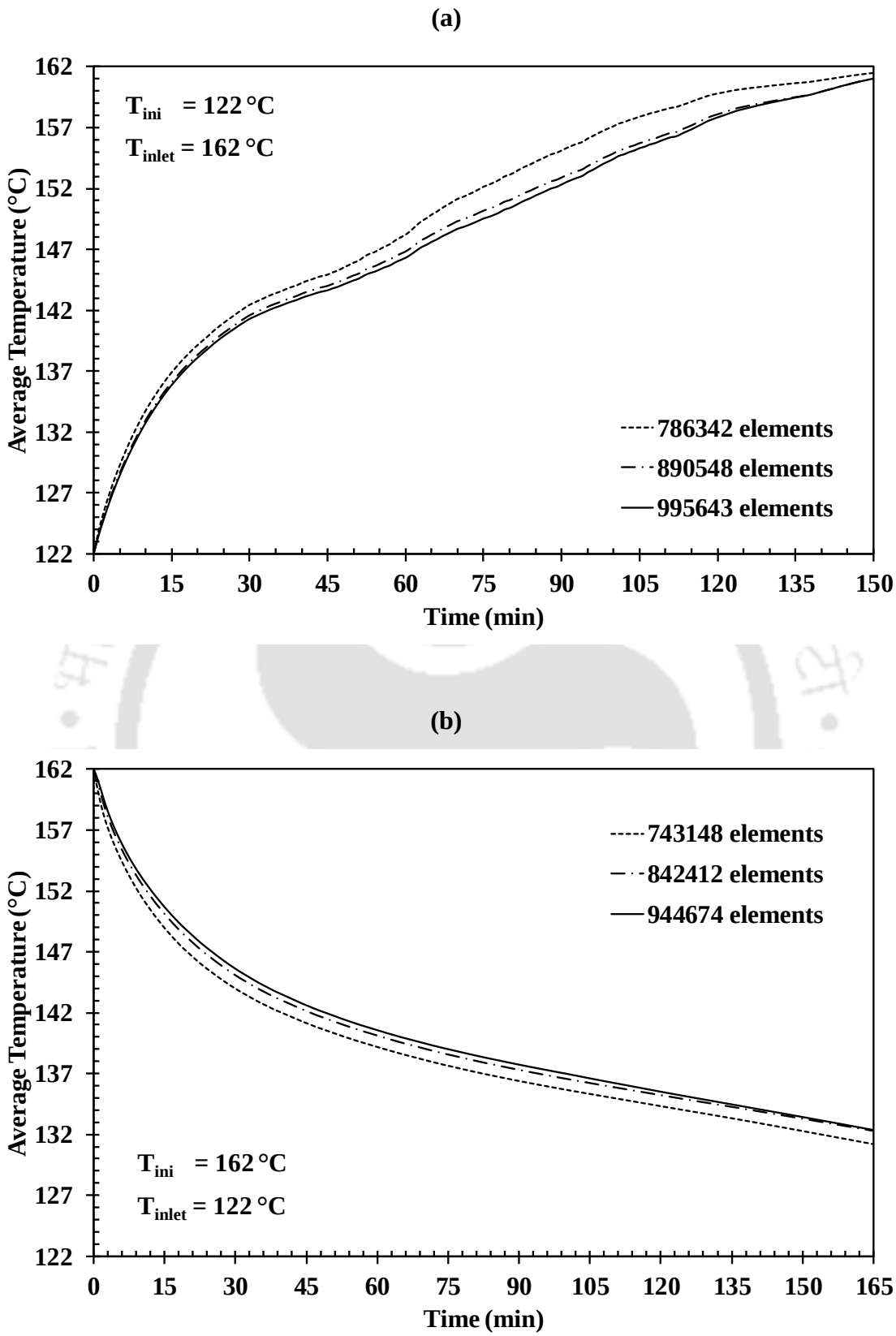

Fig. 3.6 Grid independent test of the shell-and-tube model (a) charging and (b) discharging.

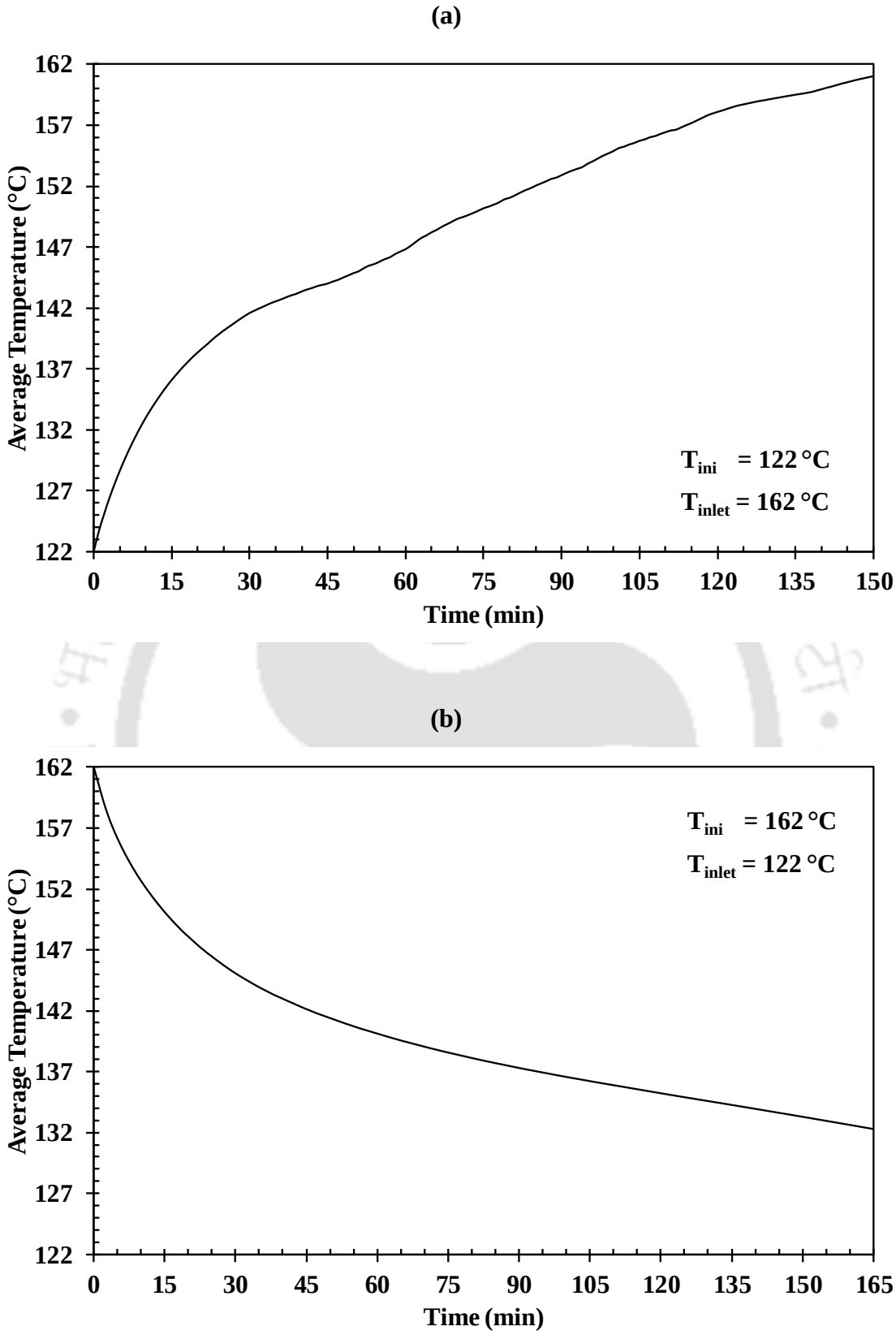

Fig. 3.7 Average temperature variation of the shell-and-tube LHS model (a) charging and (b) discharging.

3.10.5 Charging / discharging time

Fig. 3.8(a) and (b) shows the average melt fraction variations of the LHS prototype during the charging and discharging processes. Average melt fraction is the volumetric average melt fraction of all the mesh elements of the numerical model. Melt fraction is a critical performance parameter, which depicts only the latent heat storage/discharge characteristics during the charging/discharging process. It can be seen from Fig. 3.8(a) and (b) that the trend of increase/decrease of average melt fraction during charging/discharging process is initially faster due to the higher heat transfer potential and slower after a certain period due to the lower heat transfer potential between the HTF and PCM. It took about 137 / 158 min for the LHS prototype to get completely charged/discharged. The major advantage of the numerical model is the availability of data for each and every mesh element of the model. With this data, some critical decisions can be made which would be useful in planning the real-time experiments in an efficient manner. Table. 3.5 gives the charging/discharging time of partial and full heat storage/discharge. It can be understood from Table. 3.5 that, the partial charging/discharging is much efficient than the full charging/discharging process. It took only 73 % of the complete charging time for 90 % of heat storage. Similarly, it took only 70 % of the complete discharging time for 90 % of heat discharge. However, the charging/discharging time of the LHS prototype with respect to the thermocouple locations of the prototype in the experimental setup is 111 / 117 min.

Table. 3.5 Charging/discharging time for part/full storage/discharge of heat.

% of molten/solidified PCM	Charging time (min)	Discharging time (min)
50	41	45
75	74	79
90	100	110
100	137	158

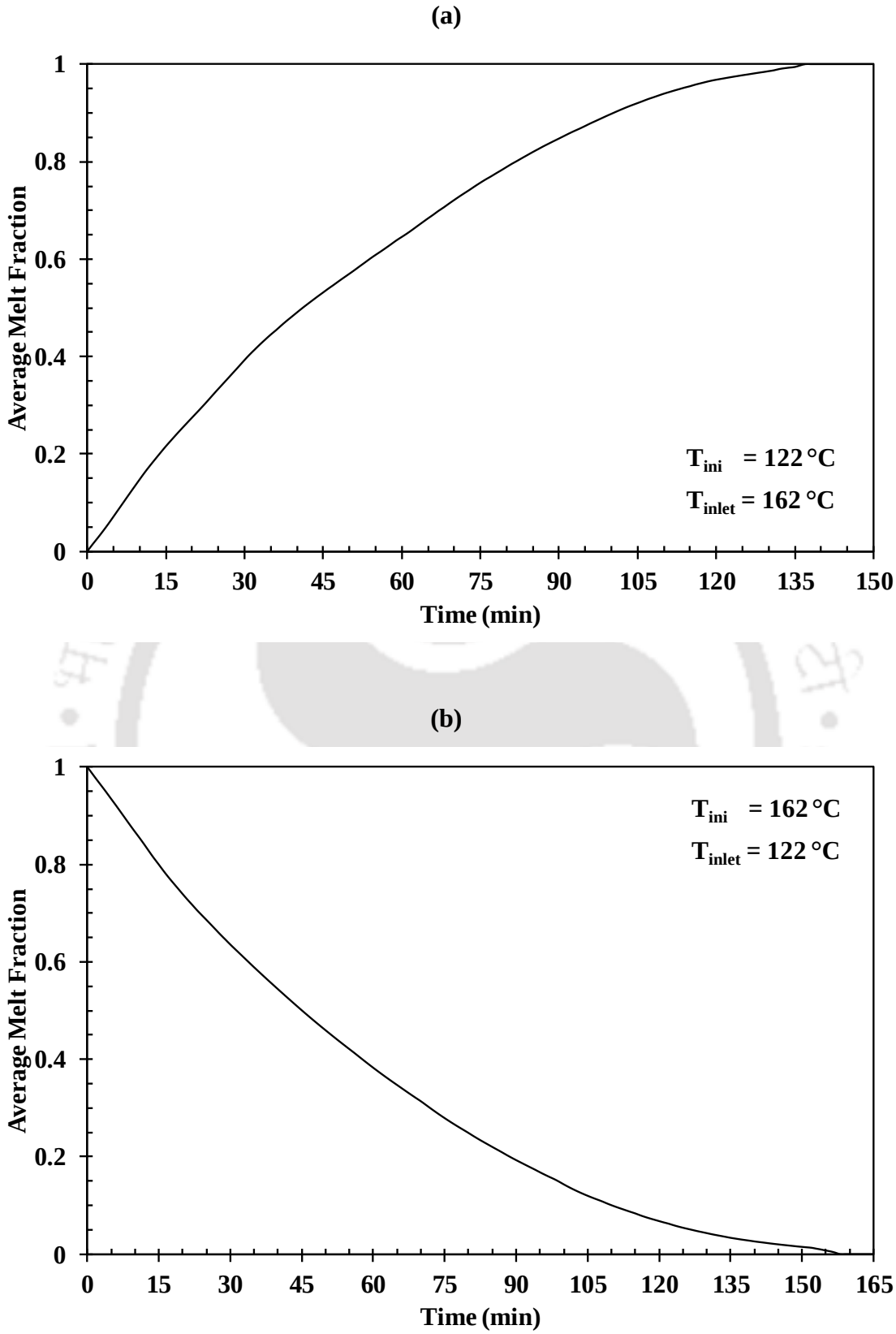

Fig. 3.8 Average melt fraction variation of the shell-and-tube LHS model (a) charging and (b) discharging.

3.10.6 Melt fraction

Fig. 3.9(a) and (b) depicts the average melt fraction contours of the LHS prototype during the charging and discharging processes. It can be seen from Fig. 3.9(a) and (b) that the average melt fraction of the LHS prototype is 0 / 1 at the start of the charging/discharging processes (t = 0 min). At time t = 50 min, it can be noted that the 1st cartridge is almost fully charged during the charging process. However, during the discharging process at the same time, the 1st cartridge is discharged to a limited extent only and not fully as in the case of charging. Hence, the charging process is faster than the discharging process. This is mainly due to the additional natural convection heat transfer present in the charging process. The effect of natural convection can be clearly seen in the LHS prototype during charging process (t = 50 min, 100 min) from the asymmetric variation of the melt fraction. Similar melt fraction variation is not noticeable in the discharging process as it is a conduction-dominated process. The axial melt fraction variation can be seen during both charging and discharging processes (t = 100 min), which is mainly due to the higher heat transfer potential availability at the entrance than the exit of the LHS prototype. It can be seen from Fig. 3.9(a) and 3.9(b) that the LHS prototype is fully charged/discharged at 150 / 160 min.

3.10.7 Energy storage / discharge rate

Fig. 3.10(a) and (b) illustrates the energy (sensible, latent and total) storage/discharge rate of the LHS prototype during the charging/discharging process. When the HTF at 162 / 122 °C is passed through the tubes, heat transfer takes place between the HTF and PCM. Initially, heat gets stored/discharged in the form of sensible heat only. Once the PCM reaches near the phase change temperature (142 °C), heat gets stored/discharged in the form of latent heat. Similarly, after phase change of PCM, heat is stored/discharged in the form of sensible heat. When the PCM reaches an average temperature of 161 °C in 150 min during the charging process, the amount of sensible, latent and total energy stored in the LHS prototype is 6.94 MJ, 10 MJ, and 16.94 MJ. The range of temperature in which the PCM stores the sensible heat is about 39 °C (122 – 161 °C). Similarly, when the PCM reaches an average temperature of 132.3 °C in 165 min during the discharging process, the amount of sensible, latent and total energy discharged from the LHS prototype is 5.29 MJ, 10 MJ, and 15.29 MJ. The range of temperature in which the PCM discharges the sensible heat is about 29.7 °C (162 – 132.3 °C).

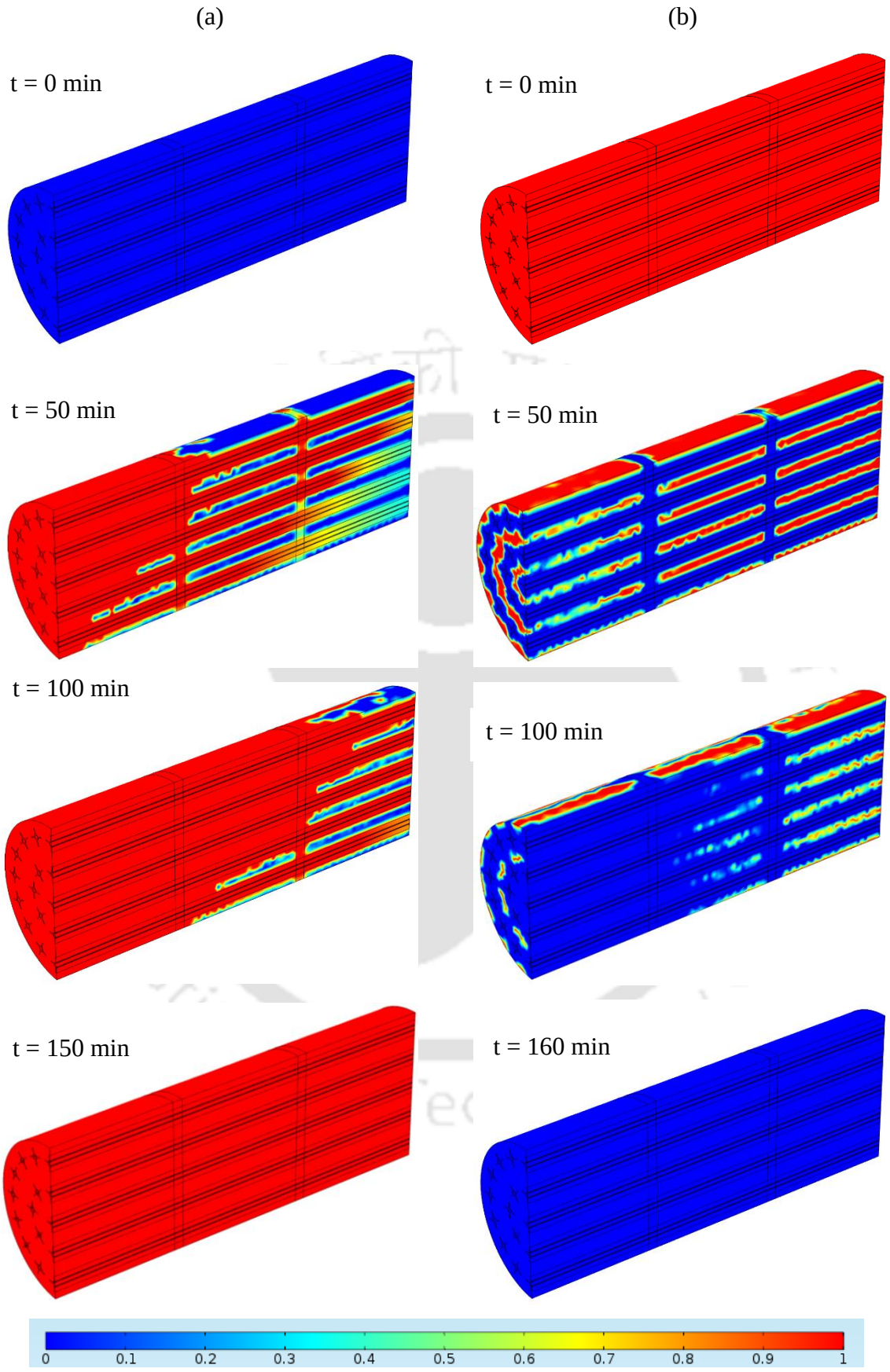

Fig. 3.9 Average melt fraction contours of the LHS model (a) charging and (b) discharging

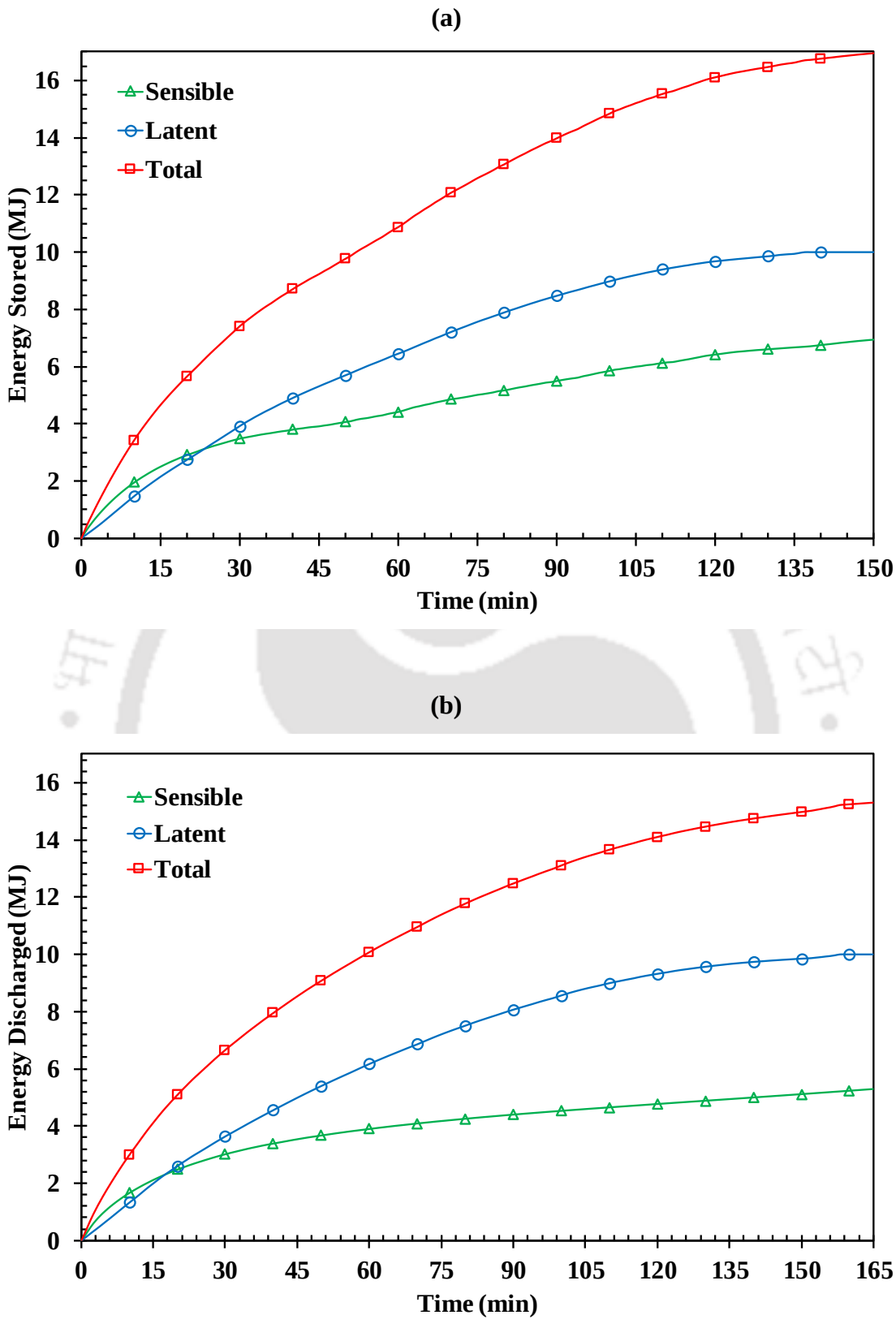

Fig. 3.10 Energy storage/discharge rate of the shell-and-tube LHS model (a) charging and (b) discharging.

3.10.8 Axial temperature variation

Fig. 3.11(a) and (b) shows the axial temperature variation of the LHS prototype during the charging and discharging processes. The volumetric average temperature of each cartridge is compared. It can be noted from Fig. 3.11(a) and (b) that PCM temperature in the cartridges in the entry portion of the LHS prototype have increased/decreased faster than the cartridges in the exit portion during charging/discharging process. This is mainly due to the existence of a higher temperature difference between the PCM and HTF at the entrance of the prototype. It can also be seen that the axial temperature variation is more in charging process than discharging process. This is due to the convective heat transfer, which increases the overall heat transfer rate of the LHS prototype. This is evident from Fig. 3.11(a) that, only after 25 min, the huge temperature difference between the cartridges started. However, there exists a uniform decrease of temperature in the cartridges during the discharging process that is mainly due to the conduction heat transfer.

3.10.9 Angular temperature variation

Fig. 3.12(a) and (b) depicts the angular temperature variation of the LHS prototype during the charging and discharging processes. Three thermocouple points of the 2nd cartridge are taken for analyzing the angular temperature variation. The thermocouple positions are shown in Fig. 3.5(a). Three straight lines in the 2nd cartridge containing the points are averaged for temperature data and are plotted during charging and discharging processes. The radial distance of the line from the center of the LHS prototype is 144 mm. It can be seen from Fig. 3.12(a) and (b) that there is a huge temperature difference exists between the top, middle and bottom portions of the LHS prototype in the charging process when compared with the discharging process. This is due to the natural convection of the molten PCM due to which the high-temperature PCM particles move to the top portion of the LHS prototype.

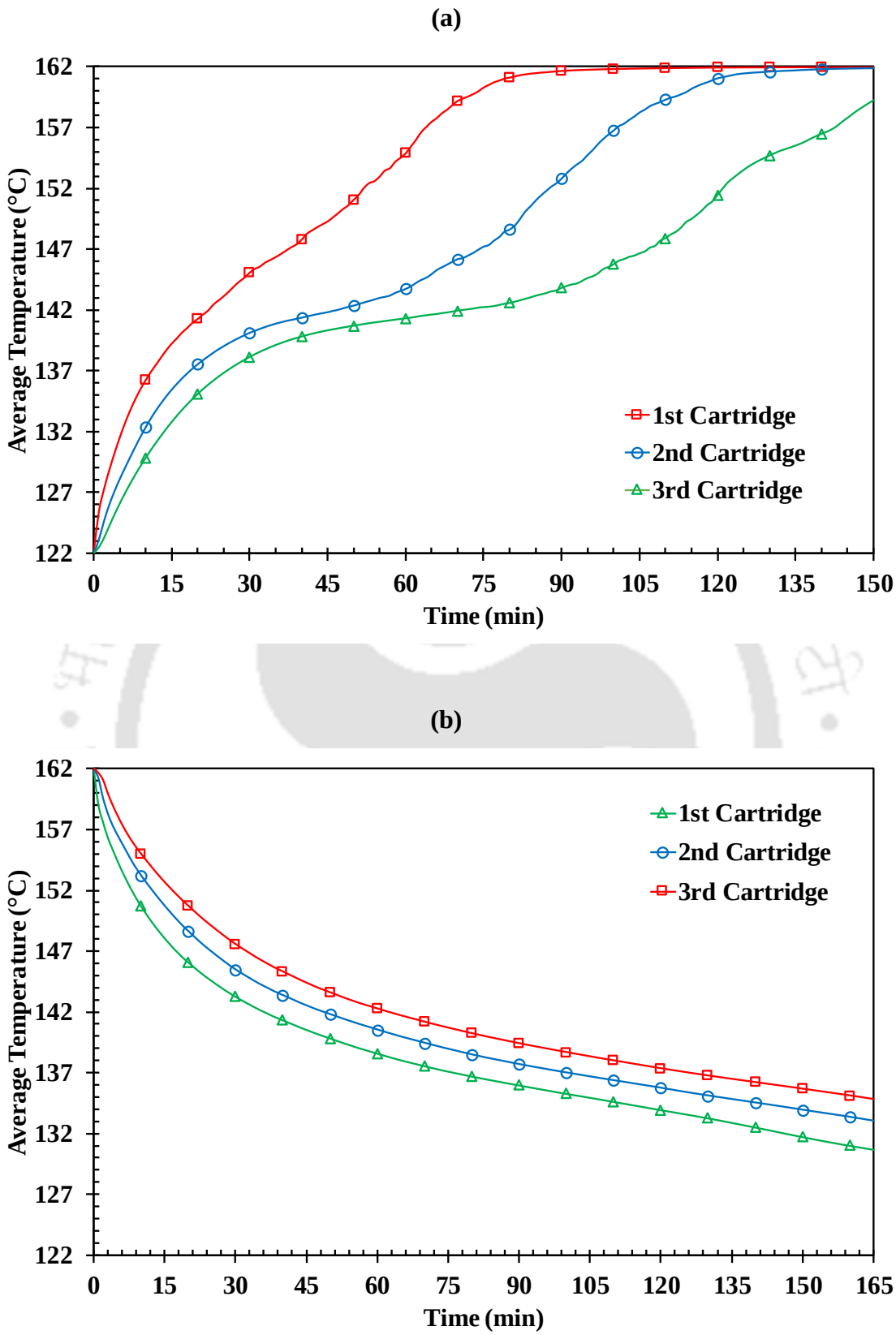

Fig. 3.11 Axial temperature variation of the shell-and-tube LHS model (a) charging and (b) discharging.

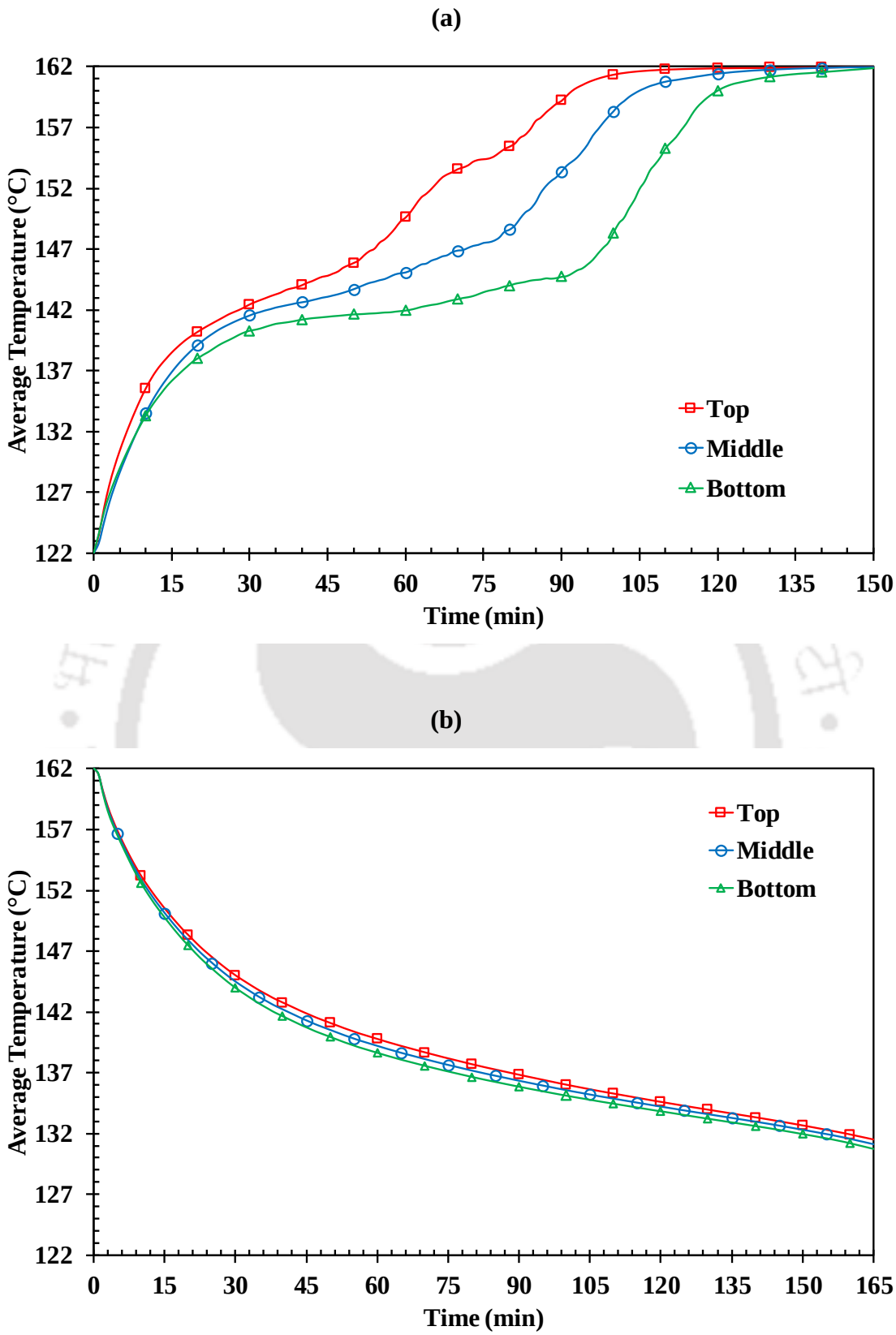

Fig. 3.12 Angular temperature variation of the shell-and-tube LHS model (a) charging and (b) discharging.

3.10.10 HTF outlet temperature

Fig. 3.13(a) and (b) shows the HTF outlet temperature and inlet-outlet temperature difference variation of the LHS prototype during the charging and discharging processes. The HTF outlet temperature variation mainly depends on the heat exchange properties of PCM and the heat transfer potential between the HTF and PCM. It can be seen from Fig. 3.13(a) and (b) that there is a steep increase/decrease of HTF outlet temperature during the commencement of the charging/discharging process. This is mainly due to the higher heat transfer potential available at the beginning of the processes. After a certain period, the increase/decrease in the rise/fall of HTF outlet temperature during charging/discharging process is reduced. This is due to the decline in the heat transfer potential that exists between the HTF and PCM, during that period. The HTF inlet-outlet temperature difference during charging reaches near about 0 at 150 min, which indicates that the PCM average temperature reaches approximately the inlet temperature of the HTF. Similarly, the HTF inlet-outlet temperature difference during discharging reaches near about 5 at 150 min, which indicates the scope of further heat extraction from the PCM. A comparison is also made between the experimental and numerical values of HTF outlet temperature and a close agreement is found between them.

3.10.11 Effect of HTF inlet temperature and flow rate

Fig. 3.14(a) and (b) illustrates the influence of HTF inlet temperature and flow rate on the charging and discharging rate of the LHS prototype. Numerical simulations were conducted with the same initial condition of T_{ini} = 122 °C for three different inlet temperatures *viz.* 157 °C, 162 °C and 167 °C during charging and T_{ini} =162 °C for three different inlet temperatures *viz.* 117 °C, 122 °C and 127 °C during discharging, at three different flow rates, *viz*. 0.3 m^3/hr, 0.45 m^3/hr and 0.6 m^3/hr respectively. It can be seen from Fig. 3.14(a) and (b) that as HTF inlet temperature increases/decreases, the charging/discharging time decreases. This is due to the higher heat transfer potential available between the HTF and PCM. Similarly, as the HTF flow rate increases, the charging/discharging time decreases. This is due to the increase in convection heat transfer coefficient in the HTF side, which enhances the overall heat transfer rate. It is found that the percentage decrease in charging time is decreasing with increase in HTF inlet temperature and flow rate. Similarly, it is also found that the percentage decrease in charging time is decreasing with a decrease in HTF inlet temperature and increase in flow rate. Varying HTF inlet temperature has a greater impact on charging/discharging time when compared with HTF flow rate. Still, the effect of HTF flow rate is more noticeable at lower/higher HTF inlet temperature during charging/discharging process.

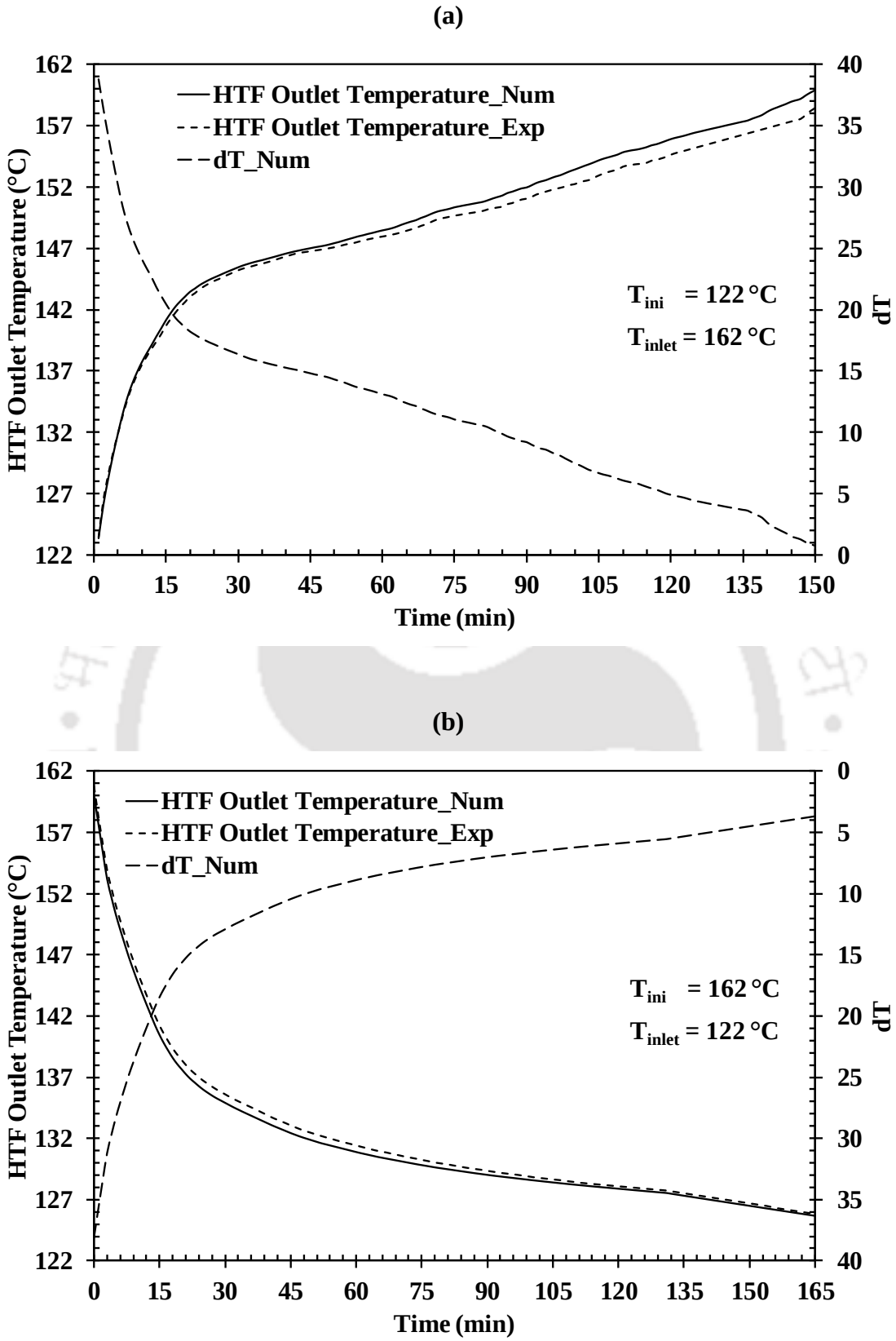

Fig. 3.13 HTF Outlet temperature variation of the shell-and-tube LHS model (a) charging and (b) discharging.

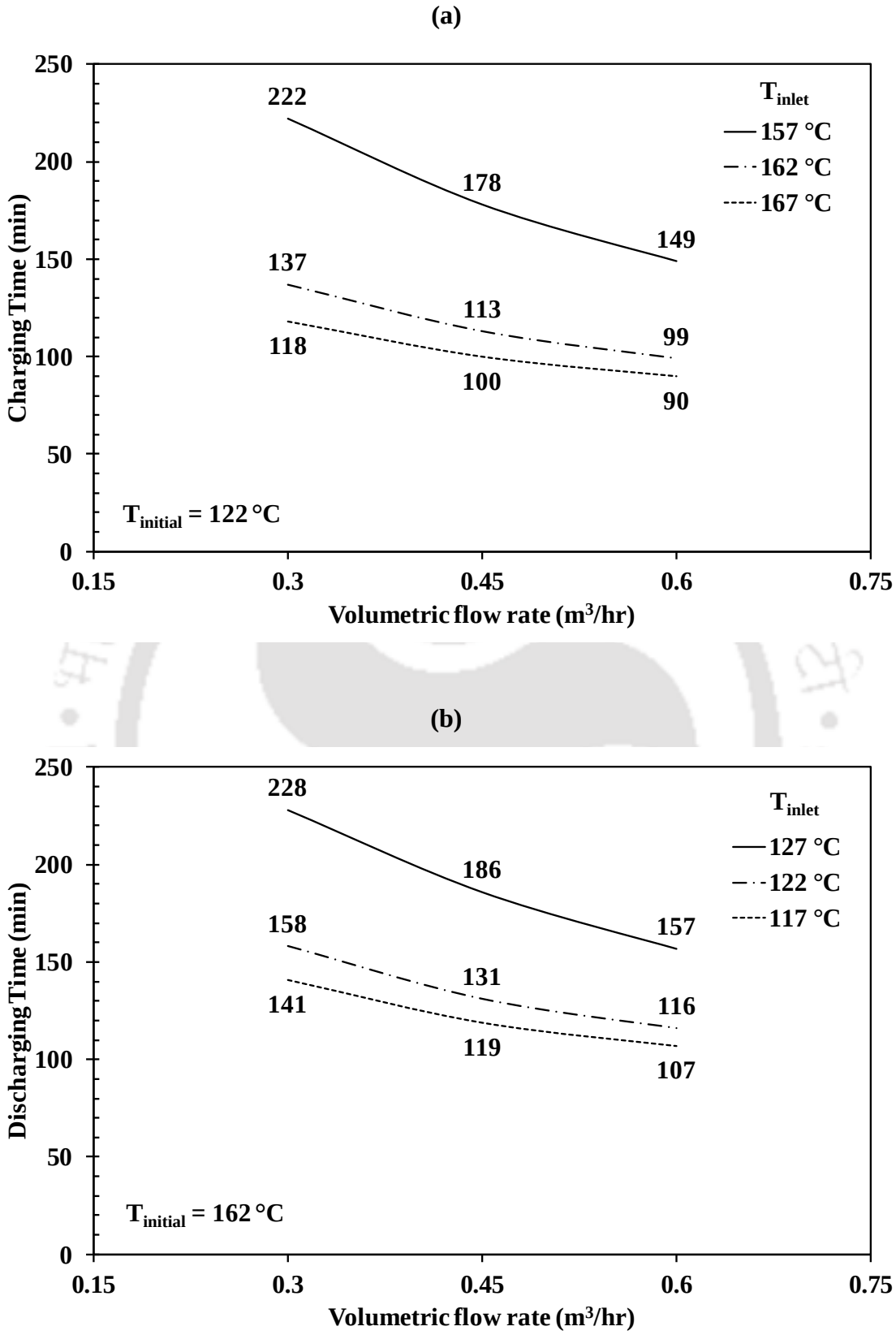

Fig. 3.14 Effect of HTF inlet temperature and flow rate on (a) charging rate and (b) discharging rate.

3.11 Summary

A 3D shell-and-tube numerical model is developed for investigating the storage characteristics of the lab-scale LHS prototype during the charging and discharging processes. Performance parameters like melt fraction, charging/discharging time, energy storage/discharge rate were evaluated at different operating conditions. An exhaustive parametric study was also conducted by varying the HTF inlet temperature and flow rate. Prior to the 3D numerical modeling, a 2D model was developed to optimize the number of tubes and fins of the LHS prototype. The following points gives a brief summary of the results of the numerical study:

- Shell-and-tube model with 25 tubes and 4 fins on each tube is found to be the optimized configuration for the lab-scale LHS prototype.
- Charging is a convection-dominated process and discharging is a conduction-dominated process. Due to this, charging is faster than discharging.
- It took about 111 / 117 min for charging/discharging of the LHS prototype with respect to the thermocouple locations of the experimental setup. For complete charging/ discharging, it took about 137 / 158 min.
- Partial charging/discharging process is efficient than the complete charging/discharging process.
- The total amount of energy, stored during charging was 16.94 MJ and discharged during discharging was 15.29 MJ.
- HTF inlet temperature variation yields a greater impact on the charging/discharging time when compared with the HTF flow rate.
- Effect of HTF flow rate is more noticeable at lower/higher HTF inlet temperature during the charging/discharging process.

Chapter 4

Lab scale Prototype – Experimental Studies

4.1 Preface

For any numerical model developed, validation with the real – time experimental data is vital for the practical applicability and further refinement of the model. In this chapter, details pertaining to the development of a shell-and-tube type lab-scale LHS prototype of 10 MJ capacity with multiple embedded HTF tubes and the corresponding experimental results are presented. Longitudinal fins are adopted on the outer surface of HTF tubes for heat transfer enhancement. The novelty of the experimental work is the simultaneous implementation of two potential things considered for commercialization of storage technology: (i) Higher storage capacity – multi-tube shell-and-tube type configuration and (ii) Heat transfer enhancement – longitudinal fins. A ternary mixture comprising of potassium nitrate, sodium nitrate and sodium nitrite in the weight proportion of 53:7:40 is selected as the PCM for the LHS prototype. Various performance parameters such as melt fraction, charging/discharging time, energy storage/discharge rate are evaluated at different operating conditions. The axial and angular temperature variation of the PCM during the charging and discharging processes are also studied. These experimental results will be useful in designing the efficient industrial scale LHS systems, which have potential applications in solar thermal power plants.

4.2 Experimental setup

The schematic of the experimental setup employed for testing the thermal storage characteristics of the LHS prototype is shown in Fig. 4.1. The experimental setup consists of an oil storage tank, a high-temperature thermic fluid pump, a thermic fluid electric heater, LHS

prototype, an expansion tank, a cooling tank, a positive displacement flow meter of the oval gear type, K-type metal-sheathed thermocouples and a data acquisition system. The oil storage tank having a 1000-liter capacity is utilized for storing the HTF. The huge storage capacity of the storage tank is mainly intended for storing the bulk heat, which aids in feeding a nearly constant temperature HTF to the LHS prototype. The HTF is circulated in the experimental loop by a high-temperature thermic fluid pump of single-stage centrifugal and horizontal end suction type. The pump provides enough pressure (about 2 bar) to overcome the pressure drop across the thermic fluid heater/cooling tank, LHS prototype and pipeline. A variable speed drive (frequency controller) is connected to the pump to achieve different flow velocities. The HTF is heated to the required operating temperature using the thermic fluid heater during the charging process. The heater is of electrical resistance type and has a heating capacity of 72 kW. The electrical load supply to the heater is tuned by a controller, based on the temperature difference between the desired HTF temperature and the heater-exit HTF temperature.

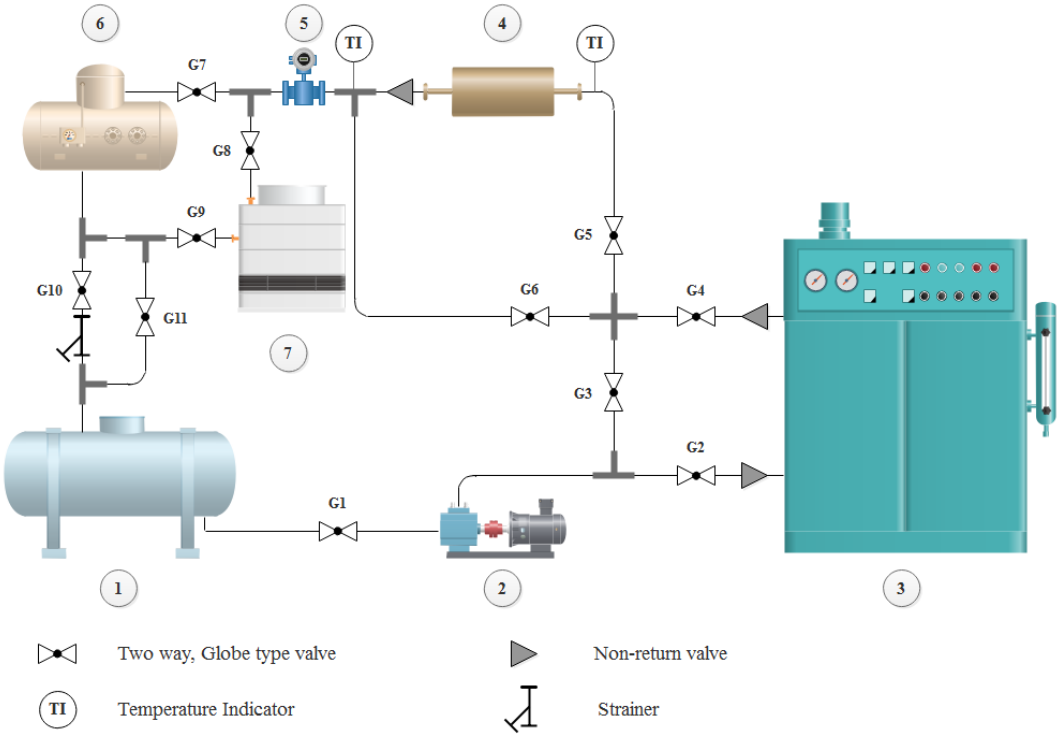

1 – Oil storage tank 2 – Thermic fluid pump 3 – Thermic fluid electric heater
4 – LHS prototype 5 – Oval gear flow meter 6 – Expansion tank 7 – Cooling tank

Fig. 4.1 Schematic diagram of the experimental setup.

The oil volume is generally increased while heating due to the thermal expansion and the excess space needed to accommodate the oil is given by the expansion tank. In addition, the expansion tank serves as a deaerator, i.e. any gases if present in the thermic oil are deaerated. A glass fluid level indicator kept adjacent to the expansion tank shows the exact level of HTF present in the expansion tank. The cooling tank used in the setup is a water based coil-type heat exchanger. The heat exchanger coils are fabricated with flexible copper tubes. Water in the cooling tank (about 750 liter) serves as the cooling medium, and the temperature of the water is maintained at near room temperature through fresh supply of water. The HTF flows through the copper tubes during the discharging process, and it is cooled down due to the heat transfer between the HTF and water. Single ported, Tee type globe valves (G1 – G11) are used to change and divert the flow of HTF during charging and discharging processes. A strainer of Y-type is kept between the expansion tank and storage tank, to filter the circulating HTF from foreign particles.

Non-return valves of clapper type are used at certain locations of the fluid line, *viz.* inlet and outlet of the thermic fluid heater and outlet of the storage prototype, to prevent backflow of the HTF. The LHS prototype, oil storage tank and the pipeline are insulated using glass wool of 50 mm thickness for avoiding heat loss to the ambient. The pictorial view of the experimental setup is presented in Fig. 4.2. During the experiment, temperature of the LHS prototype at various locations, HTF inlet and outlet temperatures and HTF flow rate are measured at a constant time interval of 5 s. A positive displacement flow meter of the oval gear type having an accuracy of ± 0.2 % is used to measure the HTF flow rate in the circuit. Nine K-type thermocouples having an accuracy of ± 0.2 ºC are fitted to the LHS prototype to measure the temperature. LHS prototype consists of three cartridges for keeping the PCM. In the middle of the three cartridges (0.135 m, 0.435 m, 0.735 m from any side of the prototype), thermocouples are placed at three different locations viz. top, middle and bottom to capture the temperature variations. Details of the thermocouple locations are given in Fig. 4.3. Two K-type thermocouples are fixed, each at the inlet and the outlet of the LHS prototype for measuring the HTF temperature. The thermocouples and the flow meter are connected to a data acquisition system, which in-turn is integrated with a computer for recording the temperature and the flow rate data. The data acquisition system consists of Agilent 34972A data logger (having a precision of ± 0.1 °C) and Agilent 34901A 20-channel multiplexer. Concrete basements are made to place the oil storage tank, thermic fluid pump and heater firmly.

(a)

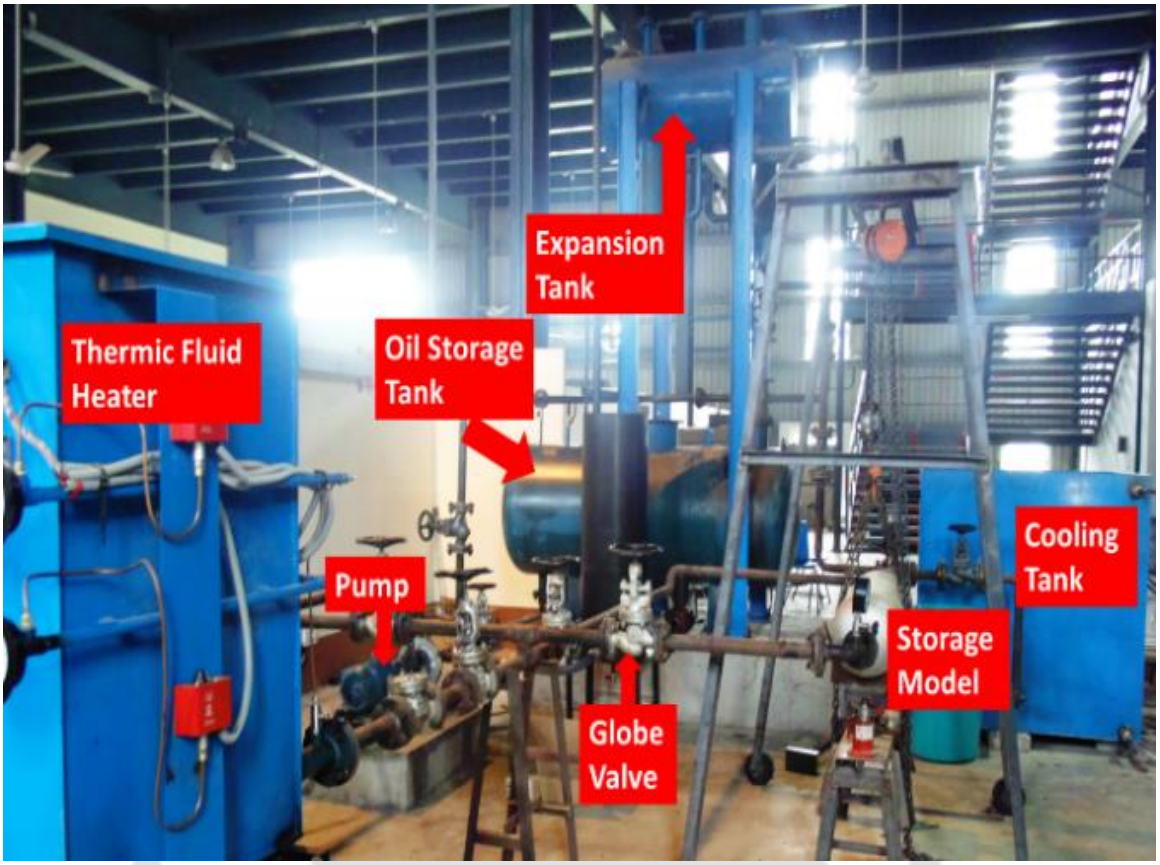

(b)

Fig. 4.2 Pictorial view of the experimental setup (a) without insulation (b) with insulation.

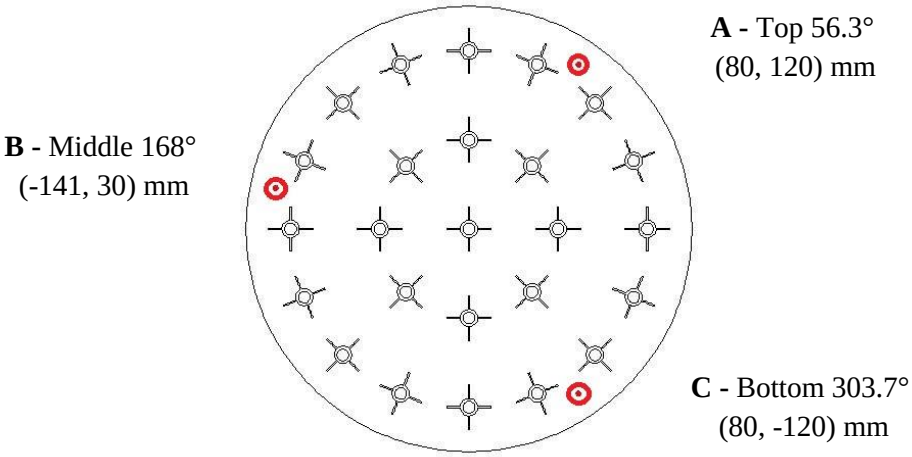

Fig. 4.3 Locations of thermocouples – cross sectional view of the LHS prototype.

4.3 Latent heat storage prototype

The schematic of the LHS prototype employed for testing the thermal storage characteristics is shown in Fig. 4.4. A ternary mixture comprising of potassium nitrate, sodium nitrate and sodium nitrite in the weight proportion of 53:7:40 is selected as the PCM for the LHS prototype. As the main focus of the present work is to evaluate the LHS characteristics of the prototype, a narrow temperature range is quite enough for the analysis. Hence, in the current study, the temperature difference between the initial temperature of the PCM and the inlet temperature of HTF is fixed as 40 °C, similar to the work reported by Alam et al. (2014). As the selected PCM has a melting point of 142 °C, the initial temperature of PCM and the inlet temperature of HTF during charging/discharging process are taken as 122 / 162 °C and 162 / 122 °C, thereby making a temperature swing of 20 °C on both sides of the melting point. The outer diameter (d) and thickness of HTF tubes are 12.7 mm and 2 mm. The height (h) and thickness (b) of the longitudinal fins attached to the tubes are 10 mm and 1 mm. The number of HTF tubes (N_T) and fins (N_F) on each tube in the optimized LHS prototype are 25 and 4. The HTF tubes and fins are made of copper. The outer shell of the prototype is made of stainless steel (SS304) of diameter 335 mm OD and 5 mm thickness. The design details of the LHS prototype is presented in Section 3.2. The physical LHS prototype with insulation and temperature sensors is given in Fig. 4.5.

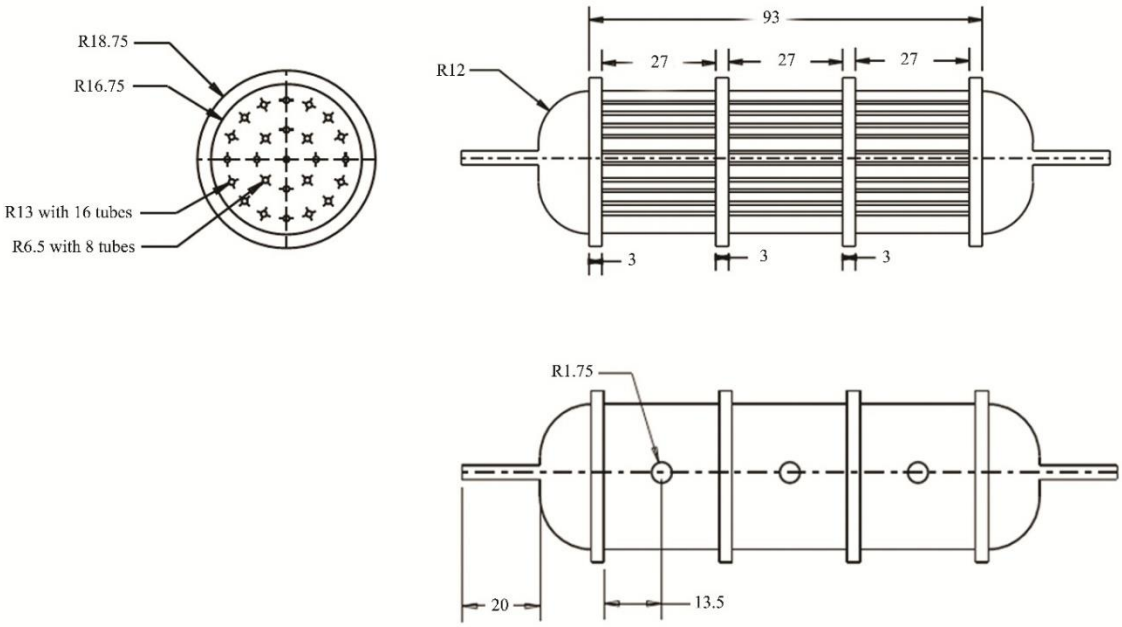

Fig. 4.4 Schematic of the LHS prototype (all dimensions are in cm).

(a)

(b)

Fig. 4.5 Pictorial view of the LHS prototype (a) with thermocouples (b) during experiments.

4.4 Experimental procedure

The entire experimental procedure can be subdivided into four processes, which should be carried out in sequence.

4.4.1 Preheating the oil – Storage prototype bypass

The HTF should be heated up to the desired HTF inlet temperature of the charging process. For achieving this, a bypass line is provided in the experimental loop so that the HTF re-circulates without entering the LHS prototype. Valves G3, G6, G8 and G9 are closed during this process. Once the HTF reaches the desired inlet temperature for charging process, this process is said to be completed.

4.4.2 Charging

When HTF reaches the desired inlet temperature for charging process, the HTF is allowed to pass through the LHS prototype to initiate the charging process. Valves G4, G6, G9 and G10 are closed during this process. The process continues until the prototype is fully charged.

4.4.3 Cooling the oil – Storage prototype bypass

Once the LHS prototype is fully charged, the HTF is then cooled down to the desired HTF inlet temperature for the discharging process. The HTF is made to flow through the cooling tank for achieving the same. Valves G3, G5 and G7 are closed during this process. Once the HTF reaches the desired inlet temperature for the discharging process, this process is said to be completed.

4.4.4 Discharging

When HTF reaches the desired inlet temperature for the discharging process, the HTF is passed through the prototype and thereby discharging of LHS prototype gets started. Valves G3, G5 and G6 are closed during this process. The process continues until the prototype is fully discharged.

4.5 Results and discussions

In the following sub-sections, various results obtained during the performance testing of the lab-scale LHS prototype during the charging and discharging processes are presented. The major implications of the results are also discussed. The initial average temperature of the LHS prototype during the charging process is 122 /162 °C and a comparatively higher/lower temperature HTF at 162 /122 °C is allowed to pass through the HTF tubes. The ambient temperature during the performance tests is about 25 °C in the charging and discharging processes.

4.5.1 Temperature variation

Fig. 4.6(a) and (b) illustrates the local temperature variation of the LHS prototype during the charging and discharging processes. When the high/low temperature HTF is passed through the HTF tubes during the charging/discharging process, heat transfer takes between the high/low temperature HTF and the comparatively low/high temperature PCM through the HTF tubes. It can be noted from Fig. 4.6(a) and (b) that the increase/decrease of temperature is faster in cartridge 1 than cartridges 2 and 3 during the charging/discharging process. A similar trend is observed between cartridge 2 and 3. This is due to the fact that there exists a higher heat transfer potential due to more temperature difference in the entry portion than the exit portion of the prototype.

It can be seen from Fig. 4.6(a) that the increase in temperature of the PCM in the top region of the prototype is faster than that of middle and bottom regions in all the cartridges. This is due to the buoyancy driven natural convection wherein the high temperature and less dense particles move to the top portion of the prototype. It can be noted from Fig. 4.6(b) that the PCM temperature in the bottom portion decreases slightly faster than the middle and top portions. This is due to the negligible natural convection that exists during the solidification process.

In addition, it can be inferred from Fig. 4.6(a) that there is a steady increase in temperature up to a certain point, after that the slope of the curve decreases and finally after a certain interval, the temperature has increased sharply. This transition is due to the melting phenomenon during which a large amount of latent heat gets stored in the PCM. However, a similar trend is not

noticeable in the temperature values of the top portion of all cartridges. This is due to the convective movement of the higher temperature particles in the top portion, by which the temperature has increased sharply. Due to the conduction heat transfer that takes place in the PCM throughout the solidification process, there exists an even temperature distribution in the radial direction of the prototype. Unlike charging process, a sharp plateau is not noticeable in the discharging process. This is because the heat source input during the discharging process is the LHS prototype itself, the potential of which is reduced while exchanging heat with the HTF. In addition, during the discharging process, a thin solid layer of PCM is formed around the HTF tube. Over a period, the thin layer becomes thicker. This increases the thermal resistance and hence, the solidification rate reduces. The distribution of the temperature in the LHS prototype during the charging/discharging process is in line with previously reported data by the other researchers (Trp et al., 2006; Avci and Yazici, 2013; Hosseini et al., 2014). The uncertainty in the temperature measurements is about ± 0.2 °C.

Fig. 4.7(a) and (b) shows the average temperature variation of the LHS prototype during the charging and discharging processes. Average temperature is the arithmetic mean of the local temperatures measured at nine locations (3 per cartridge as shown in Fig. 4.3) in the prototype. The average temperature of PCM during the charging process increases to about 160.6 °C in 150 min, which is 1.4 °C less than the HTF inlet temperature. Similarly, the average temperature of PCM during the discharging process decreases to about 131.6 °C in 165 min.

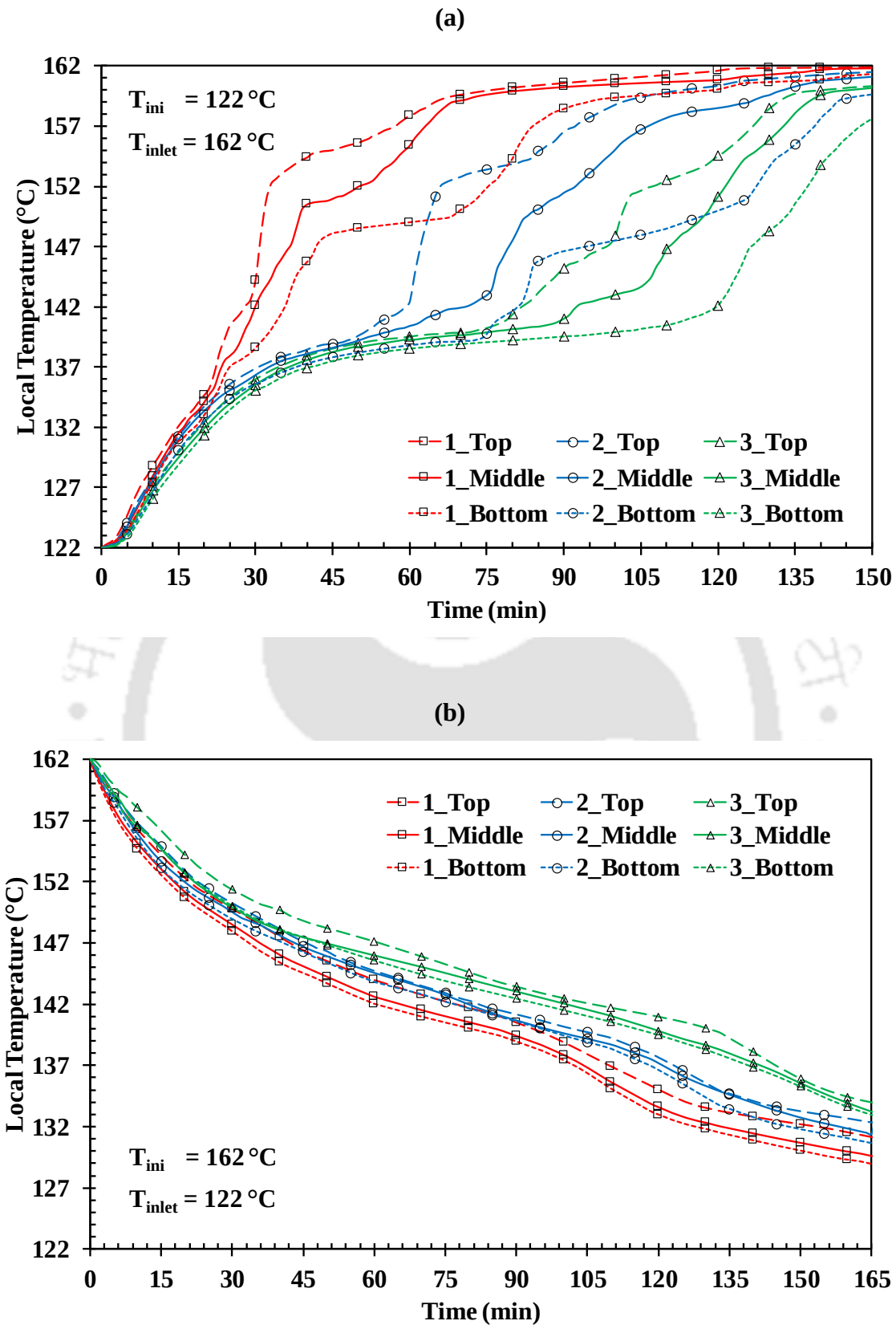

Fig. 4.6 Local temperature variation of the lab-scale LHS prototype during (a) charging and (b) discharging.

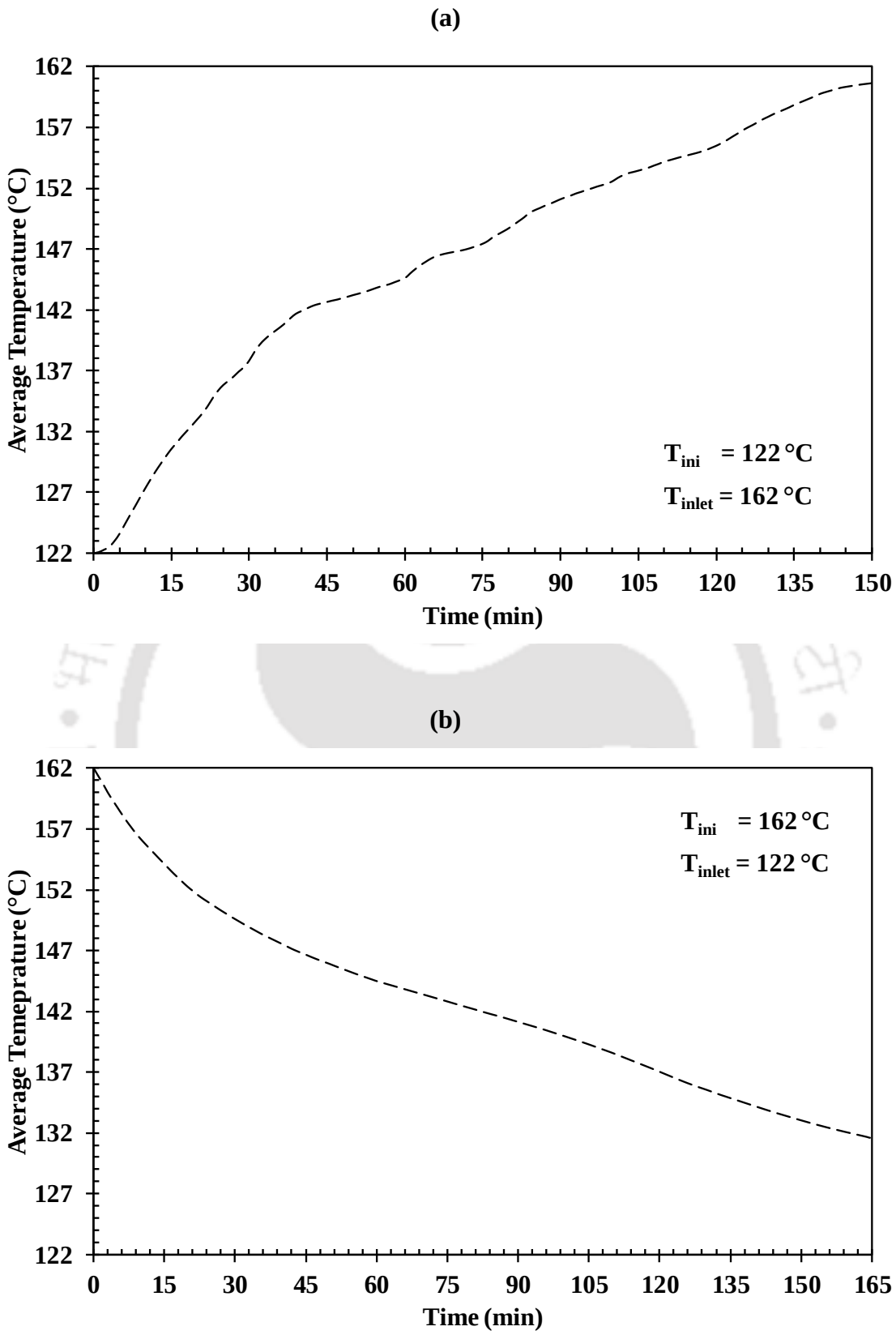

Fig. 4.7 Average temperature variation of the lab-scale LHS prototype during (a) charging and (b) discharging.

4.5.2 Charging / discharging time

Fig. 4.8(a) and (b) depicts the local melt fraction variations of the LHS prototype during the charging and discharging processes. The local melt fraction is calculated based on the temperature of the PCM (recorded at nine different locations) using the Eq. (3.10).

It is seen from Fig. 4.8(a) that the top portion of the cartridges have a steady increase in melt fraction when compared with the bottom cartridge. This is due to the convection heat transfer occurred during the melting of PCM, wherein the molten PCM moves from the bottom to the top portion of the prototype. On the contrary, it is seen from Fig. 4.8(b) that the top, middle and bottom portion of the cartridges have a steady decrease in melt fraction evenly. This is due to the uniform conduction heat transfer in the PCM. In addition, it can be seen from the above results that PCM in the 1st cartridge has melted/solidified faster than 2nd and 3rd cartridges and similar tendency is observed between 2nd and 3rd cartridges. This is due to the higher heat transfer potential available at the entrance of the LHS prototype than the exit of the prototype. The uncertainty involved in the estimation of melt fraction is about ± 0.061.

Fig. 4.9(a) and (b) shows the average melt fraction variation of the LHS prototype during the charging and discharging processes. Average melt fraction is the arithmetic mean of the local melt fractions measured at nine locations in the prototype.

It can be observed from Fig. 4.9(a) that the average melt fraction is zero until 24 min. Within this period, sensible heat gets stored in the PCM in all the cartridges. PCM in the 1st cartridge gets melted between the 25 – 38 min of the experiment. The average melt fraction is idle between 39 – 50 min. This is because the PCM in 2nd and 3rd cartridges underwent sensible heating during this period. PCM in the 2nd and 3rd cartridge gets melted between the 51 – 84 min and 72 – 123 min of the experiment. It took about 123 min for the LHS prototype to reach an average melt fraction of unity. It can be noticed from Fig. 4.9(b) that the average melt fraction is unity until 48 min. Within this period, sensible heat is discharged from the PCM in all the cartridges. PCM in the 1st, 2nd and 3rd cartridges gets solidified between 49 – 95 min, 58 – 102 min and 74 – 131 min of the experiment. It took about 131 min for the LHS prototype to reach an average melt fraction of zero.

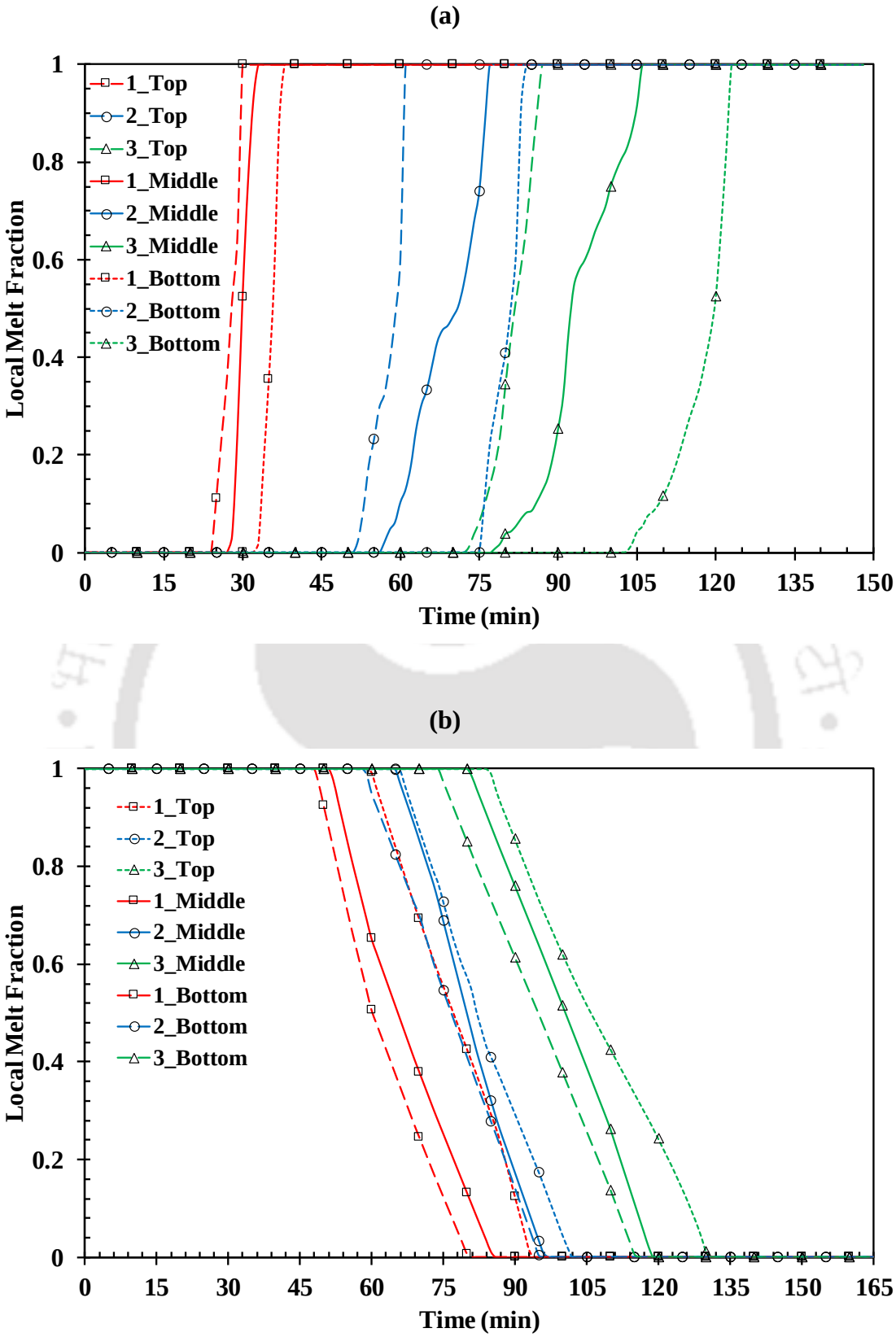

Fig. 4.8 Local melt fraction variation of the lab-scale LHS prototype during (a) charging and (b) discharging.

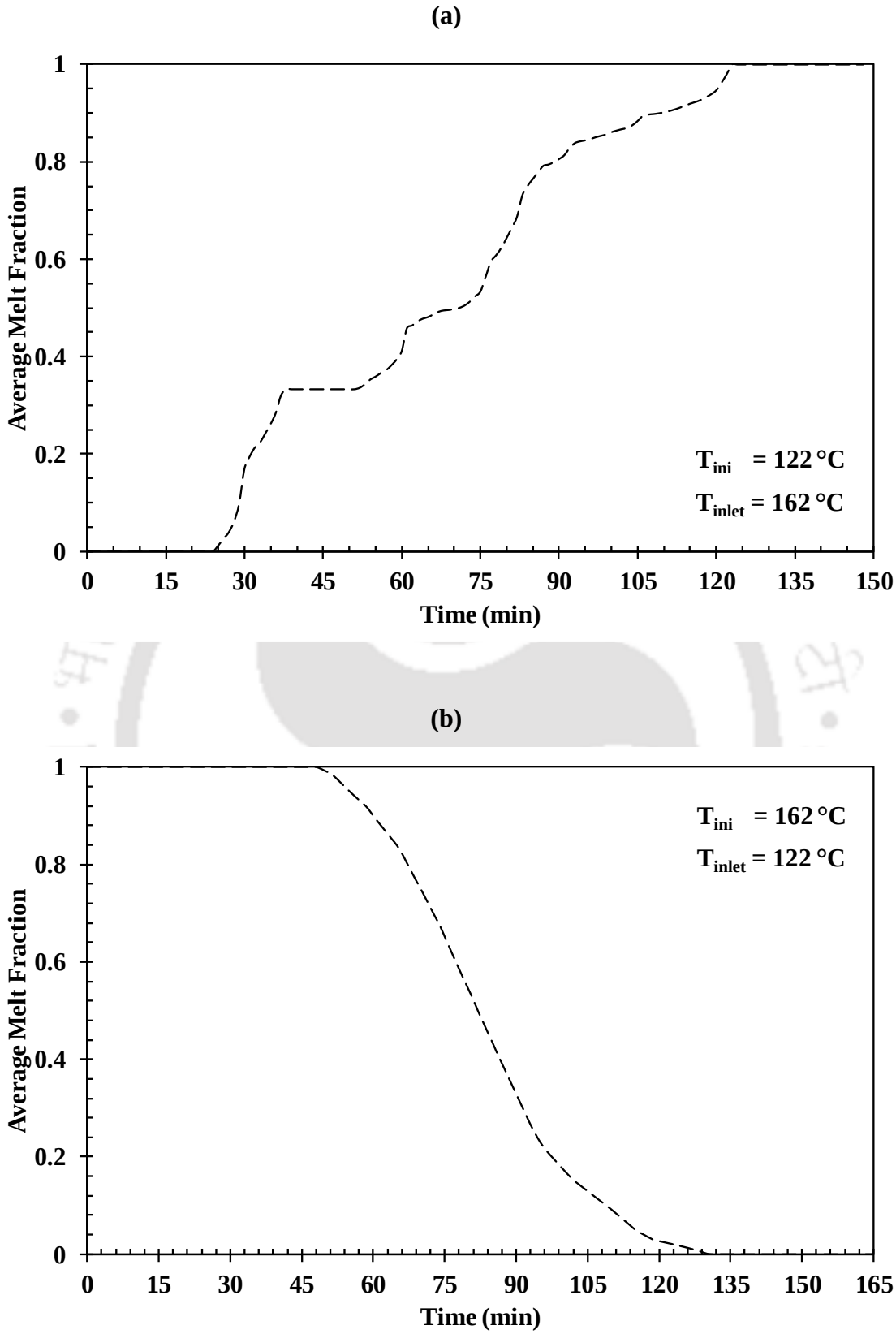

Fig. 4.9 Average melt fraction variation of the lab-scale LHS prototype during (a) charging and (b) discharging.

4.5.3 Energy storage / discharge rate

Fig. 4.10(a) and (b) illustrates the energy (sensible, latent and total) storage and discharge rate of the LHS prototype during the charging and discharging processes. Sensible, latent and total heat stored/discharged in/from the PCM are calculated using the Eq. (3.11) – (3.16), respectively. During charging, when the high-temperature HTF at 162 °C is passed through the tubes, heat from the HTF is transferred and stored in the PCM. Similarly, during discharging, when the low-temperature HTF is allowed to pass through the HTF tubes, the stored heat from the PCM is discharged to the HTF. Initially, when the PCM is in the solid/liquid state during charging/discharging, heat gets stored/discharged in the form of sensible heat only. Once the PCM reaches near the phase change temperature (142 °C), heat gets stored/discharged in the form of latent heat. Similarly, after melting/solidification of the PCM, heat is stored/discharged in the form of sensible heat.

During charging, when the PCM reaches an average temperature of 160.6 °C in 150 min, the amount of sensible, latent and total energy stored in the LHS prototype are 6.87 MJ, 10 MJ and 16.87 MJ, respectively. The range of temperature in which the PCM stores the sensible heat is about 38.6 °C (122 – 160.6 °C). During discharging, when the PCM reaches an average temperature of 131.6 °C in 165 min, the amount of sensible, latent and total energy discharged from the LHS prototype are 5.41 MJ, 10 MJ and 15.41 MJ, respectively. The range of temperature in which the PCM discharges the sensible heat is about 30.4 °C (162 – 131.6 °C).

It can also be noted from Fig. 4.10(a) and (b) that the sensible and latent energy storage/discharge rate curve has a similar trend like average temperature and melt fraction curve. Because, the sensible and latent energy stored/discharged depends only on the average temperature (Eq. 3.11 and 3.14) and the average melt fraction of the PCM (Eq. 3.12 and 3.15), provided mass, specific heat and latent heat are constant.

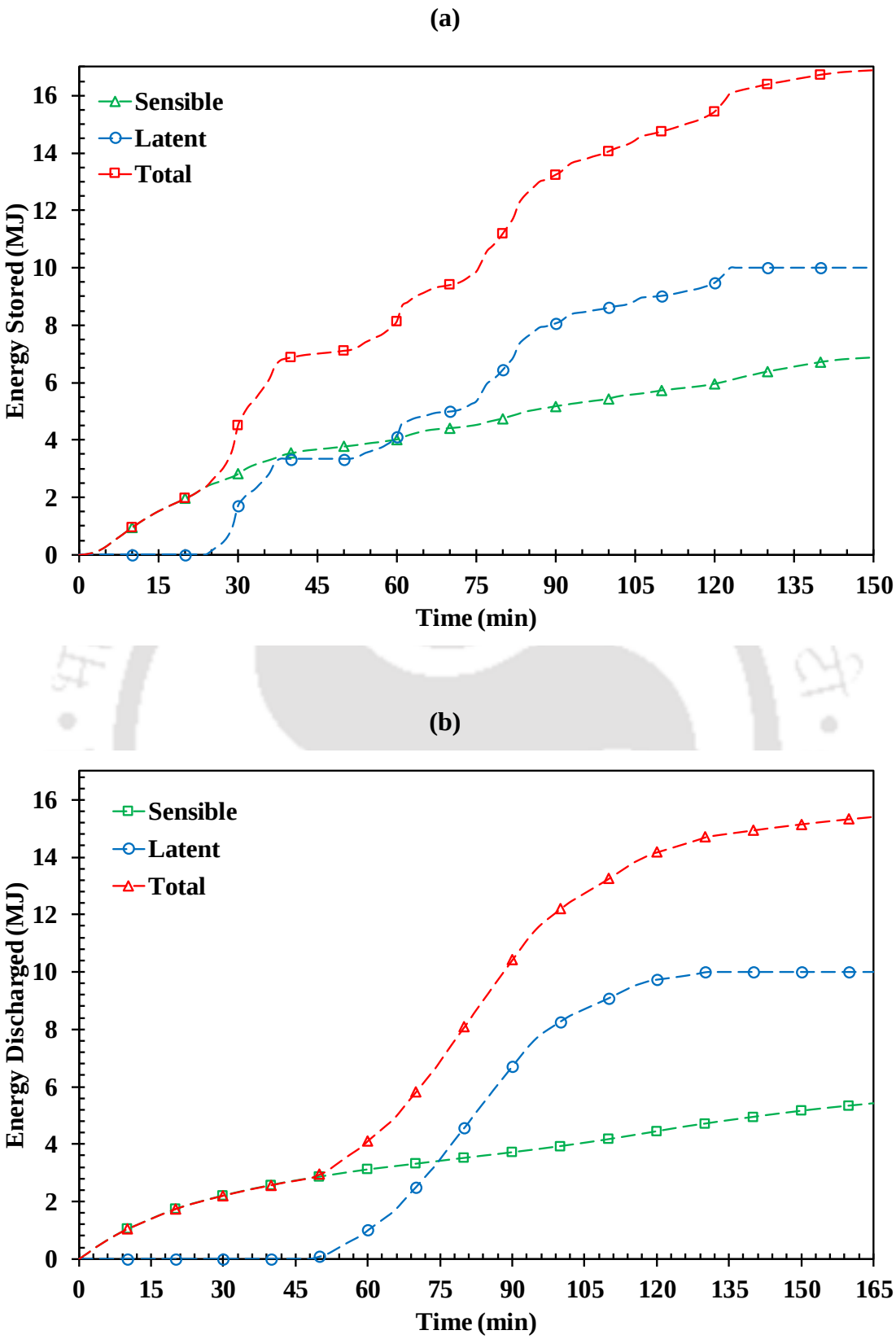

Fig. 4.10 Energy storage / discharge rate of the lab-scale LHS prototype during the experiments (a) charging and (b) discharging.

4.5.4 Axial temperature variation

Fig. 4.11(a) and (b) shows the axial temperature variation of the LHS prototype during the charging and discharging processes. Temperature measurements made at the middle portion of each of the three cartridges are compared to indicate the temperature variation in the axial direction. It can be noted from Fig. 4.11(a) and (b) that PCM temperature in the cartridges in the entry portion of the LHS prototype is increasing/decreasing faster than the cartridges in the exit portion. This is mainly due to the existence of a higher temperature difference between the PCM and HTF at the entrance of the prototype. During the flow of HTF, it exchanges heat with the PCM thereby reducing/increasing its temperature during charging/discharging. Because of this, the temperature difference between the PCM and HTF is low near the exit portion of the prototype. However, once the PCM near the entrance region gets heated/cooled up/down to a higher/lower temperature, the temperature difference between the HTF and PCM in the entrance region gets reduced. Due to this, the heat transfer rate between the HTF and PCM becomes lesser in the entrance region and the temperature reduction/increase of HTF becomes slower during charging/discharging. Hence, a relatively higher/lower temperature HTF will be available near the exit region of the LHS prototype during the end of charging/discharging. It can be noted from Fig. 4.11 (a) that after 105 min, the increase of PCM temperature in the 3rd cartridge is faster. This is due to the fact that during that time, PCM in the first two cartridges are completely melted and high temperature HTF with minor temperature drop is available for charging the 3rd cartridge.

4.5.5 Angular temperature variation

Fig. 4.12(a) and (b) illustrates the angular temperature variation of the LHS prototype during the charging and discharging processes. Temperature measurements made at the top, middle and bottom positions of the 2nd cartridge are compared to indicate the angular temperature variation. It can be noted from Fig. 4.12(a) that the PCM temperature at all the three positions during the charging process is almost same with negligible difference until about 140 °C. After that, the temperature variation profile for the three positions started deviating. The temperature of PCM in the top position has increased steeply (60 – 65 min). This is due to the natural convection, which happens after the formation of the liquid PCM. The high temperature and less dense PCM starts moving from the middle and bottom positions to the top position, leaving the cold and dense PCM in the middle and bottom positions of the LHS prototype. This steep increase in PCM temperature in the top position continues until the temperature difference

between HTF and PCM in the top position is quite enough. Once this temperature difference becomes marginal, the PCM temperature in the top position also increases slowly (66 – 85 min). During this period, the PCM temperature of the middle position increased steeply. This is due to the natural convection and presence of reasonable temperature difference between the HTF and PCM in the middle position of the LHS prototype. A similar trend with a lesser magnitude is also observed in the PCM temperature of the bottom position. After 85 min, there exists a gradual increase in PCM temperature in all the positions, due to the lesser temperature difference between the HTF and PCM. It can be observed from Fig. 4.12 (b) that the PCM temperature at all the three positions was almost same with negligible difference throughout the discharging process. PCM temperature in the bottom portion decreases slightly faster than the middle and top portions. This is due to the negligible natural convection that exists during the solidification process. The whole solidification process is a conduction-dominated process, due to which the temperature decrease is uniform throughout the PCM.

4.5.6 HTF outlet temperature

Fig. 4.13(a) and (b) depicts the HTF outlet temperature and inlet-outlet temperature difference variation of the LHS prototype during the charging and discharging processes. During the charging/discharging process, HTF passed through the tubes loses/gains heat to/from the PCM due to the temperature difference exists between them. Due to the availability of higher heat transfer potential, initially, the HTF loses/gains maximum amount of heat to/from the PCM and exits the LHS prototype at a minimum/maximum temperature during the charging/discharging process. At the same time, the increase/decrease in the overall PCM temperature of the LHS prototype is also maximum. As the LHS prototype gained/lost a certain amount of heat, the heat transfer between the HTF and PCM starts reducing. Due to this, the HTF outlet temperature also starts increasing/decreasing during the charging/discharging process. As the average PCM temperature increases/decreases faster initially in the sensible region, the increase/decrease in the HTF outlet temperature is also initially faster (0 – 30 min). During melting/solidification, there was a gradual variation in the PCM temperature, due to which the HTF outlet temperature also increases/decreases gradually. A similar trend of HTF outlet temperature variation is also reported by Mehling and Cabeza (2008). The HTF inlet-outlet temperature difference variation follows a similar trend, but opposite of the HTF outlet temperature variation.

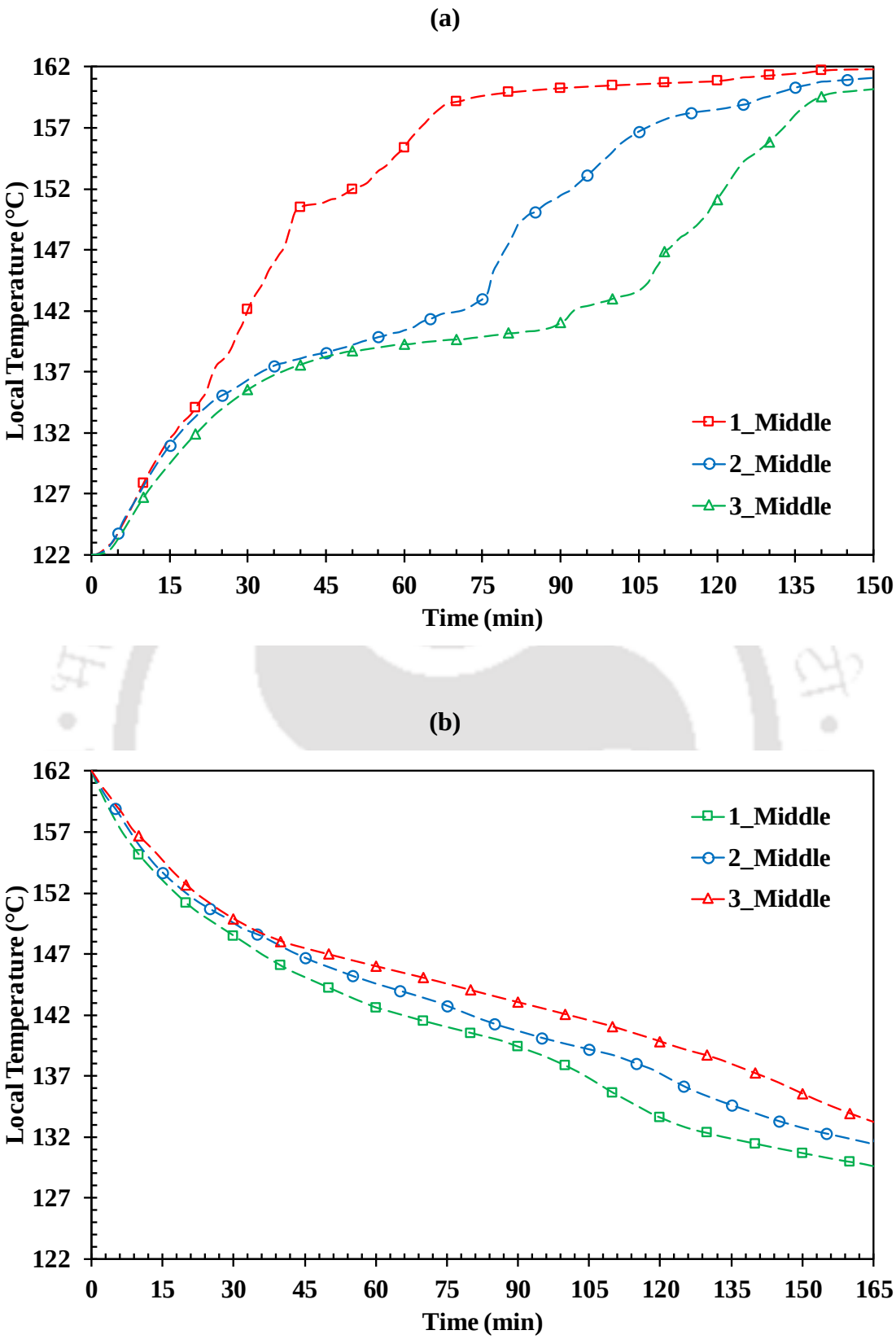

Fig. 4.11 Temperature variation of the lab-scale LHS prototype in the axial direction during the experiments (a) charging and (b) discharging.

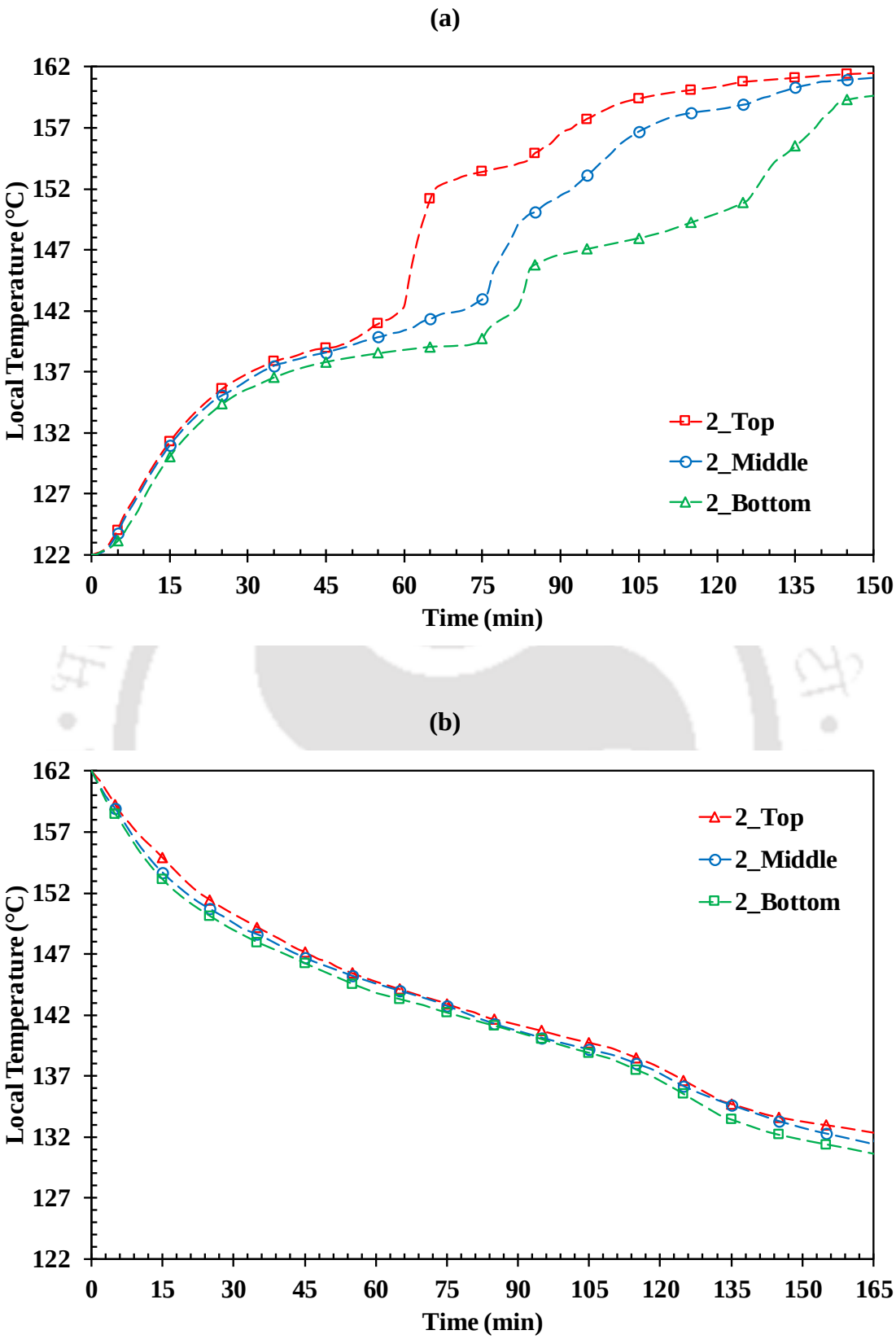

Fig. 4.12 Angular temperature variation of the lab-scale LHS prototype during the experiments (a) charging and (b) discharging.

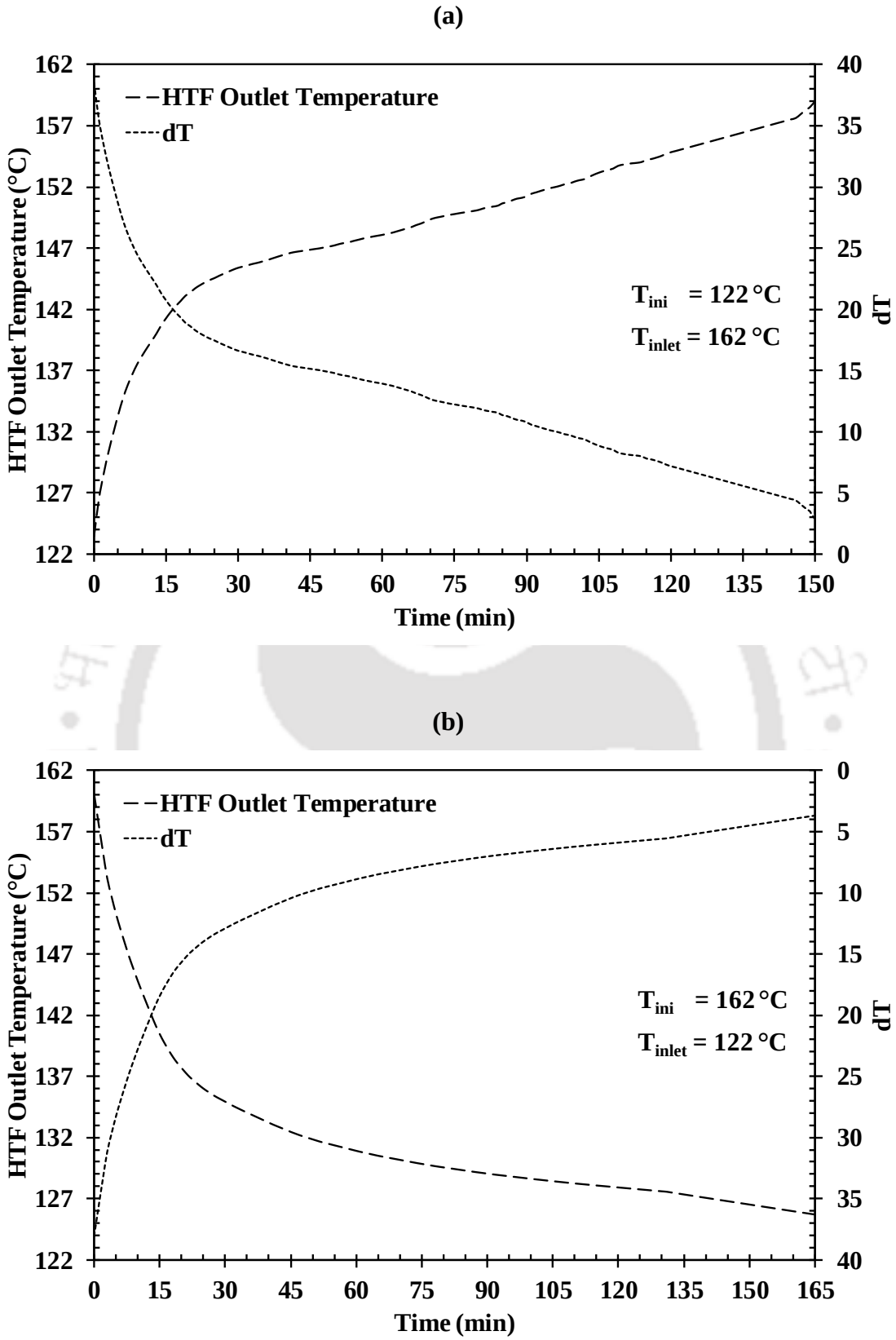

Fig. 4.13 HTF outlet temperature variation of the lab-scale LHS prototype during the experiments (a) charging and (b) discharging.

4.5.7 Effect of HTF inlet temperature and flow rate

The storage performances of the LHS prototype can be controlled by two major parameters: (1) HTF inlet temperature and (2) HTF flow rate. Hence, a detailed parametric study is vital for the better understanding of the LHS system. Fig. 4.14(a) and (b) shows the influence of the HTF inlet temperature and flow rate on the charging and discharging rates of the LHS prototype. Experiments are conducted with the same initial PCM temperature of T = 122 °C for three different HTF inlet temperatures *viz.* 157 °C, 162 °C and 167 °C, at three different HTF flow rates, *viz*. 0.3 m^3/hr, 0.45 m^3/hr and 0.6 m^3/hr. Two observations can be directly inferred from Fig. 4.14(a) and (b). (i) The charging/discharging time is lower for the higher/lower HTF inlet temperature case during the charging/discharging process. This is due to the huge temperature difference that exists between the HTF and PCM. (ii) The charging and discharging times are lower for the higher HTF flow rate case. This is due to the higher convection heat transfer coefficient in the HTF side, which enhances the overall heat transfer rate of the LHS system.

However, the charging/discharging time is lower for the higher/lower HTF inlet temperatures and higher HTF flow rates; there exists a threshold in both the parameters beyond which, the decrease in the charging/discharging time is too minimal. Because, there is a limit in the heat transfer rate of the PCM, which is mainly due to its low thermal conductivity. This phenomenon can be noted well in the cases of different HTF inlet temperatures for a specific HTF flow rate. There exists a huge reduction in the charging/discharging time between the cases with HTF inlet temperatures of 157 °C and 162 °C, than the cases with HTF inlet temperatures of 162 °C and 167 °C. Similar effect is also noticeable to a lesser extent in the cases of different HTF flow rates for a specific HTF inlet temperature. Hence, varying the HTF inlet temperature has a greater impact on the charging/discharging time when compared with HTF flow rate. Still, the effect of HTF flow rate is more pronounced at lower/higher HTF inlet temperature during the charging/discharging process. Because, at lower/higher HTF inlet temperature, the temperature difference between the HTF and PCM is less and hence, the heat transfer is dominated by the convective action of the HTF flow rather than the temperature difference between the HTF and PCM.

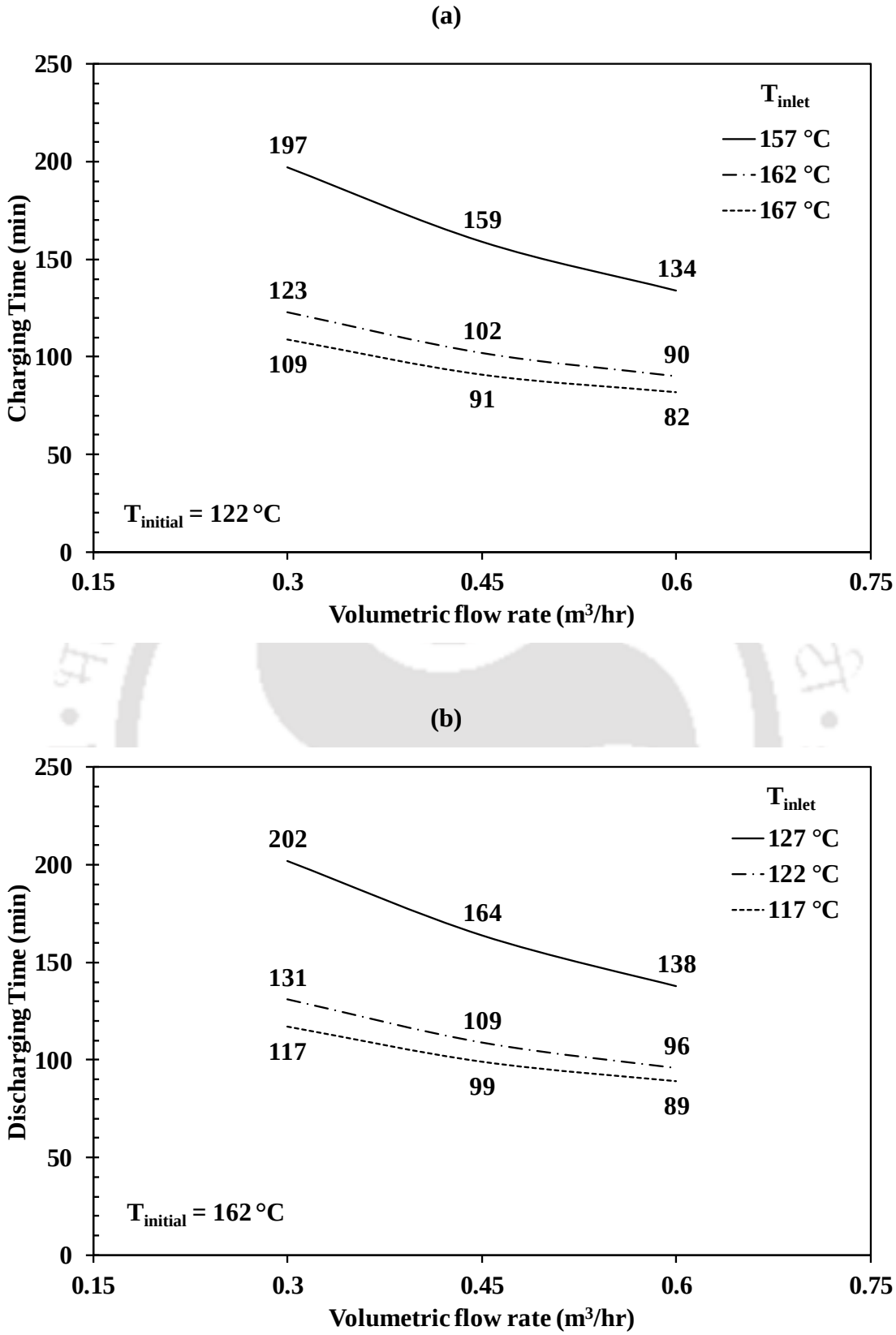

Fig. 4.14 Effect of HTF inlet temperature and flow rate on (a) charging rate and (b) discharging rate.

4.6 Summary

The results of the experimental investigation of the lab-scale LHS prototype carried out during the charging and discharging processes are presented. Performance parameters like melt fraction, charging/discharging time, energy storage/discharge rate are evaluated at different operating conditions. A detailed parametric study is also conducted at various HTF inlet temperatures and flow rates. The following points gives a brief summary of the outcomes of the experimental study:

- Natural convection plays a crucial role during charging process. It does not play a major role during the discharging process and heat transfer is conduction-dominated during solidification.
- The charging process is faster than discharging process due to the additional natural convection, which takes place after the phase change temperature.
- It took about 124 / 131 min for charging/discharging of the LHS prototype.
- The total amount of energy, stored during charging was 16.87 MJ and discharged during discharging was 15.41 MJ.
- Varying HTF inlet temperature has a greater effect on the charging/discharging time when compared with the HTF flow rate.
- Effect of HTF flow rate is more prominent at lower/higher HTF inlet temperature during the charging/discharging process.

Chapter 5
Novel Encapsulation

5.1 Preface

Steam accumulators are used as buffer storage devices between steam generators and consumers in the case of a mismatch between the steam production and consumption (Stevanovic et al., 2012; Sabihuddin et al., 2015). Steam accumulators are generally employed in several industries such as cooking (Sardeshpande and Pillai, 2012), glass and rubber (Price, 1982), metal manufacturing (Shnaider et al., 2010), textile (Goldstern, 1979), etc. Recently, electric power stations especially solar thermal power plants also started employing steam accumulators for storing the excess supply of saturated steam produced during the peak periods and use it later for the extended operation of the plant. Planta Solar 10 (PS10), a 11 MWe solar tower based concentrated solar power plant in Seville, Spain uses a steam accumulator for storing part of the saturated steam coming out from the solar receiver at 40 bar and 250 °C (SOLUCAR, 2006). Badaling, a 1 MWe solar tower based power plant in China also incorporated steam accumulator for storing the saturated steam at 23.5 bar and 220.7 °C (Xu et al., 2012). During the discharge, the pressure in the steam accumulator drops. To overcome this pressure drop, techniques such as incorporating a flash evaporator or an encapsulated latent heat storage (LHS) capsule are suggested. Due to the exergy loss by mixing in the flash evaporator system, encapsulated LHS capsule is advantageous (Steinmann and Eck, 2006).

As already explained, the major drawback of the PCMs is its lower thermal conductivity, which demands the employment of heat transfer enhancement techniques to increase the overall heat transfer rate (Da Cunha and Eames, 2016). Several techniques were reported by the researchers for improving the heat transfer in LHS devices (Jegadheeswaran and Pohekar, 2009; Khan et

al., 2016; Ibrahim et al., 2017). Encapsulation of PCMs is one of the promising techniques to improve the heat transfer characteristics of the LHS system (Alam et al., 2015). Generally, the PCMs are encapsulated in two forms; viz. flexible and stiff (Steinmann and Tamme, 2008). The flexible shells are generally made of polymer and mainly meant for low or medium temperature applications like thermal comfort in buildings. The stiff shells are made of either metals or ceramics and commonly used in high temperature applications such as power generation (Castellon et al., 2011; Liu et al., 2012; Jacob and Bruno, 2015). Over the last four decades, several experimental and numerical studies have been carried out for evaluating the storage performance characteristics of the encapsulated capsules. Certain reviews encompass the major research works carried out in the encapsulated systems (Farid et al., 2004; Su et al., 2015).

Vyshak and Jilani (2007) formulated a 1D mathematical model to compare the storage characteristics of rectangular and cylindrical capsules. Similarly, Niyas and Muthukumar (2015) developed a 2D axisymmetric model to compare the heat transfer dynamics of spherical and cylindrical capsules. For the same mass of PCM, the cylindrical capsules are found to be charging in lesser time than the rectangular and spherical capsules. Despite of several advantages like near constant temperature heat discharge, high volume-specific storage capacity, etc. (Medrano et al., 2010), the major disadvantage of cylindrical capsule is the limitation in the diameter. With an increase of diameter, the resistance to heat transfer also increases due to the low thermal conductivity of the PCM. In the present study, a novel encapsulation technique is proposed to alleviate this. The novelty proposed here is to use a tube-in-tube LHS system with a very small inner tube. With this, the heat transfer would be enhanced due to the lesser thickness of PCM and increased heat transfer area when compared to the LHS capsule having the basic encapsulation.

To compare the performance characteristics of the basic and the proposed novel encapsulation techniques, capsules having a LHS capacity of 0.5 MJ are considered. Sodium nitrate and SS304 are selected as the PCM and encapsulating material. A small tube of outer diameter 12 mm with a thickness of 2 mm is used as the inner tube for the novel capsule. The height of both the capsules considered in the study is 0.5 m. The outer diameter of the LHS capsules having basic and novel encapsulation for storing the corresponding LHS capacity (including the 2 mm capsule thickness) are found to be 65.3 mm and 66.4 mm. The design of capsules is made in such a way that the volume of PCM in both the capsules are the same.

5.2 Model description

Fig. 5.1 shows the schematic and 2D axisymmetric view of the basic and novel encapsulated cylindrical capsule containing a PCM. The LHS capsule absorbs/releases heat from/to the hot/cold heat transfer fluid in which the capsule is immersed. As both the capsule configurations are symmetric about the vertical axis, a 2D axisymmetric model is developed in the present study. A constant temperature heat/cold source is given at the boundary of the model to mimic the initiation of charging/discharging process that exists in the steam accumulator. During the charging cycle, heat is transferred from the hot boundary to the PCM through the encapsulation. Similarly, during the discharging cycle, PCM releases the stored heat due to the interaction with the cold boundary. Sodium nitrate and SS304 are selected as the PCM and the encapsulation material and their respective thermo-physical properties are given in Table. 5.1. To study the thermal storage behavior of the LHS capsule, three physical processes have to be simulated i.e. conduction, convection, and phase change. The governing equations explained in the section 3.5 is used here for predicting the heat transfer characteristics of the basic and novel LHS capsules. Similarly, the performance parameters that are involved in evaluating the storage characteristics are already explained in the section 3.6. The thermal model is developed based on following assumptions:

- The initial temperature of PCM is uniform.
- Phase change during melting/solidification occurs in a temperature interval.
- PCM is homogeneous and isotropic.

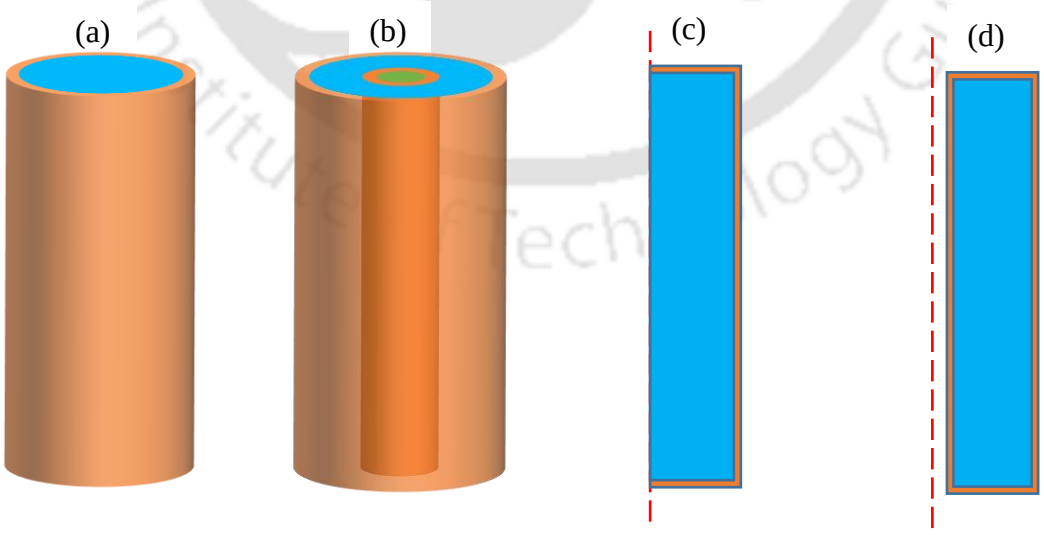

Fig. 5.1 Schematic of (a) basic and (b) novel capsules, 2D axisymmetric view of (c) basic and (d) novel capsules.

Table. 5.1 Thermo-physical properties of sodium nitrate and SS304.

Properties	**Sodium Nitrate**		**SS304**
ρ (kg m^{-3})	2130 (solid)	Bauer et al. (2012)	8000
	1908 (liquid)		
L_F (J kg^{-1})	178,000		-
μ (Pa s)	$0.0119 - 1.53 \times 10^{-5} T$	Janz et al. (1979)	-
T_M (°C)	306		-
C_P (J kg^{-1} K^{-1})	$444.53 + 2.18 T$	Lan and Kou (1991)	500
β (K^{-1})	6.6×10^{-4}		-
k (W m^{-1} K^{-1})	$0.3057 + 4.47 \times 10^{-4} T$	White and Davis (1967)	16.2

5.3 Results and discussions

In the following sub-sections, validation, grid independent test and various numerical results obtained from the simulations of the basic and novel encapsulated LHS capsules during charging and discharging processes are presented. The parametric studies are carried out by fixing the initial average temperature of the PCM as 291 / 321 °C during the charging/discharging process. Similarly, at any time (t > 0), the boundary of the capsule is given a constant temperature of 321 / 291 °C during charging/discharging process, which makes a temperature difference of 30 °C between the PCM and the capsule boundary.

5.3.1 Model validation

To ensure reliability on the numerical predictions, their results must be validated with the real–time experimental data. A shell-and-tube type LHS model with the same governing equations was already developed and validated with the lab-scale experimental results (Presented in chapter 3). Additionally, the numerical results obtained for the melt fraction of storage capsule were compared with the melt fraction values reported by Assis et al. (2007). The physical model chosen for the validation, thermo-physical properties of the PCM and initial and boundary conditions of the model are taken from the literature (Assis et al., 2007). Fig. 5.2 shows the comparison between the experimental and numerical data. The PCM and shell material considered for validation of the numerical model are RT 27 and glass. The PCM initial temperature and the capsule boundary temperature taken for the simulation are 23 °C and 40 °C. It is evident from Fig. 5.2 that the current numerical results showed a good agreement with the experimental results.

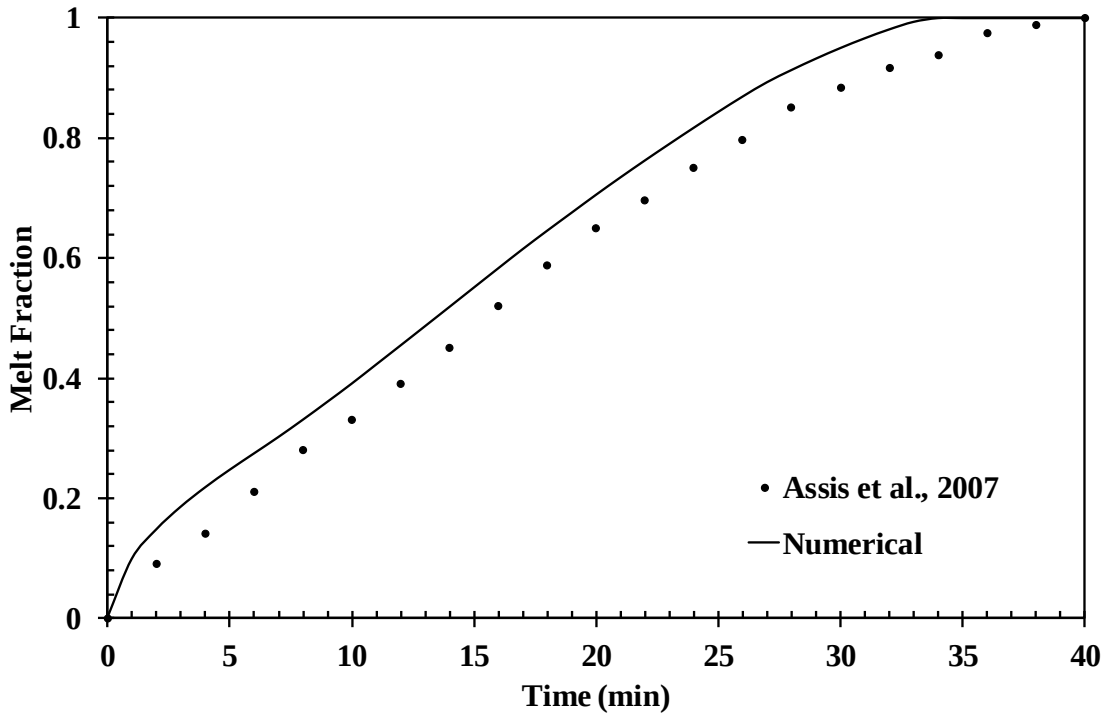

Fig. 5.2 Numerical model validation (Assis et al., 2007).

5.3.2 Grid independent test

The variation of the number of mesh elements has a major control in the numerical results of all models. To test the dependency of numerical results on the number of mesh elements, simulations with different mesh element sizes were run for charging and discharging processes. Fig. 5.3(a) and (b) shows the average temperature variation of the basic LHS capsule with a different number of mesh elements *viz*. 10283, 12127 and 14062 elements for charging process and 7487, 9414 and 11349 for discharging processes. Convergence issues were found for the developed model with mesh elements lesser than 10283 and 7487 for charging and discharging processes. It can be understood from the number of mesh elements that the charging/melting simulation demands more number of mesh elements than the discharging/solidification simulation, due to the free convective movement of the PCM. It is observed from Fig. 5.3(a) and (b) that the models with 12127 and 9414 elements are found to be grid independent for the charging and discharging processes. Similarly, grid independent test was conducted for the novel LHS capsule and model with 20770/14922 elements is found to be grid independent for the charging/discharging process.

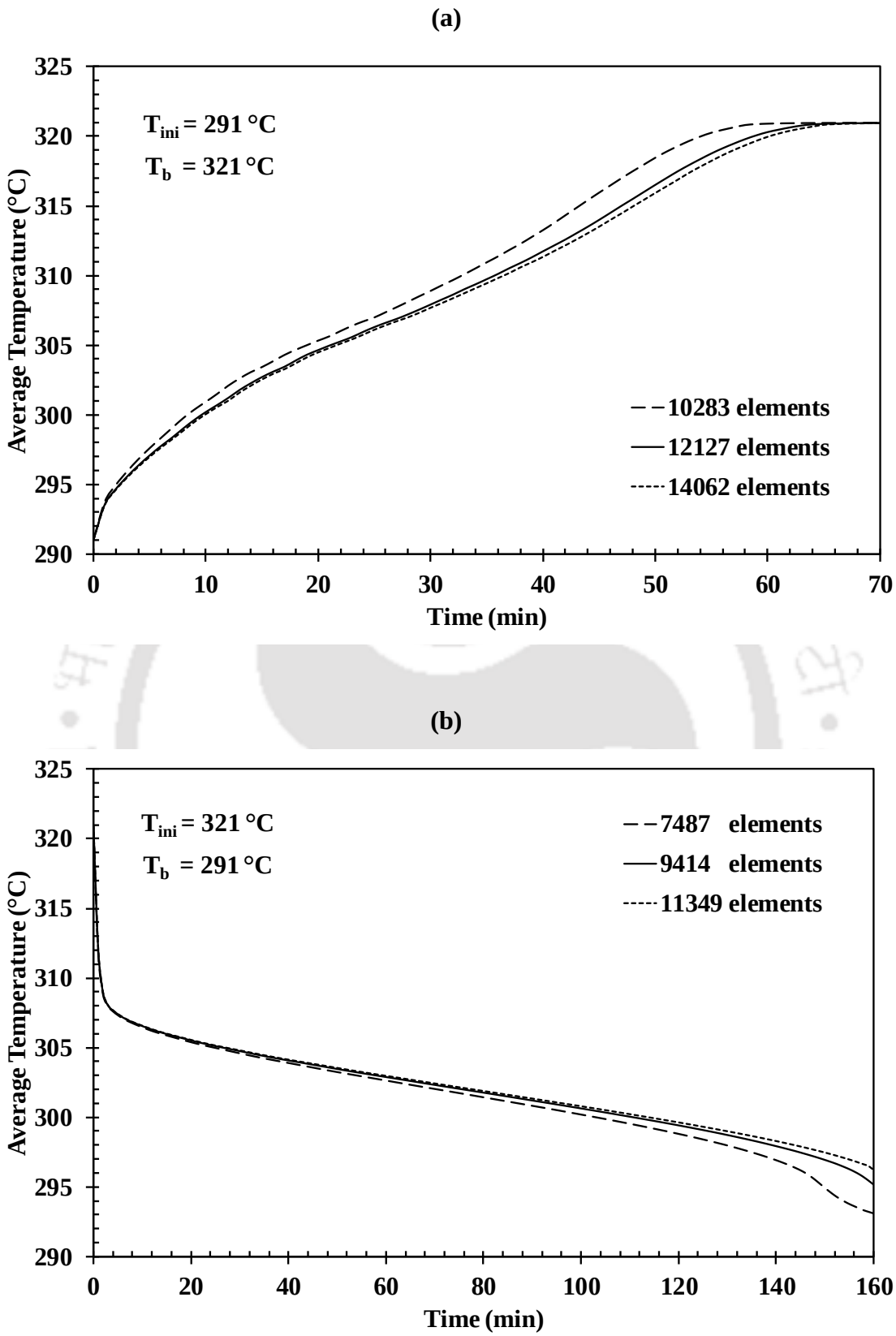

Fig. 5.3 Grid independent test of basic capsule (a) charging and (b) discharging.

5.3.3 Temperature variation

Fig. 5.4(a) and (b) shows the average temperature variation of the basic and novel LHS capsules during the charging and discharging processes. The average temperature is the volumetric average temperature of all the mesh elements of the numerical model. It can be noted from Fig. 5.4(a) and (b) that the initial part of the average temperature variation curve shows a steady increase/decrease in temperature during the charging/discharging process. This steady increase/decrease is due to the higher heat transfer potential available during the initial period of the processes. After a certain period, the slope of the temperature variation curve started reducing. During this time, LHS capsules store/discharge a large amount of latent heat. It can be observed from Fig. 5.4(a) and (b) that the increasing/decreasing rate of average temperature is higher in the case of novel capsule than the basic capsule. This is due to two reasons viz., increased surface area available for heat transfer and reduced thickness of the PCM layer in the novel capsule. The basic/novel capsule took about 65 / 39 min to reach an average temperature of 321 °C (a temperature increase of 30 °C) during the charging process. Similarly, it took about 156 / 61 min for the basic/novel capsule to reach an average temperature of 296 °C (a temperature difference of 25 °C). The increase of PCM temperature during charging is faster than the decrease of PCM temperature during discharging. This is mainly due to the additional convective heat transfer present in the charging process that increases the overall heat transfer rate of the capsule. Moreover, it can be noted from Fig. 5.4(b) that the decrease in the temperature of the PCM in both the capsules during the start of discharging is much rapid, which is even faster than the temperature increase during charging. This is due to the higher thermal conductivity of the liquid PCM. The thermal conductivity of the PCM increases in a linear fashion with respect to the temperature as given in Table. 5.1.

5.3.4 Charging / discharging time

Fig. 5.5(a) and (b) depicts the average melt fraction variations of the basic/novel LHS capsules during the charging/discharging process. Average melt fraction is the volumetric average melt fraction of all the mesh elements of the numerical model. Melt fraction is a critical performance parameter, which depicts only the latent heat storage/discharge characteristics during the charging/discharging process. It can be seen from Fig. 5.5(a) and (b) that the charging / discharging time of the novel capsules is lesser than the basic capsules. It took about 64 / 33 min and 158 / 57 min for the basic/novel capsules for complete charging (for storing a latent heat of 0.5 MJ) and discharging (for discharging a latent heat of 0.5 MJ). The reduction in the

charging/discharging time achieved by the novel capsule when compared with the basic capsule is about 48.4 / 63.9 %.

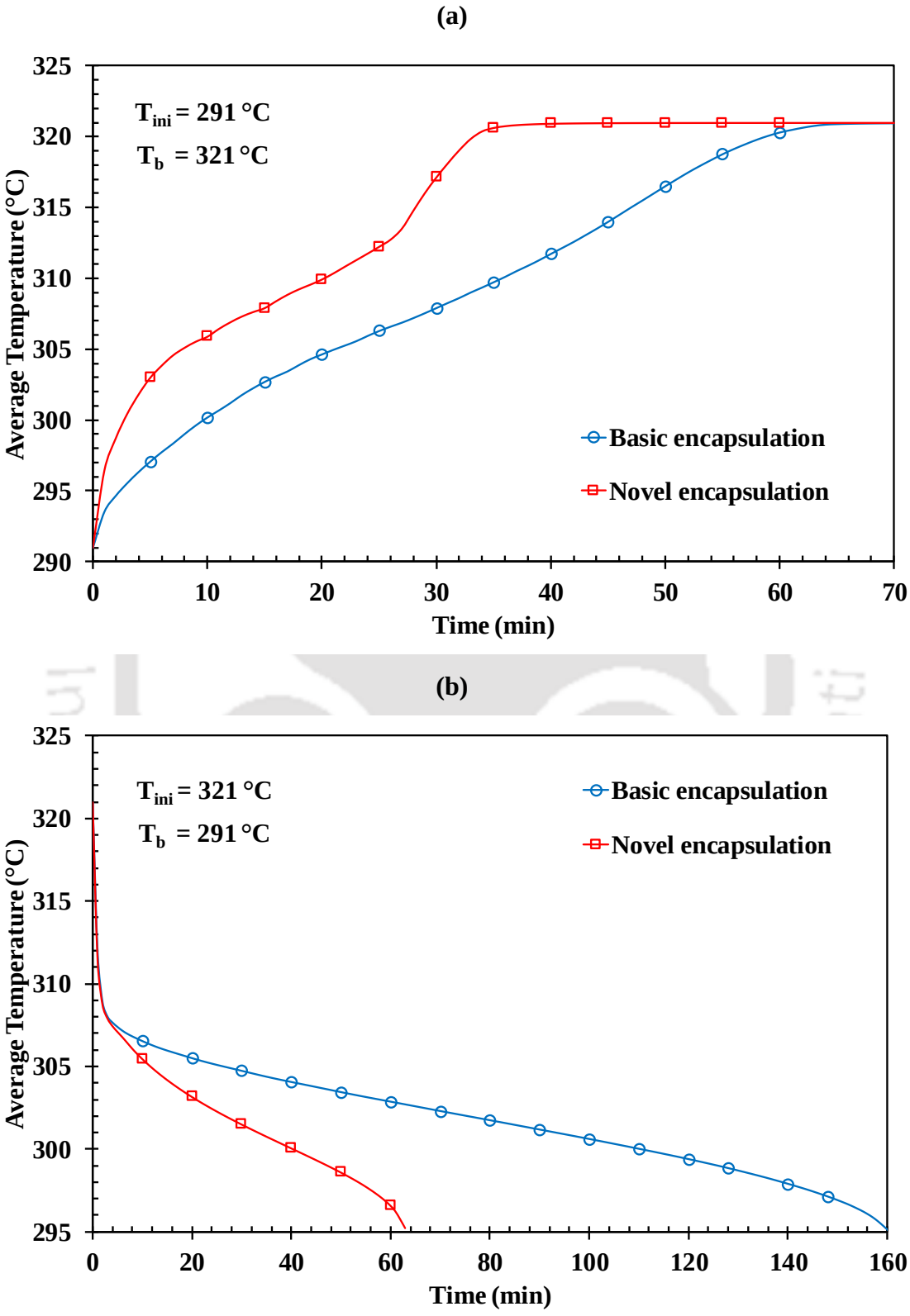

Fig. 5.4 Average temperature variation of the LHS capsules during (a) charging and (b) discharging.

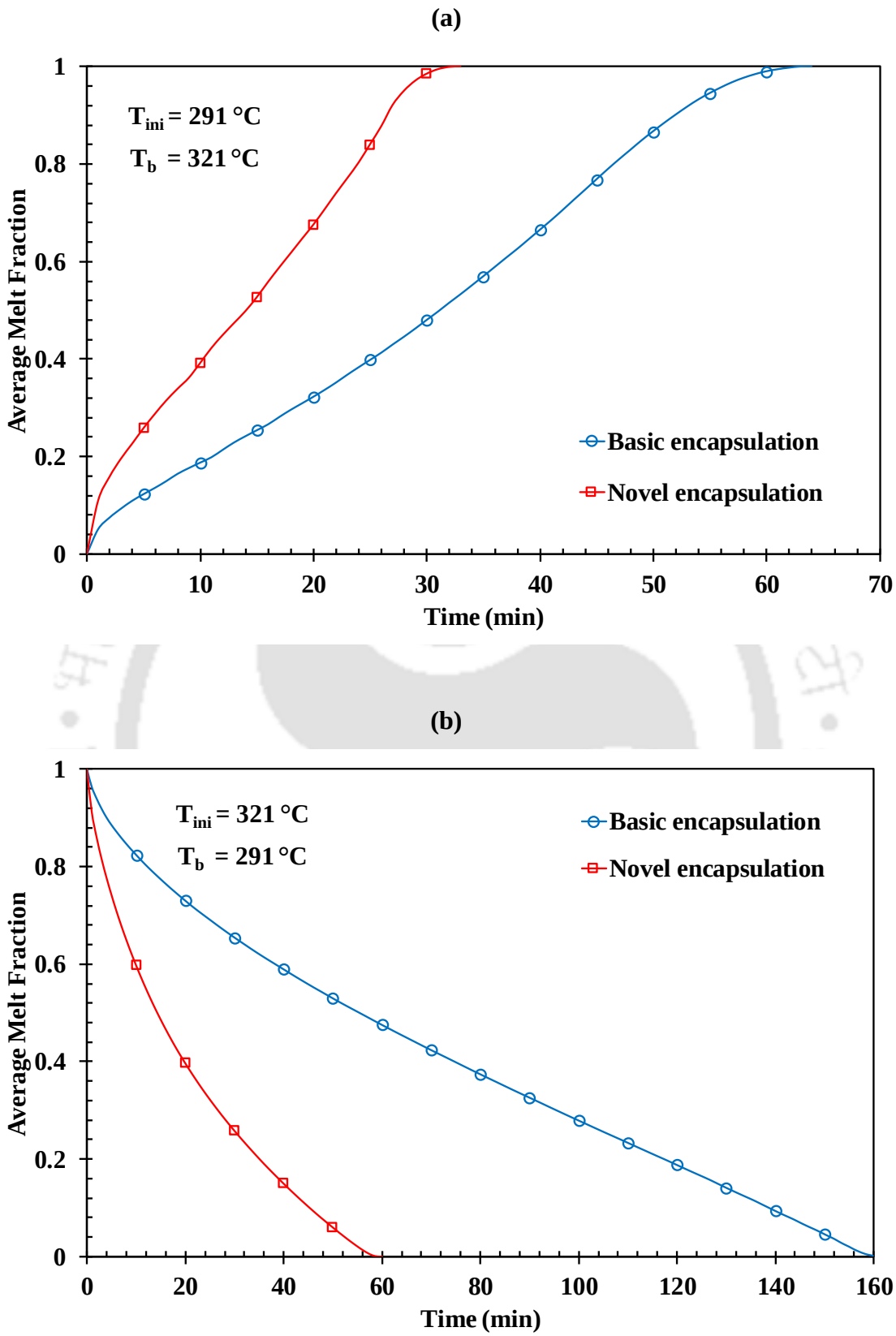

Fig. 5.5 Average melt fraction variation of the LHS capsules during (a) charging and (b) discharging.

5.3.5 Melt fraction

Fig. 5.6(a–d) shows the melt fraction contours of the LHS capsules during the charging and discharging processes. It can be seen from Fig. 5.6(a–d) that the average melt fraction of the LHS capsules is 0 / 1 at the start of the charging/discharging process (t = 0 min). At time t = 30 min, it can be seen that the basic/novel capsule is partially/almost-fully charged during the charging process. The effect of natural convection can be seen in the basic capsules clearly during the charging process (t = 30 min, 45 min) from the asymmetric variation of the melt fraction. The basic capsule is also completely charged at about 65 min. At time t = 50 min, the novel capsule has only left few molten PCM to solidify during the discharging process. However, in the basic capsule at the same time, the region near to the boundary of the capsule only was solidified. It can also be noted that the asymmetric melt fraction variation is not noticeable in the discharging process as it is a conduction-dominated process. The basic capsule is also completely discharged at about 160 min.

5.3.6 Energy storage / discharge rate

Fig. 5.7(a) and (b) illustrates the variation of total energy storage/discharge rate of the LHS capsules during the charging and discharging processes. The total energy stored/discharged in/from the PCM is calculated using the Eq. (3.13 / 3.16). Initially, the PCM stores/discharges the heat in the form of sensible heat. Once it reaches the phase change temperature, it stores/discharges the heat in the form of latent heat. Similarly, after phase change of PCM, heat is stored/discharged in the form of sensible heat again. The amount of heat stored in the basic/novel capsule during the charging process at the corresponding charging time of 64 / 33 min is about 0.63 MJ. This stored energy includes the latent heat of 0.5 MJ and the sensible heat of 0.13 MJ. Similarly, the total heat discharged from the basic/novel capsule during the discharging process at the corresponding discharging time of 158 / 57 min is about 0.61 MJ. It can be noted from Fig. 5.7(a) and (b) that the novel encapsulated capsule yields a faster energy storage/discharge than the basic encapsulated capsule.

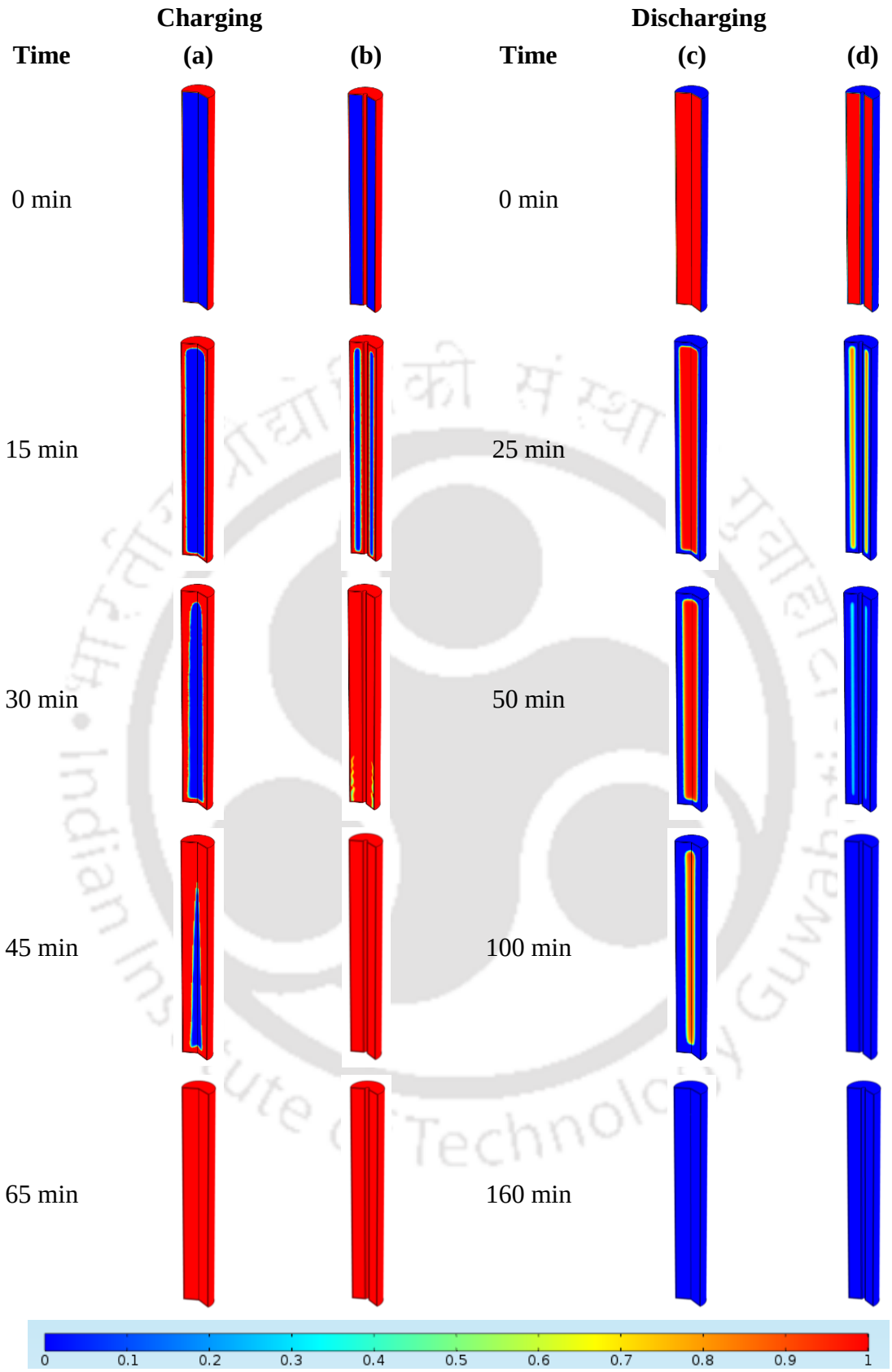

Fig. 5.6 Melt fraction contours of the LHS capsules (a & c) basic encapsulation, (b & d) novel encapsulation.

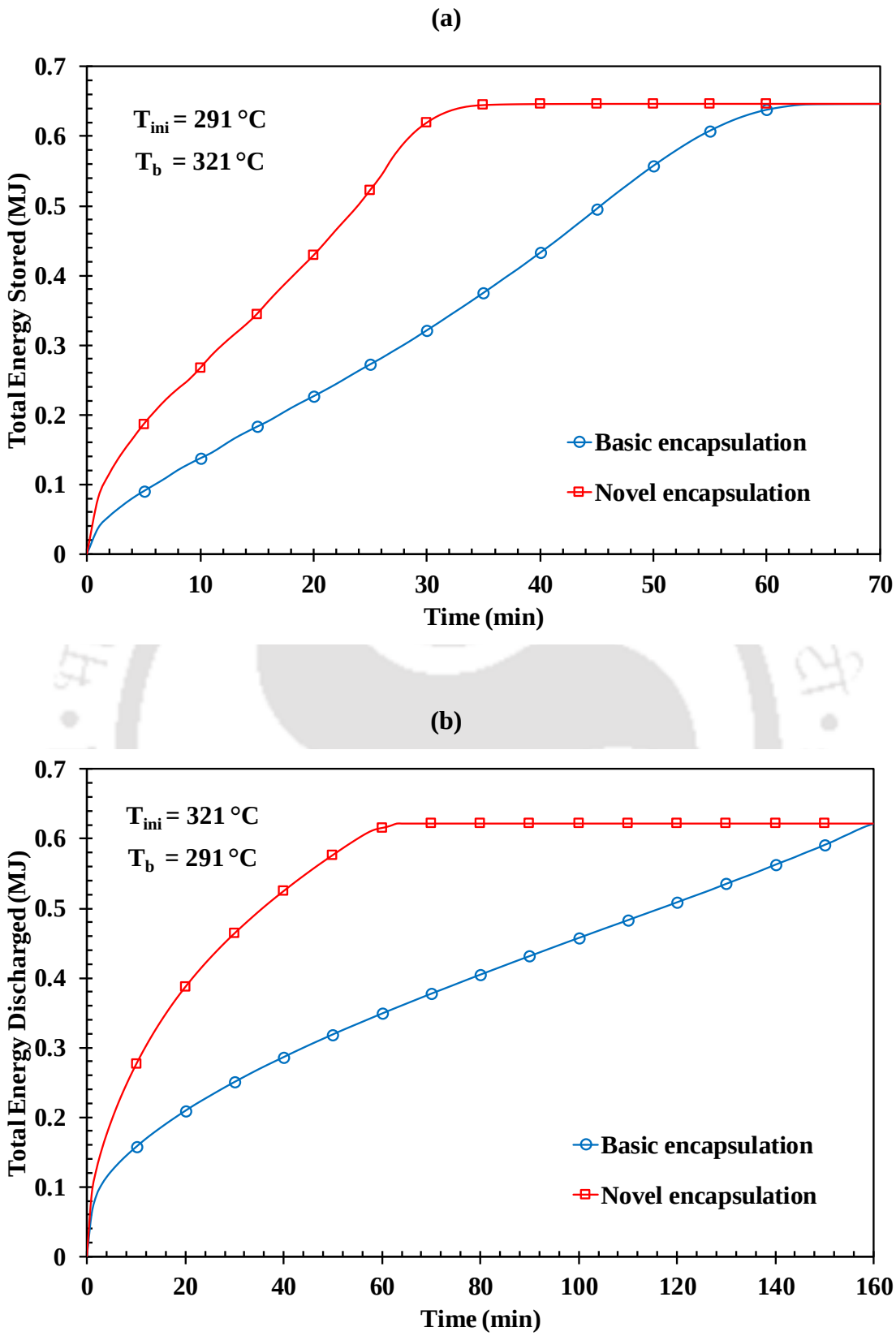

Fig. 5.7 Energy storage/discharge rate of the LHS capsules during (a) charging and (b) discharging.

5.3.7 Effect of operating temperature range

The operating temperature range of the storage capsules also influences the performance of the system due to the temperature dependence of the thermo-physical properties of the PCM. Hence, for studying this, three different temperature ranges (296 / 316 °C, 291 / 321 °C, 286 / 326 °C) with a temperature difference of 20 °C, 30 °C and 40 °C between the PCM and the capsule boundary are chosen. The charging and discharging time of basic/novel capsule for the three-temperature ranges are given in Table. 2. Fig. 5.8(a) and (b) graphically shows the influence of the operating temperature on the charging and discharging rate of the LHS capsules. It can be seen from Fig. 5.8(a) and (b) that the model with a higher temperature difference yields a lesser charging and discharging time. This is due to the higher heat transfer potential available in the model. One more important observation on the novel capsule can be inferred is that the novel capsule with the least temperature difference (20 °C) itself charges/discharges faster than the basic capsule with a higher temperature difference (30 / 40 °C).

Table. 5.2 Charging and discharging time of the capsules for different temperature ranges.

Temperature range (°C)	**Temperature difference (°C)**	**Charging time (min)**		**Discharging time (min)**	
		basic	novel	basic	novel
296 / 316	20	99	53	223	83
291 / 321	30	64	33	158	57
286 / 326	40	45	27	124	44

5.3.8 Commercial viability of the novel concept

Any novel concept to be commercialized should possess strong benefits over the conventional existing concept. The novel encapsulation technique proposed in the present study has three potential advantages over the basic encapsulation technique, which will be discussed in the forthcoming sub-sections.

(i) Better storage performance while upscaling the LHS capacity.

(ii) Effective space utilization with less volume occupancy.

(iii) Lesser encapsulation shell cost/mass with reduced capsule material.

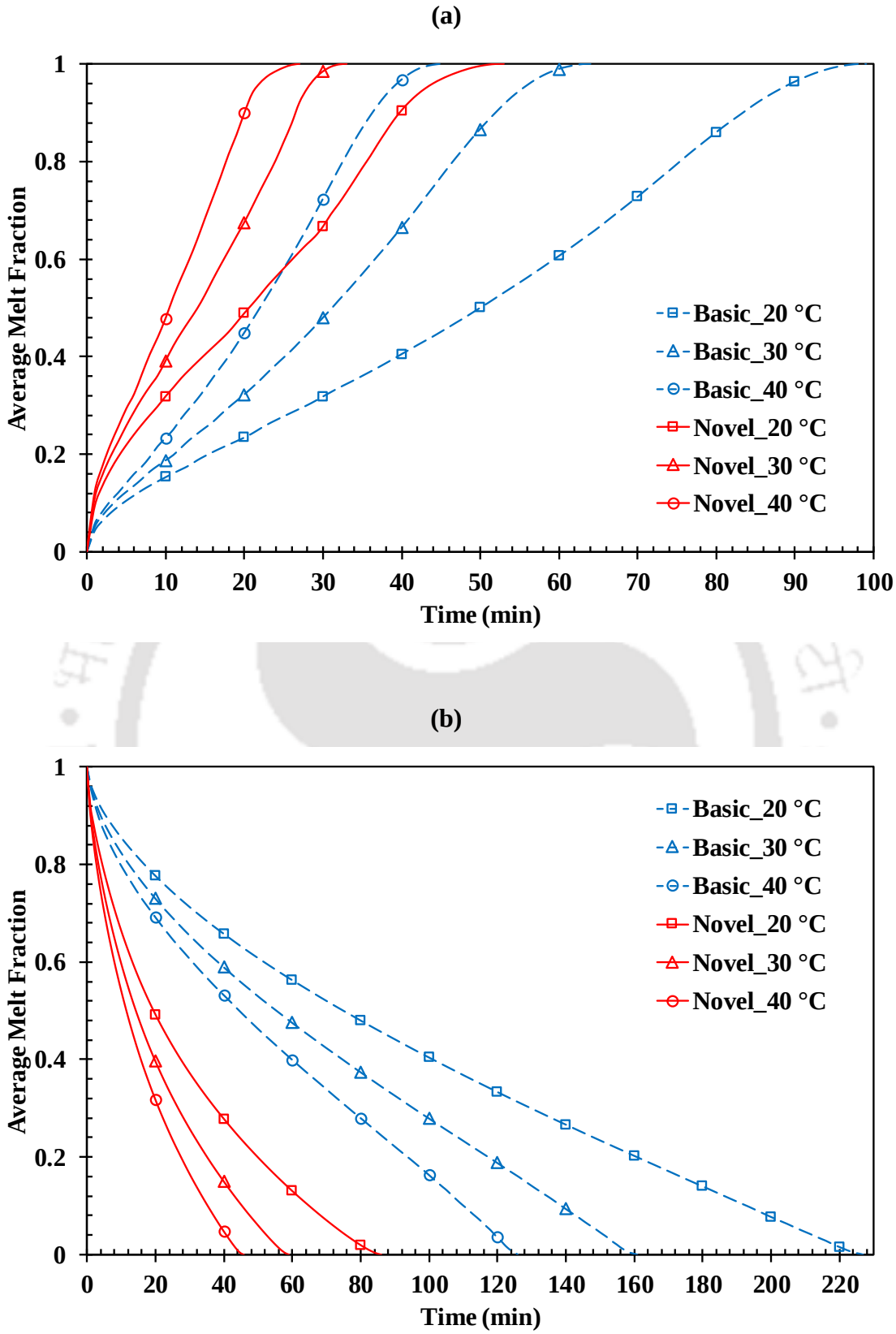

Fig. 5.8 Effect of operating temperature range in the LHS capsules during (a) charging and (b) discharging.

5.3.8.1 Upscaling

Fig. 5.9(a) and (b) depicts the influence of upscaling of the storage device on the charging and discharging rate of the LHS capsules. Three different LHS capacities namely 0.5 MJ, 1.0 MJ and 1.5 MJ are studied for the storage performance of the basic/novel capsule during the charging and discharging processes. The height of the capsules for all the three cases is the same (0.5 m) and hence the capsules differ only in the diameter. It is obvious that the capsules with a lesser storage/discharge capacity yield a lesser charging/discharging time as seen from Fig. 5.9(a) and (b). The charging and discharging time of the basic/novel capsule for the three different LHS capacities are tabulated in Table. 5.3. It can be observed from the Table. 5.3 that the novel capsule having 1.0 MJ LHS yields lesser charging time than the basic capsule with 0.5 MJ. The reduction in the charging and discharging time achieved by the novel capsule (1 MJ capacity) when compared with the basic capsule (0.5 MJ capacity) are 4.7 % and 19 %.

Table. 5.3 Charging and discharging time of the capsules for different LHS capacities.

LHS capacity	**Charging time (min)**		**Discharging time (min)**	
(MJ)	basic	novel	basic	novel
0.5	64	33	158	57
1.0	100	61	313	128
1.5	131	84	455	204

5.3.8.2 Less volume occupancy

As it is already clear from the sub-section 5.3.8.1 that the storage performance of 1.0 MJ novel capsule is better than the 0.5 MJ basic capsule, it is wise to compare the volume occupancy of one novel capsule with two basic capsules. The volume occupied by the basic/novel capsule to store 1.0 MJ heat is 0.00331 / 0.00337 m^3. The reduction in the volume of the novel capsule when compared with the basic capsule is only 1.8 % only. However, a fair decision can be made when it is compared for a certain higher storage capacity with many capsules arranged in a staggered way. Hence, an LHS capacity of 19 MJ is considered here for comparison due to the possibility of the symmetric arrangement of the 38/19 basic/novel capsules in both circular and rectangular fashions. Fig. 5.10 shows the arrangement of basic/novel capsules in circular and rectangular forms.

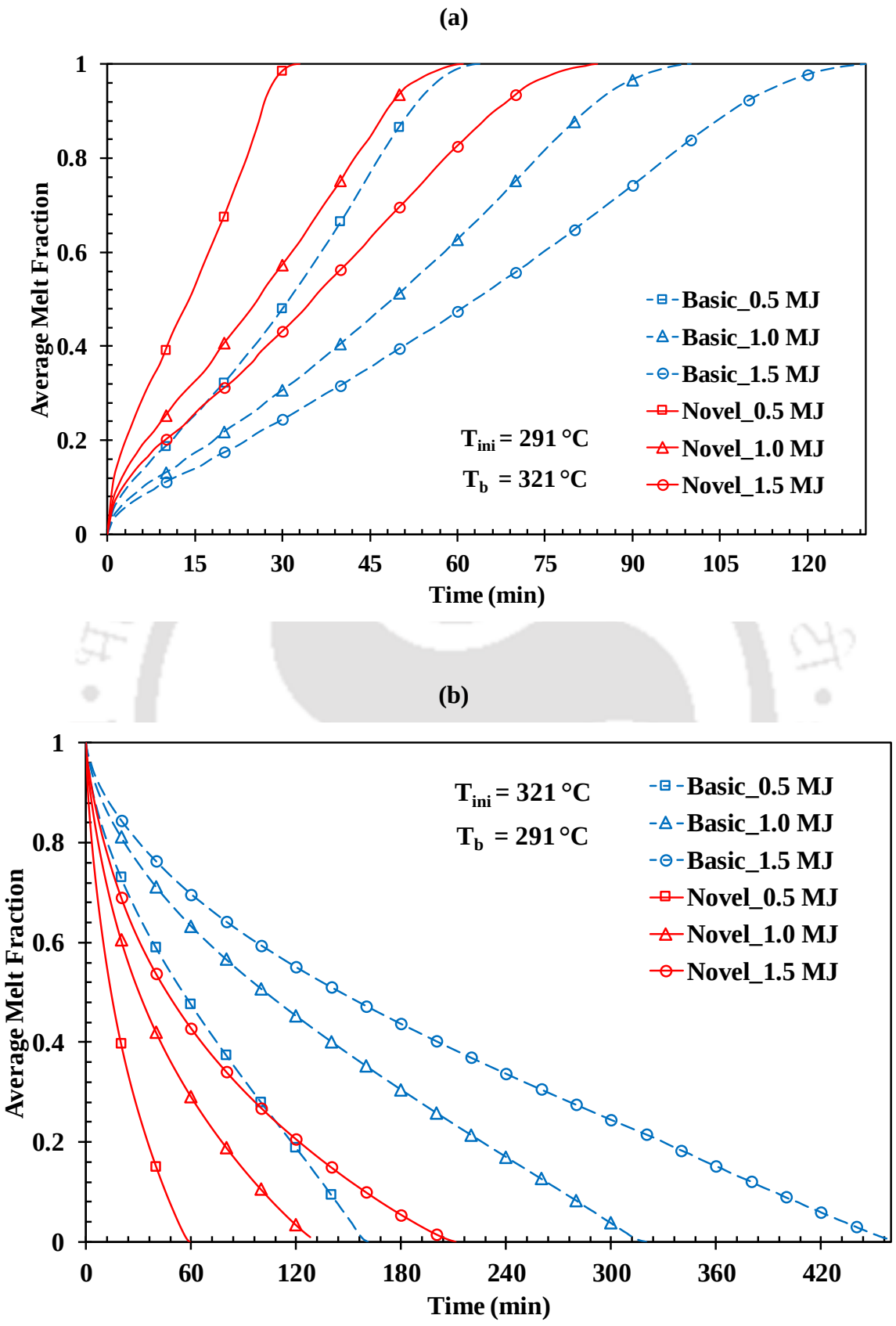

Fig. 5.9 Effect of upscaling in the LHS capsules during (a) charging and (b) discharging.

Two collocated plate type structures are used for the physical support of the encapsulated capsules. The bulk volume of the capsules with the support plates for the four arrangements is given in Table. 5.4. It is observed from Table. 5.4 that the percentage reduction of volume in the novel capsules when compared with the basic capsules is 5.1 / 3.0 in the circular/rectangular arrangement. Overall, the novel capsules arranged in the rectangular fashion occupies the least volume. Although the percentage reduction of volume is lesser in using the novel capsule when compared to the basic capsule, the charging/discharging rate reduction is much higher as explained in the sub-section 5.3.8.1.

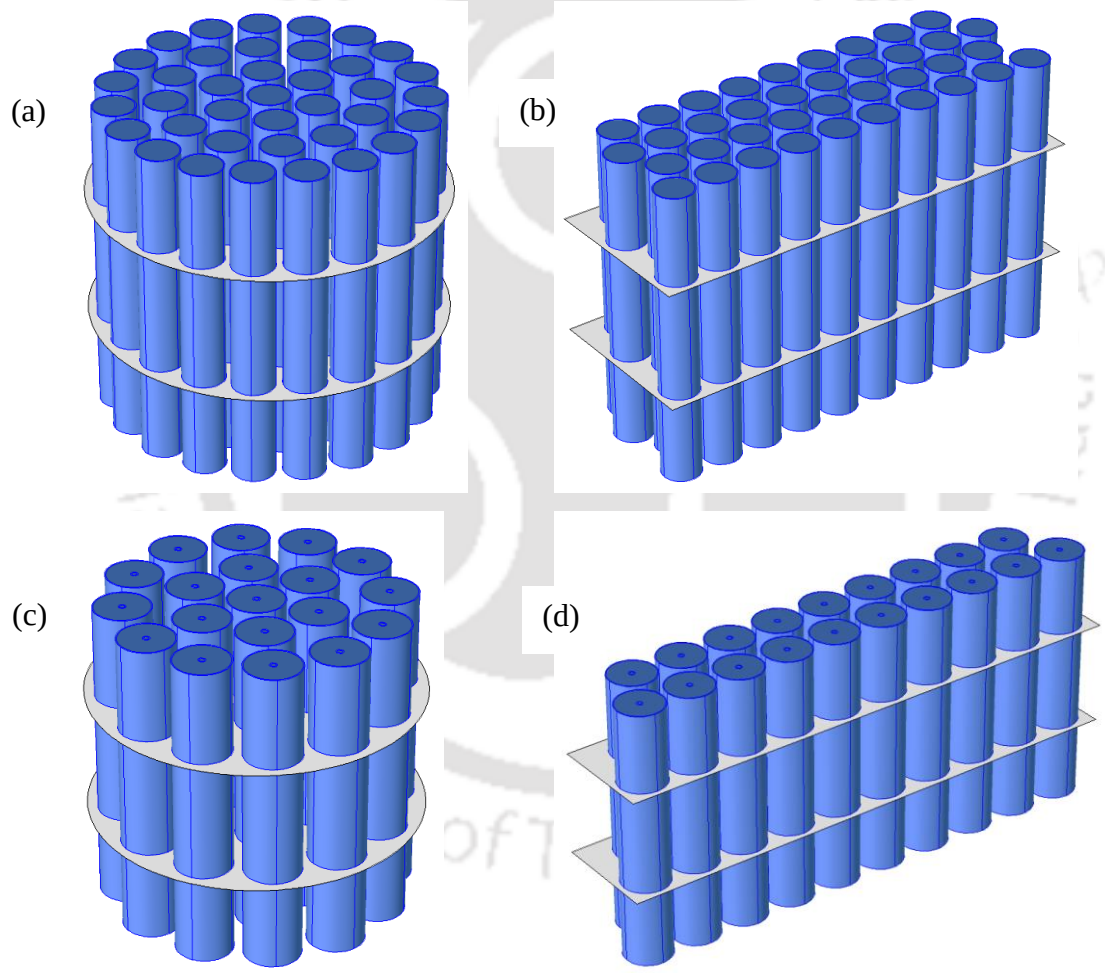

Fig. 5.10 Volume occupancy of basic capsule in (a) circular and (b) rectangular arrangement and novel capsule in (c) circular and (b) rectangular arrangement.

Table. 5.4 Bulk volume of basic/novel capsules in circular and rectangular forms.

Capsule	Arrangement of capsules	Bulk volume (m^3)	% reduction of volume
Basic	Circular	0.11057	5.1
Novel		0.11621	
Basic	Rectangular	0.10793	3.0
Novel		0.10466	

5.3.8.3 Lesser capsule material requirements

The mass of the encapsulation shell is also an important parameter to consider in the commercial LHS system with many capsules, as it is directly linked to the encapsulation material costs. Similar system of 38 / 19 basic/novel capsule having the storage capacity of 19 MJ is chosen to compare the mass of the required encapsulation material. The mass of SS304 needed for the basic/novel capsule is about 60.8 / 47.8 kg. Hence, a mass reduction of approximately 21.4 % can be achieved with the novel capsule when compared with the basic capsule in the current study.

5.4 Summary

A novel encapsulation technique is proposed for better heat transfer in LHS capsules. The storage performance of the novel capsule is studied using a numerical model. The same numerical model is used to compare the heat transfer characteristics of the basic and novel capsules. It is found from the numerical study that it took about 64 / 33 min and 158 / 57 min for the basic/novel capsules for complete charging and discharging. The reduction in the charging/discharging time achieved by the novel capsule when compared with the basic capsule is about 48.4 / 63.9 %. The scope for commercial viability of the novel concept is also explored and the results showed a positive step towards the commercialization of the novel concept.

Chapter 6

Novel Fin

6.1 Preface

Due to the low thermal conductivity of the PCM, the LHS technology has not yet commercialized to its fullest capability. Many heat-transfer enhancement techniques were studied by several researchers to improve the heat transfer of the LHS system (Kurnia et al., 2013; Li et al., 2013; Rathod and Banerjee, 2015). However, each of the techniques put forward has its own pros and cons. The disadvantages of certain major heat-transfer enhancement techniques are discussed below:

- Sprinkling of high thermal conductivity metallic particles – the metallic particles settle down due to its high density after repeated charging and discharging cycles.
- Extended heat transfer surfaces (fins) – materials having high corrosion resistance and high/moderate thermal conductivity are suitable for heat transfer enhancement in LHS systems. Materials having these properties (eg: stainless steel) are denser and hence the total weight of the system becomes high.
- Usage of multiple PCMs – proper selection of the PCMs for achieving better utilization of the heat of HTF requires extensive numerical or experimental studies with different PCMs at all the desired operating conditions.

In this chapter, a novel fin is proposed to increase the heat transfer in the LHS devices. Fig. 6.1 depicts the schematic of the tube-in-tube LHS module and the inner tube with and without novel/standard fins. The novel fin proposed here is half of the standard fin cut diagonally. This will reduce the weight and cost of the fin material by a factor of 0.5 and thereby makes the

LHS system lightweight and cost-effective. For comparing the performance characteristics of the standard and proposed novel technique, tube-in-tube modules having a LHS capacity of 0.5 MJ are considered. Sodium nitrate, air and SS304 are selected as the PCM, HTF and HTF tube, respectively. The thermo-physical properties of sodium nitrate and SS304 are given in Table. 5.1. The length of the LHS modules is fixed as 0.5 m. The height and width of the fin are 10 mm and 2 mm in the standard fin configuration. The design of LHS modules is made in such a way that the volume of PCM in all the configurations are same.

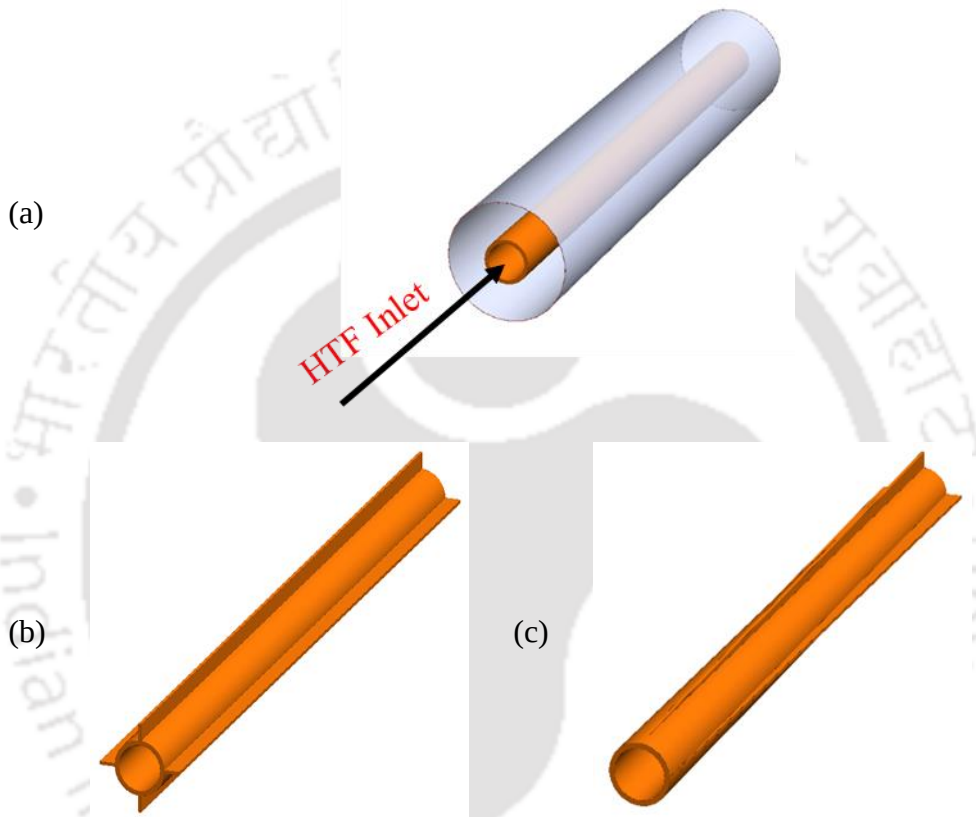

Fig. 6.1 Schematic of (a) tube-in-tube LHS module (b) inner tube with standard fin and (c) inner tube with novel fin.

6.2 Model description

The LHS unit is a regenerative type heat exchanger, which absorbs/releases heat by passing the hot/cold HTF, respectively through the tube. During the charging cycle, high-temperature HTF is supplied from one side of the model to exchange the heat through convection to the HTF tube, and this heat is further conducted to the PCM. During the discharging cycle, cold HTF is passed from the same side, which extracts the stored heat from the PCM. To study the thermal storage behavior of the tube-in-tube LHS module, four physical processes have to be simulated i.e. HTF flow, conduction, convection, and phase change. As the present model is a

simplified form of the shell-and-tube model explained in Chapter 3, the same assumptions mentioned in the section 3.4 is applicable for the current model. The governing equations explained in the section 3.5 is used here for predicting the heat transfer characteristics of the tube-in-tube LHS modules with and without standard and novel fins. Similarly, the performance parameters that are involved in evaluating the storage characteristics of the LHS modules are already explained in the section 3.6. The outer surface of the LHS model is given adiabatic condition.

6.3 Results and discussions

In the following sub-sections, the numerical results obtained from the simulations of the tube-in-tube LHS modules with or without standard and novel fins are presented. The parametric studies are carried out by fixing the initial average temperature of the PCM as 291 / 321 °C during the charging/discharging process. Similarly, at any time (t > 0), the HTF at a constant temperature of 321 / 291 °C is allowed to pass through the inner tube at a velocity of 2 m/s during the charging/discharging process, which makes an initial temperature difference of 30 °C between the initial temperature of PCM and HTF inlet temperature.

6.3.1 Temperature variation

Fig. 6.2(a) and (b) shows the comparison of the average temperature variation of the tube-in-tube LHS module with no fin, standard fin and novel fin during the charging and discharging processes. PCM kept in the modules is initially in the solid/liquid state at 291 / 321 °C during the charging/discharging process. When the HTF at 321 / 291 °C and velocity of 2 m/s is allowed to pass through the inner tube, heat transfer takes place between the fluid and PCM and the heat gets stored/discharged in/from the PCM in the form of sensible and latent heat. It is inferred from Fig. 6.2(a) and (b) that the increase/decrease of average temperature during the charging/discharging process is faster in LHS module having standard fin than that of no fin and novel fin, initially. This is due to the higher surface area available for heat transfer. But after a certain period of time, say t = 360 min, the increase/decrease of average temperature is faster in LHS module having novel fin than that of other two cases. The reason for this is the configuration of the novel fin, wherein the heat transfer area is more in the less heat transfer potential region, i.e. near the outlet portion of the model.

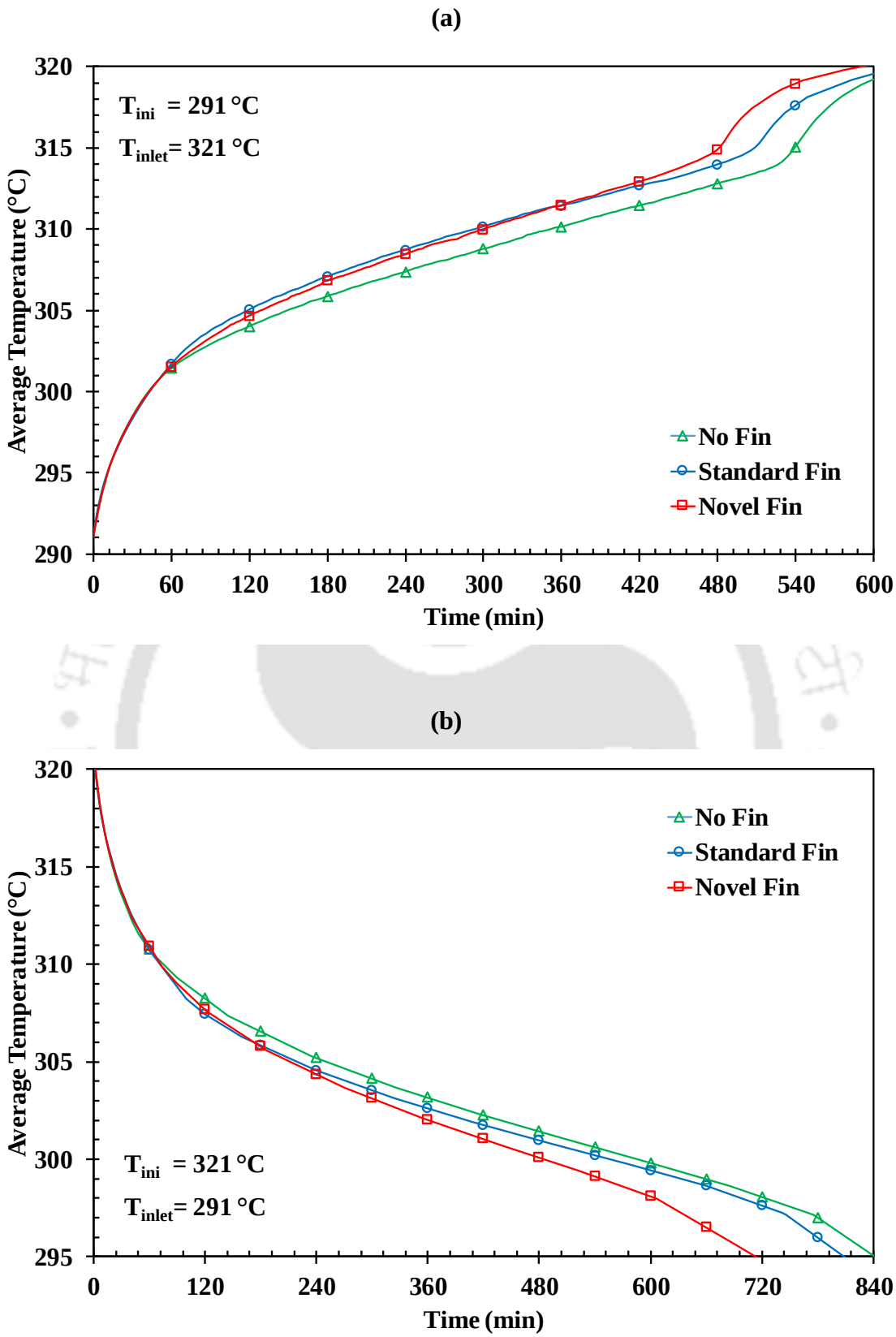

Fig. 6.2 Average temperature distribution of tube-in-tube modules with no fin, standard fin and novel fin during (a) charging and (b) discharging.

6.3.2 Charging / discharging time

Fig. 6.3(a) and (b) depicts the comparison of average melt fraction variation of the LHS modules with no fin, standard fin and novel fin during the charging and discharging processes. It can be noted from Fig. 6.3(a) and (b) that the charging/discharging time of the LHS module with novel fin configuration is lesser than that with no fin and standard fin configurations. It takes about 548 / 788 min, 514 / 742 min and 487 / 665 min for complete charging/discharging of the LHS module with no fin, standard fin and novel fin. It can be noted that the charging/discharging time has decreased by about 11.1 / 15.6 % and 5.25 /10.4 % when using novel fin configuration with respect to no fin and standard fin configurations.

6.3.3 Energy storage / discharge rate

Fig. 6.4(a) and (b) show the variation of total energy storage/discharge rate of the LHS modules during the charging and discharging processes. The total energy stored/discharged in/from the PCM is calculated using the Eq. (3.13 / 3.16). The amount of heat stored in the LHS module with no fin / standard fin /novel fin during the charging process at the corresponding charging time of 548 / 514 / 487 is about 0.63 MJ. This stored energy includes the latent heat of 0.5 MJ and the sensible heat of 0.13 MJ. Similarly, the total heat discharged from the LHS module with no fin / standard fin /novel fin during the discharging process at the corresponding discharging time of 788 / 742 / 665 min is about 0.61 MJ. It can be noted from Fig. 6.4(a) and (b) that the tube-in-tube LHS module with the novel fin configuration yields a faster energy storage/discharge than that with standard fin configuration.

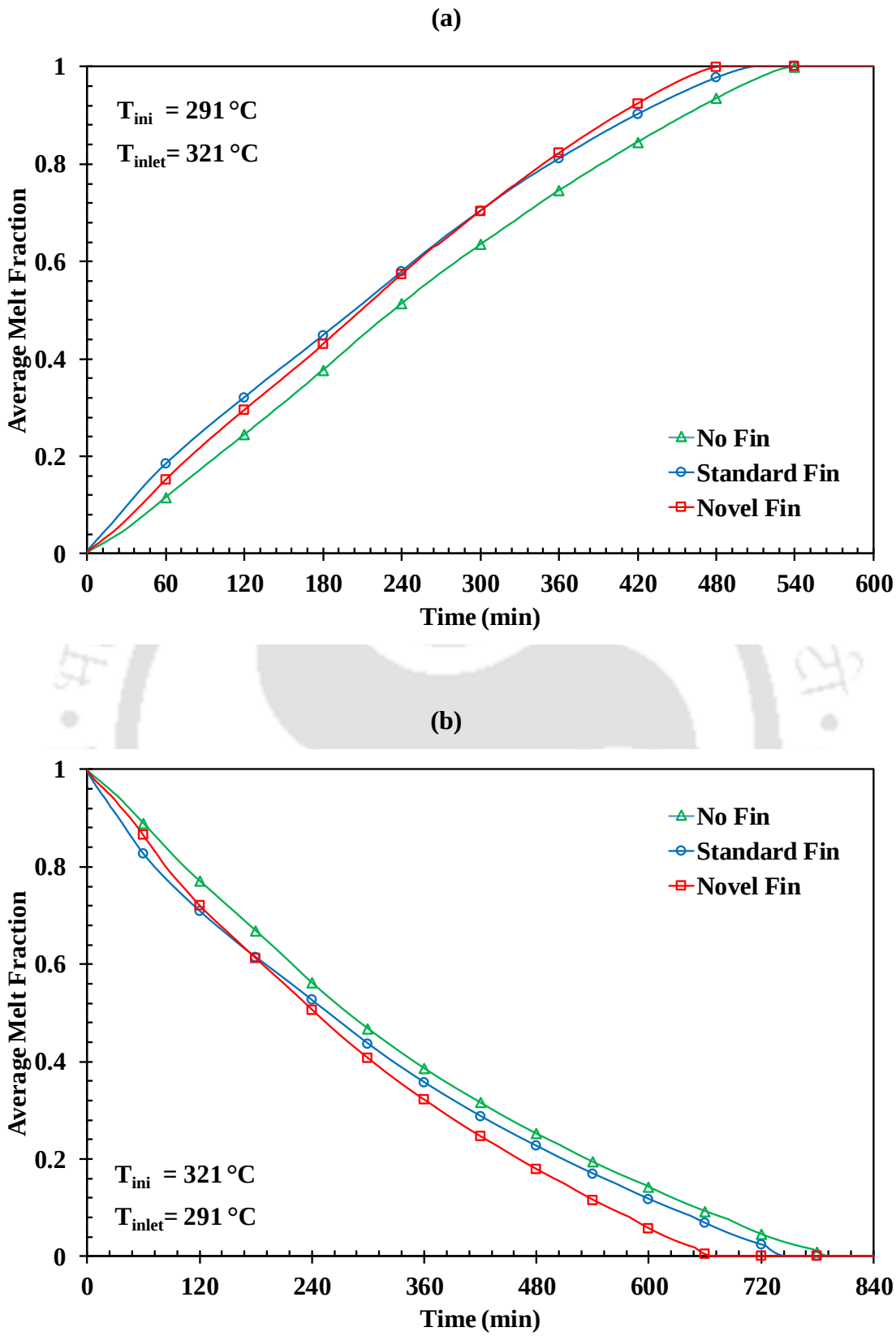

Fig. 6.3 Average melt fraction distribution of tube-in-tube modules with no fin, standard fin and novel fin during (a) charging and (b) discharging.

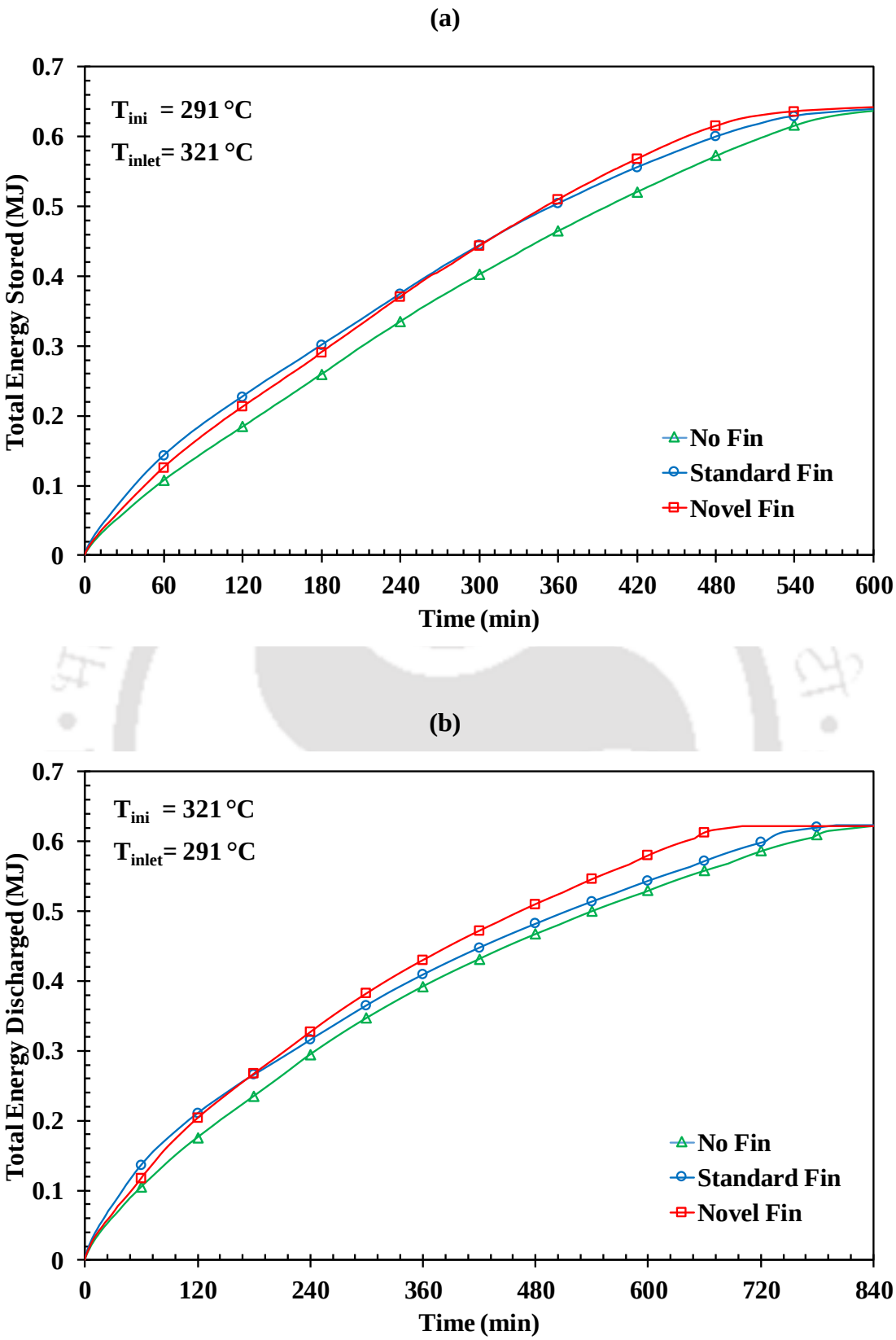

Fig. 6.4 Energy storage/discharge rate variation of tube-in-tube modules with no fin, standard fin and novel fin during (a) charging and (b) discharging.

6.4 Summary

A novel fin is proposed for effective heat transfer in tube-in-tube LHS devices. The storage performance of the novel fin is studied using a numerical model. The same numerical model is used to compare the heat transfer characteristics of the novel fin configuration with no fin and standard fin configurations. It is found from the numerical study that LHS module takes about 548 / 788 min, 514 / 742 min and 487 / 665 min for complete charging/discharging for the cases with no fin, standard fin and novel fin. It can be noted that the charging/discharging time has decreased by about 11.1 / 15.6 % and 5.25 /10.4 % when using novel fin configuration with respect to no fin and standard fin configurations. The novel fin proposed has also an additional advantage of weight and cost reduction of fins by a factor of 0.5.

Chapter 7
Conclusions and Future Scope

The major conclusions drawn from the numerical and experimental studies on the lab-scale LHS prototype are presented in this chapter. A summary of the key outcomes arrived in the numerical studies of the novel encapsulation and novel fin are also presented in this chapter.

7.1 Lab scale prototype

The performances of a lab-scale shell-and-tube type LHS prototype during charging and discharging processes were studied both numerically and experimentally. The numerical study was performed initially for the 2D shell-and-tube model for optimizing the number of HTF tubes and fins. Effective heat capacity method was employed in the model to integrate the latent heat of the PCM with the specific heat. Boussinesq approximation was used in the model to incorporate the buoyancy effect of the molten layer of the PCM. For proper modeling of velocities of the PCM, Darcy law's source term was added to the model. The governing equations involved in the model were solved using a finite element based software product, COMSOL Multiphysics 4.3a. The outcome of the optimization studies performed using the 2D numerical model yields the optimized configuration of the shell-and-tube type LHS prototype, which is used as the input for the 3D numerical model and the fabrication of the real-time experimental LHS prototype. The 3D shell-and-tube model developed was based on a conjugate heat transfer problem, which simultaneously solves the flow behavior of HTF and phase change behavior of PCM. The numerical results of the 3D model were validated with the experimental results extracted from the in-built lab scale LHS prototype and a close agreement was found between them.

Performance parameters such as melt fraction, charging / discharging time, energy storage / discharge rate were evaluated at different operating conditions. An exhaustive parametric study was also conducted by varying the HTF inlet temperature and flow rate. The conceptual conclusions arrived out from the experimental and numerical studies express a similar research flavor, and they are listed below:

- Charging is a convection-dominated process and discharging is a conduction-dominated process. Due to this, charging is faster than discharging.
- The charging / discharging time of the LHS prototype in the numerical studies was about 111 / 117 min. Similarly, it took about 124 / 131 min for charging / discharging of the LHS prototype in the experimental studies.
- As discharging process is a slower phenomenon, the optimization of the storage system should be done based on the discharging time of the prototype.
- Though addition of tubes and fins increases the conduction heat transfer during the charging and discharging processes, it slightly retards the convection heat transfer. This necessitates the optimization of the number of tubes and fins of any storage system.
- For the selected LHS capacity of 10 MJ, the optimized number of tubes and fins are found to be 25 and 4, respectively.
- Partial charging / discharging process is much efficient in the storage / retrieval of energy than the complete charging / discharging process. It took only 73 / 70 % of the complete charging / discharging time for 90 % of heat storage / discharge.
- Variation of PCM temperature in the axial direction shows a predominant change when compared with that of the angular direction.
- The axial and angular temperature variation of the PCM during the charging process is more than that of discharging process, which is mainly due to the convective heat transfer.
- The change in HTF inlet temperature yields a greater impact on the charging / discharging time when compared with the change in HTF flow rate.
- Effect of HTF flow rate is still noticeable at lower / higher HTF inlet temperature during the charging / discharging process.

7.2 Novel concepts

Two novel concepts namely novel encapsulation and novel fin were proposed in this thesis. The numerical model used for the performance evaluation of the LHS prototype was slightly modified and reused to study the storage characteristics of the novel concepts.

The novel encapsulation technique proposed is to achieve better heat transfer in LHS capsules, which has a wide application in steam accumulators. A comparison of the heat transfer characteristics of the basic and novel capsules was done using a thermal model. It was found from the numerical study that it took about 64 / 33 min and 158 / 57 min for the basic/novel capsules for complete charging/discharging. The reduction in the charging/discharging time achieved by the novel capsule when compared with the basic capsule is about 48.4 / 63.9 %. Effect of operating temperature range was also studied and it was observed that the novel capsule with the least temperature difference (20 °C) itself charges/discharges faster than the basic capsule with a higher temperature difference (30 / 40 °C). The scope for commercial viability of the novel concept is also explored and the results showed a positive step towards the commercialization of the novel concept. While upscaling, a mass reduction of approximately 21.4 % can be achieved for the encapsulation shell with the novel capsule when compared with the basic capsule for a storage capacity of 19 MJ. Different arrangements of novel and basic capsules in circular and rectangular forms are studied for less volume occupancy and it was found that the novel capsules arranged in the rectangular fashion occupies the least volume. In addition, the reduction in the charging and discharging time achieved by the novel capsule (1 MJ capacity) when compared with the basic capsule (0.5 MJ capacity) are 4.7 % and 19 %.

The novel fin proposed is to accomplish an efficient heat transfer in tube-in-tube LHS devices. A comparison of the storage characteristics of the novel fin configuration with no fin and standard fin configurations was made using the numerical model. It is found from the numerical study that it takes about 548 / 788 min, 514 / 742 min and 487 / 665 min for complete charging / discharging of the LHS module with no fin, standard fin and novel fin. It can be noted that the charging/discharging time has decreased by about 11.1 / 15.6 % and 5.25 /10.4 % when using novel fin configuration with respect to no fin and standard fin configurations. The novel fin proposed has also an additional advantage of weight and cost reduction of fins by a factor of 0.5.

7.3 Scope for future work

The works presented in this thesis offer several opportunities to broaden the research work on the LHS systems. Some of the scope for future work are given below:

- The flow regime of HTF considered in the present study is laminar. Several advantages in the heat transfer rate could be achieved if the study is extended to turbulent regime.
- Storage performance is evaluated for the medium temperature PCM having a phase transition temperature of 142 °C. Numerical and experimental studies can be carried out using high temperature PCMs.
- Development of cascaded LHS systems equipped with heat-transfer enhancement techniques such as fins.
- The performance characteristics of the novel encapsulated LHS capsules deduced using numerical models could be extended further by conducting experiments.
- The novel fin concept can be also studied for higher storage capacity.

References

Abhat A (1983). Low temperature latent heat thermal energy storage: heat storage materials. *Solar Energy*, 30(4), 313-332.

Agyenim F, Eames P, Smyth M (2009). A comparison of heat transfer enhancement in a medium temperature thermal energy storage heat exchanger using fins. *Solar Energy*, 83(9), 1509-1520.

Agyenim F, Hewitt N, Eames P, Smyth M (2010a). A review of materials, heat transfer and phase change problem formulation for latent heat thermal energy storage systems (LHTESS). *Renewable & Sustainable Energy Reviews*, 14(2), 615-628.

Agyenim F, Eames P, Smyth M (2010b). Heat transfer enhancement in medium temperature thermal energy storage system using a multitube heat transfer array. *Renewable Energy*, 35(1), 198-207.

Al-abidi AA, Bin Mat S, Sopian K, Sulaiman MY, Mohammed AT (2013). CFD applications for latent heat thermal energy storage: A review. *Renewable & Sustainable Energy Reviews*, 20, 353-363.

Alam TE, Dhau JS, Goswami DY, Rahman MM, Stefanakos E (2014). *Experimental investigation of a packed-bed latent heat thermal storage system with encapsulated phase change material*. Paper presented at the ASME 2014 International Mechanical Engineering Congress and Exposition, Montreal, Quebec, Canada.

Alam TE, Dhau JS, Goswami DY, Stefanakos E (2015). Macroencapsulation and characterization of phase change materials for latent heat thermal energy storage systems. *Applied Energy*, 154, 92-101.

Albert MR, Oneill K (1986). Moving Boundary - Moving Mesh Analysis of Phase-Change Using Finite-Elements with Transfinite Mappings. *International Journal for Numerical Methods in Engineering*, 23(4), 591-607.

Allouche Y, Varga S, Bouden C, Oliveira AC (2015). Experimental determination of the heat transfer and cold storage characteristics of a microencapsulated phase change material in a horizontal tank. *Energy Conversion and Management*, 94, 275-285.

Allouche Y, Varga S, Bouden C, Oliveira AC (2016). Validation of a CFD model for the simulation of heat transfer in a tubes-in-tank PCM storage unit. *Renewable Energy*, 89, 371-379.

Assis E, Katsman L, Ziskind G, Letan R (2007). Numerical and experimental study of melting in a spherical shell. *International Journal of Heat and Mass Transfer,* 50(9-10), 1790-1804.

Avci M, Yazici MY (2013). Experimental study of thermal energy storage characteristics of a paraffin in a horizontal tube-in-shell storage unit. *Energy Conversion and Management,* 73, 271-277.

Bauer T, Laing D, Tamme R (2012). Characterization of sodium nitrate as phase change material. *International Journal of Thermophysics,* 33(1), 91-104.

Bohlmann EG (1972). *Heat transfer salt for high temperature steam generation* (ORNL-TM-3777 Oak Ridge National Laboratory, United States).

Bonacina C, Comini G, Fasano A, Primicerio M (1973). Numerical solution of phase-change problems. *International Journal of Heat and Mass Transfer,* 16(10), 1825-1832.

Brent AD, Voller VR, Reid KJ (1988). Enthalpy-porosity technique for modeling convection-diffusion phase change: Application to the melting of a pure metal. *Numerical Heat Transfer,* 13(3), 297-318.

Buddhi D, Sahoo LK (1997). Solar cooker with latent heat storage: Design and experimental testing. *Energy Conversion and Management,* 38(5), 493-498.

Castell A, Solé C, Medrano M, Roca J, Cabeza LF (2006). *Use of external vertical fins in phase change materials modules for domestic hot water tanks*. Paper presented at the 10th International Conference on Thermal Energy Storage ECOSTOCK, Richard Stockton College of New Jersey, New Jersey, USA.

Castellon C, Martorell I, Cabeza LF, Fernandez AI, Manich AM (2011). Compatibility of plastic with phase change materials (PCM). *International Journal of Energy Research,* 35(9), 765-771.

Choi JC, Kim SD (1992). Heat-transfer characteristics of a latent-heat storage-system using MgCl2.6H2O. *Energy,* 17(12), 1153-1164.

Comini G, Del Guidice S, Lewis RW, Zienkiewicz OC (1974). Finite element solution of non-linear heat conduction problems with special reference to phase change. *International Journal for Numerical Methods in Engineering,* 8(3), 613-624.

Costa M, Buddhi D, Oliva A (1998). Numerical simulation of a latent heat thermal energy storage system with enhanced heat conduction. *Energy Conversion and Management,* 39(3-4), 319-330.

Da Cunha JP, Eames P (2016). Thermal energy storage for low and medium temperature applications using phase change materials - A review. *Applied Energy,* 177, 227-238.

Darzi AAR, Jourabian M, Farhadi M (2016). Melting and solidification of PCM enhanced by radial conductive fins and nanoparticles in cylindrical annulus. *Energy Conversion and Management,* 118, 253-263.

Dhaidan NS, Khodadadi JM, Al-Hattab TA, Al-Mashat SM (2013). Experimental and numerical investigation of melting of phase change material/nanoparticle suspensions in a square container subjected to a constant heat flux. *International Journal of Heat and Mass Transfer,* 66, 672-683.

Dimaano MNR, Watanabe T (2003). The transient behavior analysis of the capric acid and lauric acid mixture in a vertical tube. *Journal of Chemical Engineering of Japan,* 36(12), 1421-1431.

Dincer I, Rosen M (2002). *Thermal energy storage: systems and applications*: John Wiley & Sons.

Dutil Y, Rousse DR, Ben Salah N, Lassue S, Zalewski L (2011). A review on phase-change materials: Mathematical modeling and simulations. *Renewable & Sustainable Energy Reviews,* 15(1), 112-130.

Elgafy A, Lafdi K (2005). Effect of carbon nanofiber additives on thermal behavior of phase change materials. *Carbon,* 43(15), 3067-3074.

Esapour M, Hosseini MJ, Ranjbar AA, Pahamli Y, Bahrampoury R (2016). Phase change in multi-tube heat exchangers. *Renewable Energy,* 85, 1017-1025.

Esen M, Durmus A, Durmus A (1998). Geometric design of solar-aided latent heat store depending on various parameters and phase change materials. *Solar Energy,* 62(1), 19-28.

Ettouney H, Alatiqi I, Al-Sahali M, Al-Hajirie K (2006). Heat transfer enhancement in energy storage in spherical capsules filled with paraffin wax and metal beads. *Energy Conversion and Management,* 47(2), 211-228.

Fan LW, Khodadadi JM (2011). Thermal conductivity enhancement of phase change materials for thermal energy storage: A review. *Renewable & Sustainable Energy Reviews,* 15(1), 24-46.

Fan LW, Zhu ZQ, Xiao SL, Liu MJ, Lu H, Zeng Y, Yu ZT, Cen KF (2016). An experimental and numerical investigation of constrained melting heat transfer of a phase change material in a circumferentially finned spherical capsule for thermal energy storage. *Applied Thermal Engineering,* 100, 1063-1075.

Farid MM, Hamad FA, Abu-Arabi M (1998a). Phase change cool storage using dimethyl-sulfoxide. *Energy Conversion and Management,* 39(8), 819-826.

Farid MM, Hamad FA, Abu-Arabi M (1998b). Melting and solidification in multi-dimensional geometry and presence of more than one interface. *Energy Conversion and Management,* 39(8), 809-818.

Farid MM, Khudhair AM, Razack SAK, Al-Hallaj S (2004). A review on phase change energy storage: materials and applications. *Energy Conversion and Management,* 45(9-10), 1597-1615.

Fernandez AI, Martinez M, Segarra M, Martorell I, Cabeza LF (2010). Selection of materials with potential in sensible thermal energy storage. *Solar Energy Materials and Solar Cells,* 94(10), 1723-1729.

Fomin SA, Saitoh TS (1999). Melting of unfixed material in spherical capsule with non-isothermal wall. *International Journal of Heat and Mass Transfer,* 42(22), 4197-4205.

Fukai J, Kanou M, Kodama Y, Miyatake O (2000). Thermal conductivity enhancement of energy storage media using carbon fibers. *Energy Conversion and Management,* 41(14), 1543-1556.

Fukai J, Hamada Y, Morozumi Y, Miyatake O (2003). Improvement of thermal characteristics of latent heat thermal energy storage units using carbon-fiber brushes: experiments and modeling. *International Journal of Heat and Mass Transfer,* 46(23), 4513-4525.

Gil A, Medrano M, Martorell I, Lazaro A, Dolado P, Zalba B, Cabeza LF (2010). State of the art on high temperature thermal energy storage for power generation. Part 1-Concepts, materials and modellization. *Renewable & Sustainable Energy Reviews,* 14(1), 31-55.

Goldstern W (1979). Thermal energy storage in industry and power stations. *Journal of the Institute of Energy,* 52(413), 185-192.

Gong ZX, Majumdar AS (1997). Finite-element analysis of cyclic heat transfer in a shell-and-tube latent heat energy storage exchanger. *Applied Thermal Engineering,* 17(6), 583-591.

Gong ZX, Mujumdar AS (1997). Non-convergence versus non-conservation in effective heat capacity methods for phase change problems. *International Journal of Numerical Methods for Heat & Fluid Flow,* 7(5-6), 565-&.

Goodman TR, Shea JJ (1960). The Melting of finite slabs. *Journal of Applied Mechanics,* 27(1), 16-24.

Gu ZL, Liu HJ, Li Y (2004). Thermal energy recovery of air conditioning system - heat recovery system calculation and phase change materials development. *Applied Thermal Engineering*, 24(17-18), 2511-2526.

Hasnain SM (1998). Review on sustainable thermal energy storage technologies, Part I: Heat storage materials and techniques. *Energy Conversion and Management*, 39(11), 1127-1138.

Ho CJ, Gao JY (2013). An experimental study on melting heat transfer of paraffin dispersed with Al2O3 nanoparticles in a vertical enclosure. *International Journal of Heat and Mass Transfer*, 62, 2-8.

Hosseini MJ, Rahimi M, Bahrampoury R (2014). Experimental and computational evolution of a shell and tube heat exchanger as a PCM thermal storage system. *International Communications in Heat and Mass Transfer*, 50, 128-136.

Hu H, Argyropoulos SA (1996). Mathematical modelling of solidification and melting: A review. *Modelling and Simulation in Materials Science and Engineering*, 4(4), 371-396.

Huang SC (1985). Analytical solution for the buoyancy flow during the melting of a vertical semi-infinite region. *International Journal of Heat and Mass Transfer*, 28(6), 1231-1233.

Hussein HMS, El-Ghetany HH, Nada SA (2008). Experimental investigation of novel indirect solar cooker with indoor PCM thermal storage and cooking unit. *Energy Conversion and Management*, 49(8), 2237-2246.

Ibrahim NI, Al-Sulaiman FA, Rahman S, Yilbas BS, Sahin AZ (2017). Heat transfer enhancement of phase change materials for thermal energy storage applications: A critical review. *Renewable & Sustainable Energy Reviews*, 74, 26-50.

Jacob R, Bruno F (2015). Review on shell materials used in the encapsulation of phase change materials for high temperature thermal energy storage. *Renewable & Sustainable Energy Reviews*, 48, 79-87.

Janz GJ, Allen CB, Bansal N, Murphy R, Tomkins R (1979). *Physical properties data compilations relevant to energy storage. II. Molten salts: data on single and multi-component salt systems*.

Jegadheeswaran S, Pohekar SD (2009). Performance enhancement in latent heat thermal storage system: A review. *Renewable & Sustainable Energy Reviews*, 13(9), 2225-2244.

Kenisarin M, Mahkamov K (2007). Solar energy storage using phase change materials. *Renewable & Sustainable Energy Reviews,* 11(9), 1913-1965.

Khalifa A, Tan L, Date A, Akbarzadeh A (2014). A numerical and experimental study of solidification around axially finned heat pipes for high temperature latent heat thermal energy storage units. *Applied Thermal Engineering,* 70(1), 609-619.

Khan Z, Khan Z, Ghafoor A (2016). A review of performance enhancement of PCM based latent heat storage system within the context of materials, thermal stability and compatibility. *Energy Conversion and Management,* 115, 132-158.

Kheirabadi AC, Groulx D (2015). *The effect of the mushy-zone constant on simulated phase change heat transfer*. Paper presented at the ICHMT International Symposium on Advances in Computational Heat Transfer, Piscataway, USA; .

Khodadadi JM, Zhang Y (2001). Effects of buoyancy-driven convection on melting within spherical containers. *International Journal of Heat and Mass Transfer,* 44(8), 1605-1618.

Khodadadi JM, Hosseinizadeh SF (2007). Nanoparticle-enhanced phase change materials (NEPCM) with great potential for improved thermal energy storage. *International Communications in Heat and Mass Transfer,* 34(5), 534-543.

Kline SJ, McClintock FA (1953). Describing uncertainties in single-sample experiments. *Mechanical Engineering,* 3-12.

Koizumi H (2004). Time and spatial heat transfer performance around an isothermally heated sphere placed in a uniform, downwardly directed flow (in relation to the enhancement of latent heat storage rate in a spherical capsule). *Applied Thermal Engineering,* 24(17-18), 2583-2600.

Kuravi S, Kota KM, Du JH, Chow LC (2009). Numerical investigation of flow and heat transfer performance of nano-encapsulated phase change material slurry in microchannels. *Journal of Heat Transfer-Transactions of the Asme,* 131(6).

Kuravi S, Trahan J, Goswami DY, Rahman MM, Stefanakos EK (2013). Thermal energy storage technologies and systems for concentrating solar power plants. *Progress in Energy and Combustion Science,* 39(4), 285-319.

Kurklu A (1998). Short-term thermal performance of a built-in solar storage for frost prevention in a greenhouse. *International Journal of Energy Research,* 22(2), 169-174.

Kurnia JC, Sasmito AP, Jangam SV, Mujumdar AS (2013). Improved design for heat transfer performance of a novel phase change material (PCM) thermal energy storage (TES). *Applied Thermal Engineering,* 50(1), 896-907.

Lacroix M (1993). Numerical-simulation of a shell-and-tube latent-heat thermal-energy storage unit. *Solar Energy*, 50(4), 357-367.

Laing D, Bauer T, Breidenbach N, Hachmann B, Johnson M (2013). Development of high temperature phase-change-material storages. *Applied Energy*, 109, 497-504.

Lamberg P (2004). Approximate analytical model for two-phase solidification problem in a finned phase-change material storage. *Applied Energy*, 77(2), 131-152.

Lamberg P, Lehtiniemi R, Henell AM (2004). Numerical and experimental investigation of melting and freezing processes in phase change material storage. *International Journal of Thermal Sciences*, 43(3), 277-287.

Lan CW, Kou S (1991). Effects of rotation on heat transfer, fluid flow and interfaces in normal gravity floating zone crystal growth. *Journal of Crystal Growth*, 114(4), 517-535.

Li TX, Lee JH, Wang RZ, Kang YT (2013). Enhancement of heat transfer for thermal energy storage application using stearic acid nanocomposite with multi-walled carbon nanotubes. *Energy*, 55, 752-761.

Liu M, Saman W, Bruno F (2012). Review on storage materials and thermal performance enhancement techniques for high temperature phase change thermal storage systems. *Renewable & Sustainable Energy Reviews*, 16(4), 2118-2132.

Lynch DR (1982). Unified approach to simulation on deforming elements with application to phase change problems. *Journal of Computational Physics*, 47(3), 387-411.

Mat S, Al-Abidi AA, Sopian K, Sulaiman MY, Mohammad AT (2013). Enhance heat transfer for PCM melting in triplex tube with internal-external fins. *Energy Conversion and Management*, 74, 223-236.

Medrano M, Gil A, Martorell I, Potau X, Cabeza LF (2010). State of the art on high-temperature thermal energy storage for power generation. Part 2-Case studies. *Renewable & Sustainable Energy Reviews*, 14(1), 56-72.

Mehling H, Cabeza L (2008). *Heat and cold storage with PCM*: Springer Berlin Heidelberg.

Merlin K, Soto J, Delaunay D, Traonvouez L (2016). Industrial waste heat recovery using an enhanced conductivity latent heat thermal energy storage. *Applied Energy*, 183, 491-503.

Meyer GH (1973). Multidimensional Stefan problems. *Siam Journal on Numerical Analysis*, 10(3), 522-538.

Morgan K, Lewis RW, Zienkiewicz OC (1978). An improved algorithm for heat conduction problems with phase change. *International Journal for Numerical Methods in Engineering*, 12(7), 1191-1195.

Najjar A, Hasan A (2008). Modeling of greenhouse with PCM energy storage. *Energy Conversion and Management*, 49(11), 3338-3342.

Neumann F (1912). Lectures Given in the 1860's. *Die Partiellen Differential-Gleichungen der Mthematischen Physik*, 117-121.

Ng KW, Gong ZX, Mujumdar AS (1998). Heat transfer in free convection-dominated melting of a phase change material in a horizontal annulus. *International Communications in Heat and Mass Transfer*, 25(5), 631-640.

Niyas H, Muthukumar P (2015). *Comparison of thermal storage characteristics of phase change materials encapsulated in different capsule configurations*. Paper presented at the 23rd National and 1st International ISHMT-ASTFE Heat and Mass Transfer Conference, Liquid Propulsion Systems Centre, Indian Space Research Organization, Thiruvananthapuram, India.

Ogoh W, Groulx D (2012). Effects of the heat transfer fluid velocity on the storage characteristics of a cylindrical latent heat energy storage system: A numerical study. *Heat and Mass Transfer*, 48(3), 439-449.

Ona EP, Zhang X, Kyaw K, Watanabe F, Matsuda H, Kakiuchi H, Yabe M, Chihara S (2001). Relaxation of supercooling of erythritol for latent heat storage. *Journal of Chemical Engineering of Japan*, 34(3), 376-382.

Panayiotou GP, Kalogirou SA, Tassou SA (2016). Evaluation of the application of phase change materials (PCM) on the envelope of a typical dwelling in the Mediterranean region. *Renewable Energy*, 97, 24-32.

Paterson S (1952). Propagation of a Boundary of Fusion. *Proceedings of the Glasgow Mathematical Association*, 1(1), 42-47.

Perez M, Perez R (2015). Update 2015-A Fundamental look at supply side energy reserves for the planet. *Natural Gas*, 2(9), 215.

Poirier D, Salcudean M (1988). On Numerical Methods Used in Mathematical Modeling of Phase Change in Liquid-Metals. *Journal of Heat Transfer-Transactions of the Asme*, 110(3), 562-570.

Prakash J, Garg HP, Datta G (1985). A solar water heater with a built-in latent-heat storage. *Energy Conversion and Management*, 25(1), 51-56.

Price N (1982). Steam accumulators provide uniform loads on boilers. *Chemical Engineering*, 89(23), 131-135.

Rathod MK, Banerjee J (2015). Thermal performance enhancement of shell and tube latent heat storage unit using longitudinal fins. *Applied Thermal Engineering*, 75, 1084-1092.

Regin AF, Solanki SC, Saini JS (2006). Latent heat thermal energy storage using cylindrical capsule: Numerical and experimental investigations. *Renewable Energy,* 31(13), 2025-2041.

Rieger H, Projahn U, Beer H (1982). Analysis of the heat-transport mechanisms during melting around a horizontal circular-cylinder. *International Journal of Heat and Mass Transfer,* 25(1), 137-147.

Sabihuddin S, Kiprakis AE, Mueller M (2015). A numerical and graphical review of energy storage technologies. *Energies,* 8(1), 172-216.

Saitoh T, Hirose K (1986). High performance phase change thermal energy storage using spherical capsules. *Chemical Engineering Communications,* 41(1-6), 39-58.

Sardeshpande V, Pillai IR (2012). Effect of micro-level and macro-level factors on adoption potential of solar concentrators for medium temperature thermal applications. *Energy for Sustainable Development,* 16(2), 216-223.

Sari A, Kaygusuz K (2002a). Thermal and heat transfer characteristics in a latent heat storage system using lauric acid. *Energy Conversion and Management,* 43(18), 2493-2507.

Sari A, Kaygusuz K (2002b). Thermal performance of a eutectic mixture of lauric and stearic acids as PCM encapsulated in the annulus of two concentric pipes. *Solar Energy,* 72(6), 493-504.

Sawin JL, Sverrisson F, Seyboth K, Adib R, Murdock HE, Lins C, et al. (2016). *Renewables 2016 Global Status Report Key findings - A Record Breaking Year for Renewable Energy: New Installations, Policy Targets, Investment and Jobs mainstreaming renewables.*

Schenk O, Gartner K (2004). Solving unsymmetric sparse systems of linear equations with PARDISO. *Future Generation Computer Systems,* 20(3), 475-487.

Seddegh S, Wang XL, Henderson AD (2015). Numerical investigation of heat transfer mechanism in a vertical shell and tube latent heat energy storage system. *Applied Thermal Engineering,* 87, 698-706.

Seddegh S, Wang XL, Henderson AD (2016). A comparative study of thermal behaviour of a horizontal and vertical shell-and-tube energy storage using phase change materials. *Applied Thermal Engineering,* 93, 348-358.

Shamsundar N, Sparrow EM (1975). Analysis of multidimensional conduction phase change via the enthalpy model. *Journal of Heat Transfer,* 97(3), 333-340.

Sharma SD, Buddhi D, Sawhney RL, Sharma A (2000). Design, development and performance evaluation of a latent heat storage unit for evening cooking in a solar cooker. *Energy Conversion and Management,* 41(14), 1497-1508.

Sharma SD, Sagara K (2005). Latent heat storage materials and systems: A review. *International Journal of Green Energy,* 2(1), 1-56.

Shenoy AV, Mashelkar RA (1978). Laminar natural convection heat transfer to a viscoelastic fluid. *Chemical Engineering Science,* 33(6), 769-776.

Shnaider DA, Divnich PN, Vakhromeev IE (2010). Modeling the dynamic mode of steam accumulator. *Automation and Remote Control,* 71(9), 1994-1998.

Shyy W, Udaykumar HS, Liang SJ (1993). An Interface Tracking Method Applied to Morphological Evolution during Phase-Change. *International Journal of Heat and Mass Transfer,* 36(7), 1833-1844.

Siva K, Lawrence MX, Kumaresh GR, Rajagopalan P, Santhanam H (2010). Experimental and numerical investigation of phase change materials with finned encapsulation for energy-efficient buildings. *Journal of Building Performance Simulation,* 3(4), 245-254.

Soares N, Gaspar AR, Santos P, Costa JJ (2015). Experimental study of the heat transfer through a vertical stack of rectangular cavities filled with phase change materials. *Applied Energy,* 142, 192-205.

SOLUCAR (2006). *PS10: 10MW solar thermal power plant for southern Spain, NNE5-1999-356.*

Sparrow EM, Larson ED, Ramsey JW (1981). Freezing on a finned tube for either conduction-controlled or natural-convection-controlled heat-transfer. *International Journal of Heat and Mass Transfer,* 24(2), 273-284.

Stefan J (1891). Ueber die Theorie der Eisbildung, insbesondere über die Eisbildung im Polarmeere. *Annalen der Physik,* 278(2), 269-286.

Steinmann WD, Eck M (2006). Buffer storage for direct steam generation. *Solar Energy,* 80(10), 1277-1282.

Steinmann WD, Tamme R (2008). Latent heat storage for solar steam systems. *Journal of Solar Energy Engineering-Transactions of the Asme,* 130(1), 0110041-0110045.

Stevanovic VD, Maslovaric B, Prica S (2012). Dynamics of steam accumulation. *Applied Thermal Engineering,* 37, 73-79.

Su W, Darkwa J, Kokogiannakis G (2015). Review of solid-liquid phase change materials and their encapsulation technologies. *Renewable & Sustainable Energy Reviews,* 48, 373-391.

Tan FL, Leong KC (1999). An experimental investigation of solidification in a rectangular enclosure under constant heat rate condition. *International Communications in Heat and Mass Transfer*, 26(7), 925-934.

Tan G, Zhao DL (2015). Study of a thermoelectric space cooling system integrated with phase change material. *Applied Thermal Engineering*, 86, 187-198.

Tayeb AM (1993). A simulation model for a phase change energy storage system - Experimental and verification. *Energy Conversion and Management*, 34(4), 243-250.

Tiari S, Qiu SG, Mahdavi M (2015). Numerical study of finned heat pipe-assisted thermal energy storage system with high temperature phase change material. *Energy Conversion and Management*, 89, 833-842.

Trp A, Lenic K, Frankovic B (2006). Analysis of the influence of operating conditions and geometric parameters on heat transfer in water-paraffin shell-and-tube latent thermal energy storage unit. *Applied Thermal Engineering*, 26(16), 1830-1839.

Vakilaltojjar SM, Saman W (2001). Analysis and modelling of a phase change storage system for air conditioning applications. *Applied Thermal Engineering*, 21(3), 249-263.

Velraj R, Seeniraj RV, Hafner B, Faber C, Schwarzer K (1999). Heat transfer enhancement in a latent heat storage system. *Solar Energy*, 65(3), 171-180.

Veremachi A, Cuamba BC, Zia A, Lovseth J, Nydal OJ (2016). PCM heat storage charged with a double-reflector solar system. *Journal of Solar Energy*, 2016, 8.

Verma P, Varun, Singal SK (2008). Review of mathematical modeling on latent heat thermal energy storage systems using phase-change material. *Renewable & Sustainable Energy Reviews*, 12(4), 999-1031.

Voller VR, Prakash C (1987). A fixed grid numerical modeling methodology for convection-diffusion mushy region phase-change problems. *International Journal of Heat and Mass Transfer*, 30(8), 1709-1719.

Vyshak NR, Jilani G (2007). Numerical analysis of latent heat thermal energy storage system. *Energy Conversion and Management*, 48(7), 2161-2168.

White LR, Davis HT (1967). Thermal conductivity of molten alkali nitrates. *Journal of Chemical Physics*, 47(12), 5433-5439.

Wu ZG, Zhao CY (2011). Experimental investigations of porous materials in high temperature thermal energy storage systems. *Solar Energy*, 85(7), 1371-1380.

Xu E, Wang Z, Wei G, Zhuang J (2012). Dynamic simulation of thermal energy storage system of Badaling 1 MW solar power tower plant. *Renewable Energy*, 39(1), 455-462.

Yang H, He Y (2010). Solving heat transfer problems with phase change via smoothed effective heat capacity and element-free Galerkin methods. *International Communications in Heat and Mass Transfer,* 37(4), 385-392.

Yao LS, Cherney W (1981). Transient phase-change around a horizontal cylinder. *International Journal of Heat and Mass Transfer,* 24(12), 1971-1981.

Yazici MY, Avci M, Aydin O, Akgun M (2014a). On the effect of eccentricity of a horizontal tube-in-shell storage unit on solidification of a PCM. *Applied Thermal Engineering,* 64(1-2), 1-9.

Yazici MY, Avci M, Aydin O, Akgun M (2014b). Effect of eccentricity on melting behavior of paraffin in a horizontal tube-in-shell storage unit: An experimental study. *Solar Energy,* 101, 291-298.

Zhai XQ, Cheng XW, Wang C, Wang RZ (2015). Experimental investigation and performance analysis of a fin tube phase change cold storage unit for high temperature cooling application. *Energy and Buildings,* 89, 9-17.

Zhang P, Xiao X, Meng ZN, Li M (2015). Heat transfer characteristics of a molten-salt thermal energy storage unit with and without heat transfer enhancement. *Applied Energy,* 137, 758-772.

Zhang Y, Du K, He JP, Yang L, Li YJ (2014). Impact factors analysis of the enthalpy method and the effective heat capacity method on the transient nonlinear heat transfer in phase change materials (PCMs). *Numerical Heat Transfer Part A-Applications,* 65(1), 66-83.

Zhang YW, Chen ZQ, Wang QJ, Wu QJ (1993). Melting in an enclosure with discrete heating at a constant rate. *Experimental Thermal and Fluid Science,* 6(2), 196-201.

Appendix A

Derivation of Energy Stored / Discharged

The thermal model developed is based on a conjugate heat transfer problem, which simultaneously solves the flow behavior of HTF and phase change behavior of PCM. The biggest problem associated in the modelling of an LHS model is the incorporation of latent heat required to melt/solidify the PCM. This concern is solved by using the effective heat capacity (EHC) method, which includes both specific heat and latent heat of the PCM in a single term called EHC. The heat capacity of the PCM is modified as shown in Eq. (A.1) and the EHC is calculated using Eq. (A.2).

$$C_P = \begin{cases} C_{P,S} \; for \; T < T_S \\ C_{P,EFF} \quad for \; T_S \le T \le T_L \\ C_{P,L} \; for \; T > T_L \end{cases} \tag{A.1}$$

$$C_{P,EFF} = \frac{C_{P,S} + C_{P,L}}{2} + \frac{L_F}{T_L - T_S} \tag{A.2}$$

For explicit calculation of the amount of latent heat stored / discharged during the charging/discharging process, the specific heat term should be deducted from the effective specific heat. The latent heat stored/discharged are expressed in Eq. (A.3) and (A.4), after excluding the specific heat term.

$$\begin{aligned} E_{L,C} &= m\left(C_{P,EFF} - \frac{C_{P,S} + C_{P,L}}{2} \right)\left(T - T_S \right) \\ &= m\left(\frac{L_F}{T_L - T_S} \right)\left(T - T_S \right) \\ &= m L_F \, \theta \end{aligned} \tag{A.1}$$

$$\begin{aligned} E_{L,D} &= m\left(C_{P,EFF} - \frac{C_{P,S} + C_{P,L}}{2} \right)\left(T_L - T \right) \\ &= m\left(\frac{L_F}{T_L - T_S} \right)\left[\left(T_L - T \right) - \left(T_S - T_S \right) \right] \\ &= m\left(\frac{L_F}{T_L - T_S} \right)\left[\left(T_L - T_S \right) - \left(T - T_S \right) \right] \\ &= m L_F \left(1 - \theta \right) \end{aligned} \tag{A.2}$$

Appendix B

Error Analysis

Kline and McClintock (1953) proposed a methodology for estimating the uncertainty of any dependent parameter, which depends on certain measured quantities of the experimental studies. If a parameter N depends on the independent variables such as u1, u2, u3 ….un then N can be expressed as a function of all the independent variables as given in Eq. (B.1)

$$N = N\left(u_1, u_2, u_3 ... u_n\right) \tag{B.1}$$

Then the total uncertainty of the parameter (ΔN) is given by Eq. (B.2)

$$\Delta N = \sqrt{\left[\frac{\partial N}{\partial u_1}\Delta u_1\right]^2 + \left[\frac{\partial N}{\partial u_2}\Delta u_2\right]^2 + \left[\frac{\partial N}{\partial u_3}\Delta u_3\right]^2 + \cdots + \left[\frac{\partial N}{\partial u_n}\Delta u_n\right]^2} \tag{B.2}$$

The major performance parameters estimated in the experimental studies are melt fraction, energy stored and energy discharged. The major independent parameter involved in the experiments is the temperature, which is measured with metal-sheathed K Type thermocouples having an accuracy of ± 0.2 °C. The uncertainty in the mass of the PCM is assumed ± 2 %.

Melt Fraction

Melt fraction is a non-dimensional parameter, which quantifies the percentage of liquid phase in the mushy region. Melt fraction of the PCM can be calculated based on the lever rule applied between the solidus and liquidus temperatures and it is given by Eq. (B.3).

$$\theta = \frac{T - T_S}{T_L - T_S} = \frac{T - T_S}{2\ \Delta T_M} = \begin{cases} 0 \ \ for\ T < T_S \\ 0-1 \ \ for\ T_S \le T \le T_L \\ 1 \ \ for\ T > T_L \end{cases} \tag{B.3}$$

Applying the Kline – McClintock's rule, we have

$$\Delta\theta = \sqrt{\left[\frac{\partial\theta}{\partial T}\Delta T\right]^2 + \left[\frac{\partial\theta}{\partial T_S}\Delta T_S\right]^2 + \left[\frac{\partial\theta}{\partial \Delta T_M}\Delta\left(\Delta T_M\right)\right]^2}$$

$$= \sqrt{\left(0.125\times 0.2\right)^2 + \left(-0.125\times 0.2\right)^2 + \left(-0.125\times 0.4\right)^2}$$

$$= \pm 0.061$$

where,

$$\frac{\partial\theta}{\partial T} = \frac{1}{2\cdot\Delta T_M} = 0.125$$

$$\frac{\partial\theta}{\partial T_S} = -\frac{1}{2\cdot\Delta T_M} = -0.125$$

$$\frac{\partial\theta}{\partial \Delta T_M} = \frac{\left(T - T_S\right)}{2}\cdot\frac{\left(-1\right)}{\left(\Delta T_M\right)^2} = -0.125$$

Energy Stored / Discharged

The amount of energy stored/discharged in/from the PCM depends on mass, temperature difference, specific heat, latent heat and melt fraction. Energy stored/discharged in/from the PCM is calculated using the Eq. (B.4) and (B.5). The uncertainty of mass, temperature difference and melt fraction have an impact in the uncertainty of the amount of energy stored/discharged.

$$E_{T,C} = m\left[C_p\left(T - T_{ini}\right) + L_F\,\theta\right] = m\left[C_p\,\Delta T_C + L_F\,\theta\right] \quad \text{(B.4)}$$

$$E_{T,D} = m\left[C_p\left(T_{ini} - T\right) + L_F\,(1-\theta)\right] = m\left[C_p\,\Delta T_D + L_F\,(1-\theta)\right] \quad \text{(B.5)}$$

Applying the Kline – McClintock's rule, we have

$$\Delta E_{T,C} = \sqrt{\left[\frac{\partial E_{T,C}}{\partial m}\Delta m\right]^2 + \left[\frac{\partial E_{T,C}}{\partial \Delta T_C}\Delta\left(\Delta T_C\right)\right]^2 + \left[\frac{\partial E_{T,C}}{\partial \theta}\Delta\theta\right]^2}$$

$$= \sqrt{\left(137.5\times 0.02\right)^2 + \left(178\times 0.2\right)^2 + \left(10000\times 0.4\right)^2}$$

$$= \pm 614\ kJ$$

$$= \pm 0.614\,MJ$$

$$\Delta E_{T,D} = \sqrt{\left[\frac{\partial E_{T,D}}{\partial m}\Delta m\right]^2 + \left[\frac{\partial E_{T,D}}{\partial \Delta T_D}\Delta\left(\Delta T_D\right)\right]^2 + \left[\frac{\partial E_{T,D}}{\partial \theta}\Delta\theta\right]^2}$$

$$= \sqrt{\left(125.6\times 0.02\right)^2 + \left(178\times 0.2\right)^2 + \left(10000\times 0.4\right)^2}$$

$$= \pm 614\ kJ$$

$$= \pm 0.614\,MJ$$

where,

$$\frac{\partial E_{T,C}}{\partial m} = C_P\cdot\Delta T_C + L_F\theta = 137.5$$

$$\frac{\partial E_{T,D}}{\partial m} = C_P\cdot\Delta T_D + L_F\theta = 125.6$$

$$\frac{\partial E_{T,C}}{\partial \Delta T_C} = \frac{\partial E_{T,D}}{\partial \Delta T_D} = m\cdot C_P = 178$$

$$\frac{\partial E_{T,C}}{\partial \theta} = \frac{\partial E_{T,D}}{\partial \theta} = -m\cdot L_F = 10000$$

Summary

The uncertainties involved in the estimation of melt fraction and energy stored / discharged are ± 0.061 and ± 0.614 MJ, respectively.

List of Publications

International Journal Papers

1. Niyas H, Prasad S, Muthukumar P. Performance investigation of a lab–scale latent heat storage prototype – Numerical results. **Energy Conversion and Management**. 2017; 135:188-199.
2. Niyas H, Rao CRC, Muthukumar P. Performance investigation of a lab–scale latent heat storage prototype – Experimental results. **Solar Energy**. 2017; 155:971-984.
3. Niyas H, Prasad L, Muthukumar P. Performance investigation of high-temperature sensible heat thermal energy storage system during charging and discharging cycles. **Clean Technologies and Environmental Policy**. 2015; 17(2):501-513.
4. Niyas H, Muthukumar P. A novel encapsulation technique for performance improvements in latent heat storage system (Submitted to **Applied Energy**, April 2017).
5. Rao CRC, Niyas H, Muthukumar P. Performance tests on lab-scale sensible heat storage prototypes (Submitted to **Applied Thermal Engineering**, Aug 2017).

International Conference Papers

1. Prasad L, Niyas H, Muthukumar P. Performance analysis of high temperature sensible heat thermal energy storage system during charging and discharging cycles. **4th International conference on Advances in Energy Research**, Indian Institute of Technology Bombay, Mumbai, India, 10-12 December 2013.
2. Niyas H, Muthukumar P. Performance analysis of latent heat storage systems. **International conference on Emerging Trends in Renewable Energy**. C.V. Raman College of Engineering, Bhubaneswar, India, 27-28 December 2013.
3. Niyas H, Shukla AK, Muthukumar P. Thermal characterization of phase change materials used for thermal energy storage in solar thermal power plants. **23rd International conference on Processing and Fabrication of Advanced Materials**, Indian Institute of Technology Roorkee, Roorkee, India, 05-07 December 2014.

4. Niyas H, Muthukumar P. Performance investigation of packed bed thermal energy storage system. **3rd International conference on Polygeneration**, College of Engineering Guindy, Anna University, Chennai, India, 18-20 February 2015.
5. Niyas H, Muthukumar P. Novel encapsulation technique to upscale latent heat storage capacity in steam accumulators. **ISES Solar World Congress**, Exco, Daegu, Korea, 8-12 November 2015.
6. Niyas H, Muthukumar P. Novel fin for effective heat transfer in shell-and-tube latent heat storage system. **ISES Solar World Congress**, Exco, Daegu, Korea, 8-12 November 2015.
7. Niyas H, Muthukumar P. Comparison of thermal storage characteristics of phase change materials encapsulated in different capsule configurations. **23rd National and 1st International ISHMT – ASTFE Heat and Mass Transfer Conference**, Liquid Propulsion Systems Centre, Indian Space Research Organization, Thiruvananthapuram, India, 17-20 December 2015.
8. Niyas H, Muthukumar P. Appropriate sizing prediction and performance evaluation of the shell-and-tube latent heat storage unit. **24th National and 2nd International ISHMT – ASTFE Heat and Mass Transfer Conference**, BITS Pilani, Hyderabad, India, 27-30 December 2017 (Under Review).

Book Chapters

1. Muthukumar P, Niyas H. Comparison of thermal characteristics of sensible and latent heat storage materials encapsulated in different capsule configurations, In: Chandra L, Dixit A. **Concentrated Solar Thermal Energy Technologies, Springer Proceedings in Energy**, 2018.
2. Rao CRC, Niyas H, Prasad L, Muthukumar P. Performance investigation of lab-scale sensible heat storage system, In: Chandra L, Dixit A. **Concentrated Solar Thermal Energy Technologies, Springer Proceedings in Energy**, 2018.